Cryogel-integrated hepatic cell culture microchips for liver tissue engineering

Lilandra Boulais

Par **Lilandra BOULAIS**

Cryogel-integrated hepatic cell culture microchips for liver tissue engineering

Thèse présentée
pour l'obtention du grade
de Docteur de l'UTC

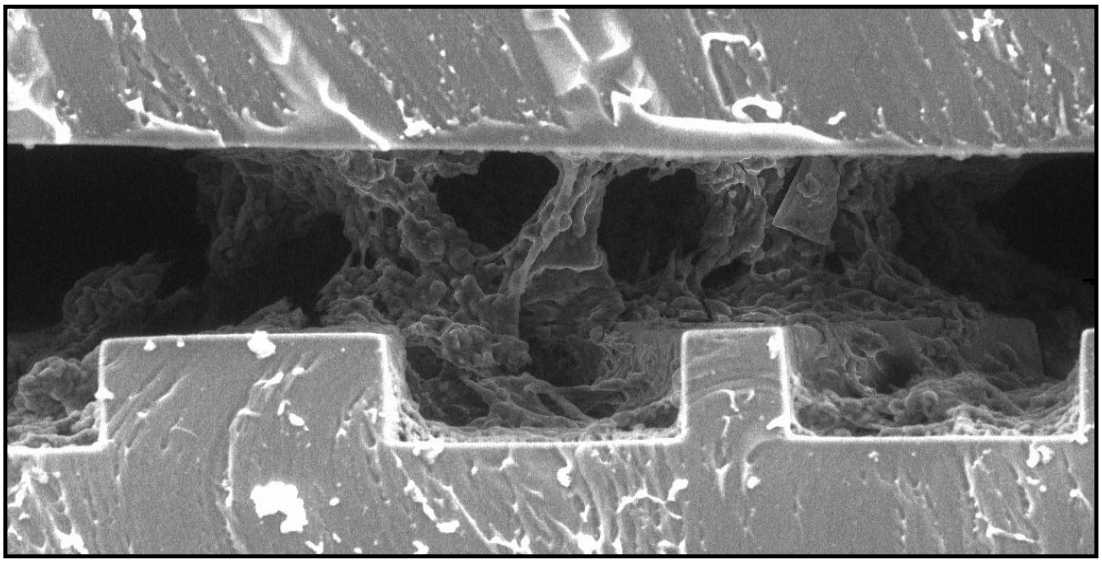

Soutenue le 31 août 2020
Spécialité : Bio-ingénierie : Unité de Recherche Biomécanique et Bio-ingénierie (UMR-7338)
D2561

THÈSE DE DOCTORAT

Ecole doctorale 71 : Sciences pour l'ingénieur
Spécialité de doctorat : Bioingénierie

Cryogel-integrated hepatic cell culture microchips for liver tissue engineering

---

Présentée et soutenue publiquement par
Lilandra BOULAIS

le 31 août 2020

Pour obtenir le grade de docteur de
UNIVERSITÉ DE TECHNOLOGIE DE COMPIÈGNE

Directeurs de thèse: Dr. Cécile LEGALLAIS, Dr. Sidi BENCHERIF

Laboratoire de BioMécanique et BioIngénierie (BMBI)
Equipe Cellules Biomatériaux Bioréacteurs (CBB)
CNRS UMR 7338

Jury:

Sidi Bencherif	Assistant Professor, Northeastern University	Directeur de thèse
Dominique Collard	DR CNRS, UMI CNRS 2820, LIMMS Tokyo	Rapporteur
Bertrand David	CR CNRS, UMR CNRS 8579, Centrale Supelec	Examinateur
Nathalie Maubon	CEO/CSO HCS Pharma	Examinateur
Cécile Legallais	DR CNRS, UMR CNRS 7338, UTC	Directrice de thèse
Nathalie Picollet D'hahan	Chercheur HDR, CEA	Rapporteur
Muriel Vayssade	Professeur, UMR CNRS 7338, UTC	Examinateur

Contents

Acknowledgements/Remerciements

Je souhaite d'abord remercier les membres de mon jury qui ont accepté d'évaluer mes travaux de thèse : Dominique Collard et Nathalie Picollet D'hahan pour leurs rapports et leurs questions ainsi que Bertrand David, Nathalie Maubon et Muriel Vayssade pour les échanges sur leurs domaines d'expertise respectif.

Je remercie également mes directeurs de thèse, Cécile Legallais et Sidi Bencherif, de m'avoir donné l'opportunité de réaliser cette thèse, tout en poursuivant des activités annexes. Un grand merci à Cécile pour sa disponibilité, l'autonomie et la confiance accordée, ainsi que la relecture de ce manuscrit. Merci à Sidi de m'avoir accueillie dans son laboratoire à l'université Northeastern à Boston et pour ses remarques constructives.

Merci à Anne Le Goff et Anne Dubart Kupperschmitt d'avoir fait partie de mon comité de suivi scientifique. J'ai apprécié échanger avec vous et voir votre optimisme qui me motivait chaque année.

J'aimerais également remercier toutes les personnes avec qui j'ai pu travailler pendant ces 4 années. Frédéric Nadaud pour le temps passé à observer les échantillons au microscope électronique à balayage et Caroline Lefebvre pour sa formation au microscope confocal. Merci également à Margaux, Solène, Anna, Darlène et Lauretta, qui m'ont aidé à différents moments du projet et que j'ai eu le plaisir d'encadrer pendant leur stage.

Merci à tout le laboratoire BMBI et en particulier l'équipe CBB qui m'a accompagnée pendant ce doctorat. Rachid, Ulysse, Pascale, un grand merci pour vos conseils, votre disponibilité et votre écoute. Vous avez toujours su m'aider et me remonter le moral. Vanessa, Murielle, Christophe, Muriel, Patrick, merci pour les moments partagés et la bonne humeur que vous apportez au laboratoire. Je remercie tout particulièrement les doctorants, Mégane, Alex, Mattia, Augustin, Félix, Claire, Antoine, Manon, Sabrina, Mathilde, Amal, Delphine, Doriane. Merci pour tous les moments que nous avons passés ensemble, au laboratoire et à l'extérieur, qui m'ont beaucoup apporté et qui ont pleinement contribué à mon épanouissement pendant ce doctorat.

Je tiens également à remercier ma famille et mes amis qui m'ont toujours guidée et supportée dans mes choix, et qui se sont toujours intéressés à mon sujet de recherche même s'ils ne comprenaient pas toujours tout.

Une thèse est faite de plein de rebondissements et celle-ci en a eu un peu plus que prévu : coupures électriques, contaminations des cultures cellulaires, travaux d'agrandissement, canicule, confinement... Malgré cela j'ai toujours essayé d'avancer et je suis fière de vous présenter les résultats de ce projet de recherche dans ce manuscrit et vous en souhaite bonne lecture.

Abstract

Today, one of the challenges for the pharmaceutical industry is to develop accurate *in vitro* liver models to improve the predictability of preclinical studies, in particular the study of the toxicity and efficacy of drug candidates. In recent years, tissue engineering, a multidisciplinary approach to develop tissues, has led to the development of new cell culture methods. Among them, cell cultures in 3D or in perfusion allowed to obtain hepatic activities similar to those observed *in vivo*. The objective of this thesis is to combine these two cell culture methods to create an even more accurate *in vitro* liver model. To do so, we are seeking to develop an alginate cryogel integrated into a microchip with mechanical properties adaptable to those of the liver depending on the physiological state to be reproduced (healthy or pathological liver).

In the first part, we develop and characterize the alginate cryogel at the microscopic and macroscopic level, outside (cylindrical samples) and then inside the biochip. Three parameters are studied here: the cryopolymerization temperature, the alginate concentration and the quantity of cross-linking agents. Mechanical properties, porosity, absorption, pore interconnectivity and flow resistance are analyzed.

The second part aims to culture liver cells within this new device. For this feasibility study the HepG2/C3A cell line is used. The results show viable and functional cells (albumin production, APAP transformation). In addition, we observe a 3D tissue structure, which is maintained after removal of the alginate cryogel.

The last part aims to complexify the hepatic model, in particular by co-cultures. To get closer to the sinusoid structure, liver cells are cultured with endothelial cells (HUVEC) according to two approaches. In addition, the possibility to follow circulating tumor cells (MDA-MB-231) in the system is studied.

Resume

L'un des enjeux de l'industrie pharmaceutique aujourd'hui est de développer des modèles de foie *in vitro* fidèles pour améliorer la prédictivité des études précliniques, notamment l'étude de la toxicité et de l'efficacité des médicaments candidats. Ces dernières années, l'ingénierie tissulaire, approche multidisciplinaire pour développer des tissus, a mené au développement de nouvelles méthodes de culture cellulaire. Parmi elles, les cultures de cellules en 3D ou en perfusion ont permis d'obtenir des activités hépatiques similaires à celles observées *in vivo*. L'objectif de cette thèse est de combiner ces deux méthodes de culture cellulaire pour créer un modèle de foie *in vitro* encore plus fidèle. Pour cela, nous cherchons à développer un cryogel d'alginate intégré en micropuce avec des propriétés mécaniques adaptables à celles du foie en fonction de l'état physiologique à reproduire (foie sain ou pathologique).

Dans la première partie, nous développons et caractérisons le cryogel d'alginate au niveau microscopique et macroscopique, à l'extérieur (échantillons cylindriques) puis à l'intérieur de la biopuce. Trois paramètres sont étudiés ici : la température de cryopolymérisation, la concentration d'alginate ainsi que la quantité d'agents réticulants. Les propriétés mécaniques, la porosité, l'absorption, l'interconnectivité des pores et la résistance au flux sont analysés.

La deuxième partie vise à cultiver des cellules hépatiques au sein de ce nouveau dispositif. Pour cette étude de faisabilité la lignée cellulaire HepG2/C3A est utilisée. Les résultats montrent des cellules viables et fonctionnelles (production d'albumine, transformation d'APAP). De plus, nous observons une structure tissulaire 3D, qui se maintient après retrait du cryogel d'alginate.

La dernière partie a pour but de complexifier le modèle hépatique, notamment par des co-cultures. Pour se rapprocher de la structure du sinusoïde, des cellules hépatiques sont cultivées avec des cellules endothéliales (HUVEC) selon deux approches. De plus, la possibilité de suivre des cellules tumorales circulantes (MDA-MB-231) dans le système est étudiée.

List of Figures

List of Tables

Abbreviation

AAD: Adipic acid dihydrazide
ADME: Absorption, distribution, metabolism, excretion
APAP: N-acetyl-para-aminophenol, acetaminophen, paracetamol
APAP-GLUC: APAP glucuronide
APAP-GSH: APAP glutathione
APAP-SULF: APAP Sulfate
ATCC: American type culture collection
CTC: Circulating tumor cells
CYP: Cytochrome P450
DC: Degree of pore connectivity
DILI: Drug induced liver failure
ECM: Extracellular matrix
ECVAM: European centre for the validation of alternative methods
EDC: 1-Ethyl-3-(3-dimethylaminopropyl)carbodiimide
FBS: Fetal bovine serum
G: α-L-guluronate
GFP: Green fluorescent protein
GST: Glutathione S-transferase
HSC: Hepatic stellate cells
HUVEC: Human umbilical vein endothelial cells
ICCVAM: Interagency coordinating committee on the validation of alternative methods
IDCCM: Integrated dynamic cell cultures in microsystems
iLite: Innovations for liver tissue engineering
iPSCs: Induced pluripotent stem cells
LDH: Lactate dehydrogenase
LSEC: Liver sinusoidal endothelial cells
M: β-D-mannuronate
MEM: Minimum essential medium
MES: 2-(N-morpholino)ethanesulfonic acid
NAPQI: N-acetyl-p-benzoquinone imine
NAT: N-acetyltransferase
NHS: N-hydroxysuccinimide
NPC: Non-parenchymal cells
PBPK: Physiologically based pharmacokinetics
PBS: Phosphate buffered saline

PDMS: Polydimethylsiloxane
PFA: Paraformaldehyde
PHH: Primary human hepatocyte
PK/PB: Pharmacokinetics/Pharmacodynamics
Q_M: Swelling ratio
QSAR: Quantitative structure activity relationship
RGD: Arginine (R), glycine (G), aspartate (D)
SDS: Sodium dodecyl sulfate
SEM: Scanning electron microscopy
SULT: Sulfotransferase
UDP: Uridine diphosphate
UGT: UDP-glucuronosyltransferase
YM: Young modulus

Introduction

The "bioartificial liver" program within BMBI laboratory consists in the optimization of liver functions thanks to reconstructed liver tissues using multiple tissue engineering approaches. This program is directed since several years at UTC by Dr. C. Legallais, one of my supervisor, research director at CNRS and expert in liver tissue engineering. On the one hand, the culture of liver cells in microbioreactors, i.e. biochips, introduced by Dr. E. Leclerc, showed improved cellular responses in terms of biotransformation after the administration of drugs or toxic substances. On the other hand, the culture of hepatocytes, individually or in the form of aggregates within alginate beads resulted in the development of a suitable extracorporeal bioartifcial organ. Most of this work, carried out in bioreactors, has highlighted the critical role of the "cell microenvironment" in biological responses such as cell-cell interactions, cell-matrix interactions, the effect of shear stress on cells induced by a perfusion, etc.

To better understand the impacts of the microenvironment on liver cells and more broadly on liver tissue regeneration, we aim here at implementing and investigating the culture of hepatocytes in cryogel-based matrices integrated in microfluidic devices. Dr. S. Bencherif, my PhD co-supervisor, recruited as CNRS researcher at BMBI in 2015 and currently associate professor at Northeastern University, is expert in such scaffolds. We therefore propose here a strategy to prepare and evaluate a new generation of liver-on-chip, which should combine the advantages of 3D culture and of perfused microsystems. As complex *in vitro* model, it can potentially be used for drug screening or as a platform to better understand phenomena occurring in native or pathological liver tissues.

This PhD thesis was initially supported by the Ligue contre le Cancer (comité de l'Oise) and rapidly integrated the PIA RHU iLite (Innovations in liver tissue engineering) program led by Prof. J-C. Duclos Vallée (Centre Hépatobiliaire, Villejuif). A specific work package, under the supervision of Prof. B. Lepioufle (ENS Cachan) is dedicated to liver-on-chip and its applications. Meanwhile, we also join another research consortium led by Dr A. Treizebré at IEMN, dealing with the *in vitro* modeling of circulating tumor cells' behaviour in the liver. These different collaborations allowed us to evaluate the system we developed for different applications.

The PhD manuscript is divided in six chapters. The first one brings the general context justifying the development of liver models for the pharmaceutical industry. Chapter 2 proposes a review of the literature on engineered *in vitro* liver models. The chapter 3 describes the materials and methods. In chapter 4, we justify how we design the cryogel-integrated microchip taking into account physical and mechanical properties. Chapter 5 is dedicated to the biological proof of concept using a human hepatic cell line,

HepG2/C3A. In the last chapter, we finally propose to evaluate the potential of the new microchip in different conditions that bring it closer to the applications: culture of primary human hepatocytes, co-culture of HepG2/C3A with endothelial cells, and finally behavior of circulating breast tumor cells in the system.

Chapter 1

Liver and drugs, a close relationship

1.1 Drug development

Every year, tens of thousands of molecules are tested in pharmaceutical and biotechnological companies for their potential to treat diseases. However, only a handful of these candidates will end up in our pharmacies years later. It is estimated that out over 10 000 discovered compounds, only one is approved as a market drug after 10 to 15 years process.

1.1.1 A long, difficult and costly process

The development of a new drug follows a long process that extends over several years. It is divided into several stages from research to market (Figure 1.1) [1]–[3].

- Drug discovery: this step takes place in laboratories. Thousands of molecules are tested on a biological target and those presenting the best potential of interest are selected for the following steps.

- Preclinical testing: to predict potential safety problems, pharmaceutical and toxicological studies are conducted on *in vitro* or *in vivo* models, on animals. These studies are mandatory prior to initiate clinical phase. Once the studies performed, an application for approval to conduct clinical studies is submitted to the regulatory body. In the United States of America (USA), the application, called an Investigational New Drug application (IND), has to be submitted to the Food and Drug Administration (FDA). In the European Union (EU), each state is governed by its own regulatory body therefore the application can be done to one or several states.

- Clinical trials: at this stage, studies are performed on human subjects with increasing number. Trials are divided into 3 phases:
  - Phase I aims to study the safety and the pharmacokinetics of the drug candidates. This involves testing them on 20 to 80 healthy subjects.
  - During phase II, the therapeutic activity of the drug is investigated, in particular dose response relationship and dose range, called PK/PD studies (pharmacokinetics/pharmacodynamics). This involves testing 100 to 300 subjects with the targeted condition.

- The goal of phase III is to confirm and validate the previous results by monitoring the side effects. It involves 1000 to 3000 subjects with the targeted condition.

- Marketing authorisation: in case of successful clinical trials, a marketing authorization application is submitted to the regulatory authorities. In the USA, the New Drug Application (NDA) is reviewed by the FDA. In the EU, 4 pathways are possible: the centralized process for designated drugs through the European Medicines Agency (EMA), the national process, the mutual recognition that extends the approval in one state to another one and the decentralized procedure with simultaneous approval in several states.

- Manufacturing/Post approval: also known as phase IV, this stage corresponds to pharmacovigilance. This involves monitoring the side effects that could be associated to the drug on the whole population.

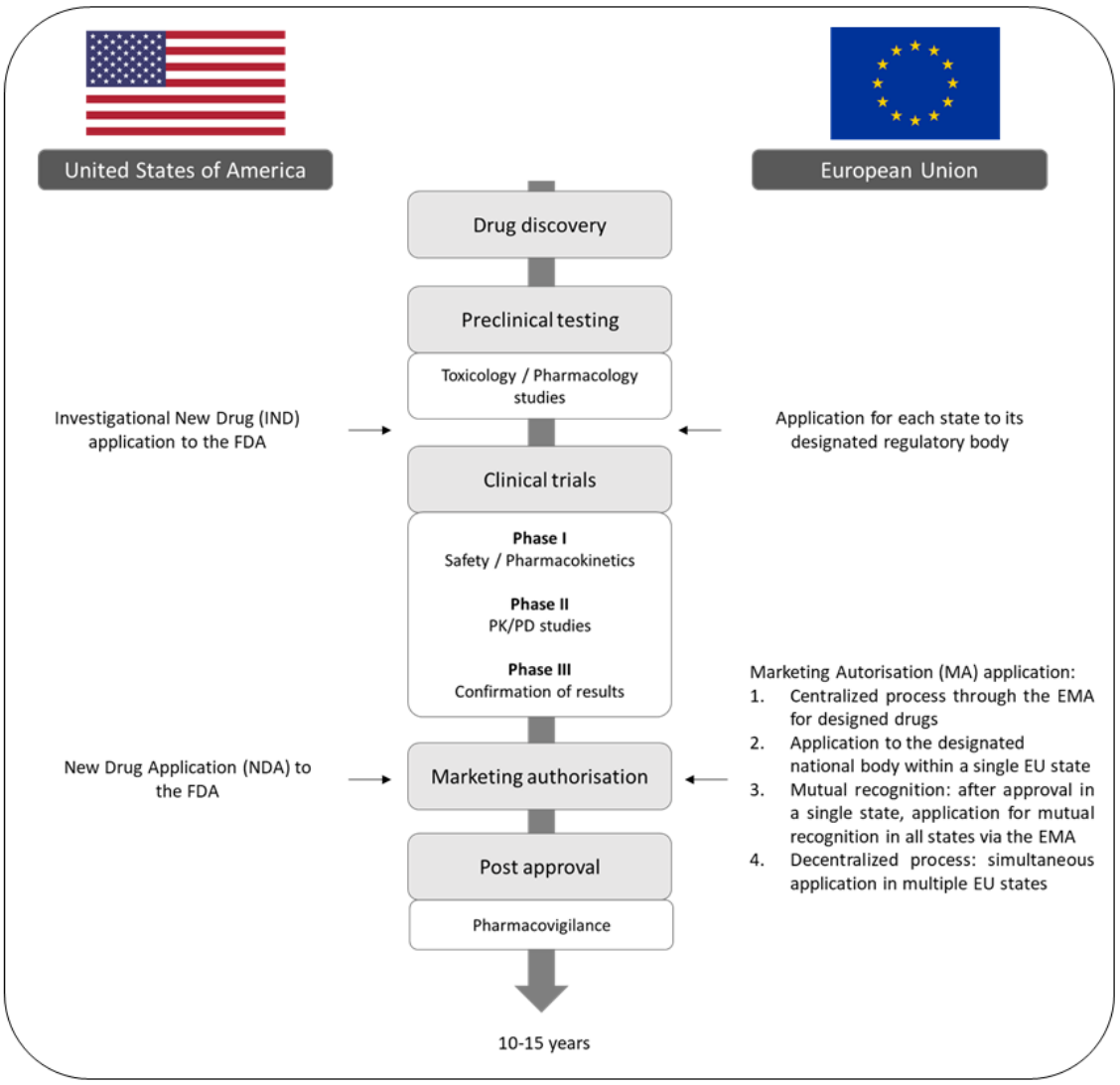

FIGURE 1.1: Drug development process in the USA and in the UE.

This drug development process takes up to 10 to 15 years to be achieved. Moreover, the number of drug candidates decreases considerably as the stages go on. The attrition rate is high: about 63% of compounds pass the preclinical phase, 48% of them transition from Phase I into Phase II, 29% from Phase II to Phase III and 67% will be submitted to market application [4]. Thus, it is estimated that only 6% of the drug candidates will successfully reach the drug market. This attrition rate is mainly due to a lack of efficacy and safety (Fig. 1.2) [5], [6]. This leads pharmaceutical industries to spend several millions of dollars per drug, a cost that is continuously increasing [7]–[9]. As clinical trials are the most expensive stages in the drug development, it has become financially and temporally relevant to investigate in a more reliable way to determine efficacy and, in particular, potential toxicity of drug candidates during preclinical phase [10].

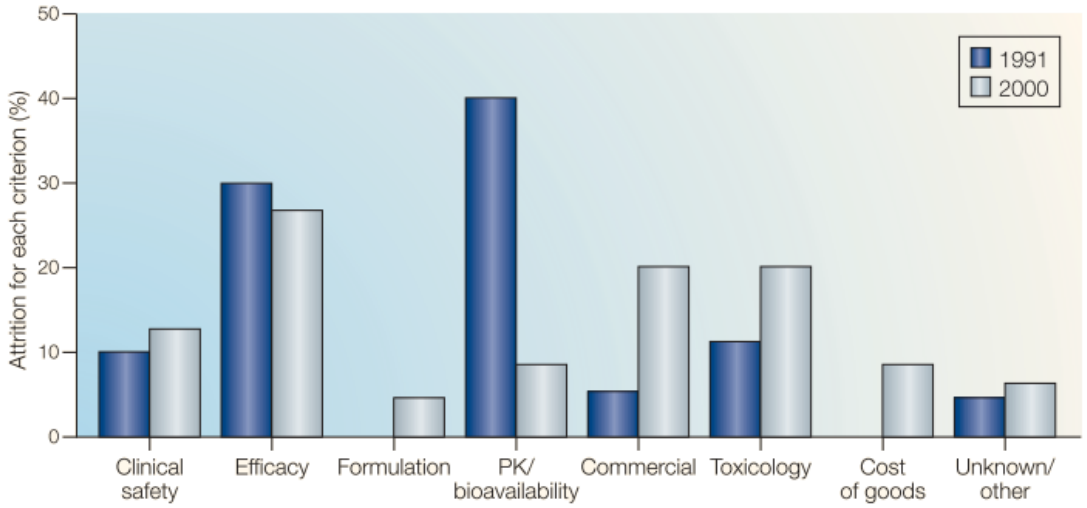

FIGURE 1.2: Reasons for attrition. PK: pharmacokinetics [5].

1.1.2 Drug safety

After a first selection during the drug discovery phase, the drug candidates must pass various tests to guarantee security. These safety tests are performed during preclinical phase. They are composed of toxicological and pharmacological studies in order to reveal any potential danger and any side effects of the drug candidates.

Toxicology

As a drug can have diverse effects on the organisms, different types of toxicological studies must be conducted.

The acute toxicity, aims at determine the median lethal dose corresponding to the dose required to kill half of the animals. It also evaluates the maximum tolerated concentration corresponding to the No-Observed-Adverse-Effect Level (NOAEL). These tests are performed with single dose and last for at least 14 days to observe adverse effects.

The chronic toxicity assesses the adverse effects of the drug on a long term exposure. It determines the nature, the frequence or the evolution of these effects. These tests are performed with repeated doses at low concentration and over at least 6 months in Europe.

The effects on the reproduction are also assessed. Male and female fertility tests are performed. In the same way, other complementary assessments may be conducted such as embryonic development, peri and neonatal toxicity.

The mutagenic potential is determined by gene mutation and chromosomal aberration tests. The carcinogenic potential is evaluated over 2 years on animals with the maximum tolerated dose.

Pharmacology

Pharmacological studies must be done in order to further deepen the knowledge around the drug, study its efficacy, determine its mechanism of action and thus the drug /organism interactions. They are separated into pharmacodynamics, analyzing the effects of the drug on the body, and pharmacokinetics, analyzing the effects of the body on the drug. These two studies are closely linked since some drugs become toxic only after their transformation by the organism. In doing so, the drug pathway in the body has to be followed and is composed of 4 phases: absorption, distribution, metabolism, and excretion (ADME)(Fig. 1.3).

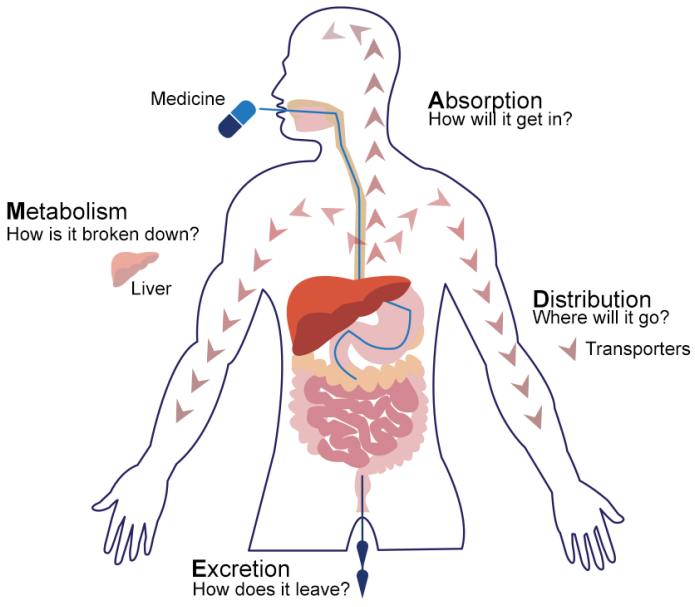

FIGURE 1.3: Schematic representation of the ADME process [11].

The absorption is the process by which a drug reaches the bloodstream from its delivery site. This step involves the passage of biological barriers that protect the organism against xenobiotic substances. The adsorption depends on the mode of administration (oral, subcutaneous, intravenous...) and on the galenic form (solution, capsule...).

Once the drug is in the bloodstream, it can reach any organs rapidly by being transported throughout the body and especially its effector site. The distribution depends on various factors: the blood flow in the organ, the vascular permeability, the drug affinity for the tissue and the local pH. Thus, the drug distribution is unequal in the body and the highly perfused organs receive more drug quantities like the heart or the liver.

As a xenobiotic, the drug is transformed by the organism to be eliminated. The metabolism is performed by different organs such as lungs, kidney, intestine but mainly by the liver. In this organ it is the enzymatic reactions called phase I and II which intervene in the biotransformation of the drug. The products of these transformations, the metabolites, can be either inactive, toxic or with another drug activity.

The excretion is the final step of the drug path in the body. It leads to the elimination of the xenobiotic from the body. It is mainly excreted via the urine and feces. In the first case, the obtained metabolites return to the bloodstream and are filtered by the kidney. In the other case, they are excreted in the bile and go then to the intestine. They can also be excreted in saliva, lungs in expired air...

The safety of drugs is thus estimated by these different studies. However, after approval and marketing, a higher number of patients are exposed to the drugs than in clinical studies, leading to the discovery of rare toxic effects, including hepatotoxicity [12], [13]. Drug induced liver injury (DILI) is a non negligeable adverse reaction: it is estimated that DILI is responsible for approximately 50% of acute liver failure in the United States and in Western Europe (Table 1.1) [14]. Due to its high vascularization and its xenobiotic activities, the liver is the principal organ in interaction with the drugs. In addition, as it is also an essential organ for the proper functioning of the human body, a damage to it can lead to serious complications.

Causes	Germany	United Kingdom	United States
Drugs	29	68	52
Hepatitis virus (A, B, E)	22	8	11
Other	28	7	19
Unknown	21	17	18

TABLE 1.1: Causes of acute liver failure in Europe and in the USA [14].

1.2 The liver: an essential organ in the metabolism of xenobiotics

1.2.1 Structure

Weighing around 1.5 kg and measuring about 15 cm wide, the liver is one of the largest organ of the human body but also one of the most essential. Located in the abdominal area, just below the diaphragm, it is easily recognizable by its brown colour and its smooth sponge-like texture.

From a macroscopic view, the liver is composed of two parts, a left and a right lobes separated by the falciform ligament and held together in a thin capsule called Glisson's capsule. Highly vascularized, the liver receives about 2 L/min of blood via two main vessels: the hepatic artery and the portal vein. Around 70% of the volume comes from the portal vein that carries a blood low in oxygen but rich in nutrients after passing through the digestive system, the pancreas and the spleen. The last 30% comes from the hepatic artery that carries oxygen-rich blood from the aorta. The blood from both vessels mixes and is distributed through the liver by a network of capillaries called sinusoids. Blood is collected out of the liver by the hepatic vein and continues its cycle in the human body. The macroscopic anatomy of the liver is described in the figure 1.4.

From a microscopic view, each lobe is composed of several hepatic lobules, the functional unit of the liver [15], [16]. These lobules present a hexagonal shape with a well-organized structure. At each lobule's corner, a branch of the hepatic artery, a branch of the portal vein and a bile duct form the portal triad. The blood flows in the sinusoids from the portal triad to the central vein, located at the centre of the hexagon, and then to the hepatic veins. During its flow through the sinusoids, exchanges with cells take place resulting in blood's composition changes. Thus, the lobule is commonly divided in 3 zones according to the Rappaport acinus model (Figure 1.4) [17]. The first one, the periportal zone, is the closest to the portal triads and so corresponds to a blood rich in oxygen, nutrients and xenobiotics. At the opposite the third one, the closest to the central vein, called the pericentral zone, corresponds to a blood poor in oxygen, nutrients and xenobiotics. Between them, the transitional zone is the zone 2 corresponding to an intermediary. This structural zonation leads also in a functional zonation that is detailed later. Bile flows through bile canaliculi in parallel to blood but in the opposite direction that is to say towards the bile duct of the portal triad. Then, bile leaves the liver by the common hepatic duct and joins the gallbladder to be stored.

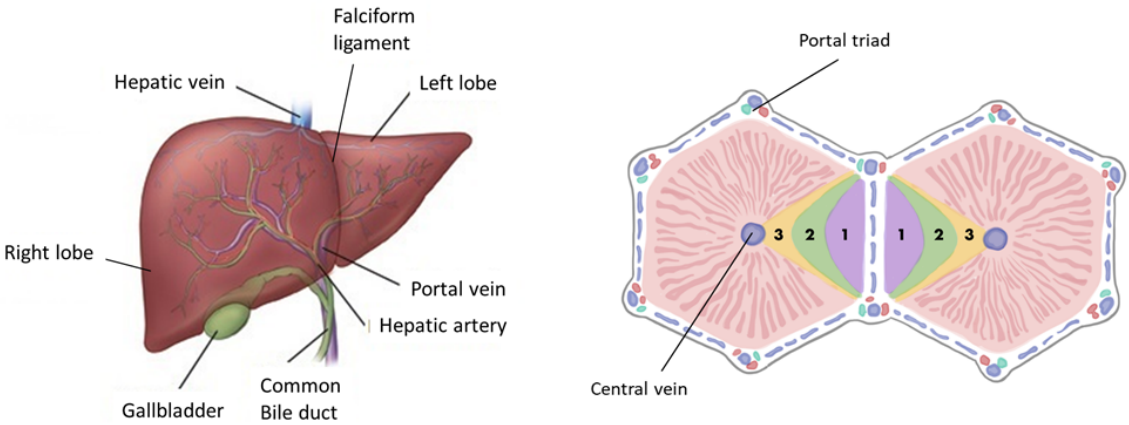

FIGURE 1.4: Liver anatomy and schematic representation of two hepatic lobules and their zonation: 1)periportal zone, 2)intermediate zone, 3)centrilobular zone. Adapted from [18], [19].

1.2.2 Cells and organization

The liver is composed of different cell types. Hepatocytes represent with 60% the great majority and constitute the parenchymal cells of this organ, ensuring its functional part. The non-parenchymal cells (NPC) are in majority liver sinusoidal endothelial cells (LSEC), Kupffer cells and hepatic stellate cells (HSC) [20], [21]. All these cell types are present in the hepatic lobules and well organized around the sinusoid as shown in the figures 1.5 and 1.6.

The sinusoid is composed of LSEC which are the specific endothelial cells of the liver. Without organized basal lamina and presenting open pores with diameters around 100 nm, called fenestrae, they allow the exchanges of molecules between the blood on one side and the hepatocytes on the other. They also play a role in inflammatory reactions as they can detect pathogen-associated molecular patterns. It has been shown that they participate in the establishment of the liver microarchitecture and in the guidance of hepatocytes proliferation during liver regeneration.

In the sinusoid lumen, lining the walls, the Kupffer cells are the macrophages of the liver. They destroy any bacteria flowing through the sinusoid by phagocytosis but also cellular debris such as old red blood cells or hemoglobin that are broken down into bilirubin. They can modulate the activities of hepatocytes by secreting the cell signaling protein cytokines.

In the other side of the sinusoidal barrier are the HSC, also known as Ito cells. These pericytes cells are located in the space of Disse that separates the sinusoid from the hepatocytes. They store most of the vitamin A and can also secrete cytokines to modulate the inflammatory response. Moreover, they are involved in the liver regeneration process.

The hepatocytes are separated from the sinusoid by the space of Disse. They are organized in plates of one cell thick and form by joining their membrane an intercellular space which is the bile canaliculi. These cubical cells are polarized [22]: their basal membrane is on the space of Disse side and their apical membrane is exposed to the bile canaliculi. They are involved in the majority of the metabolic functions and ensured the xenobiotic activity of the liver.

1.2.3 Functions

Although the liver is known from centuries, its functions remain partially understood. The number of functions is generally estimated around 500 comprising molecule's production or degradation, storage and blood detoxification. The liver plays a major role in many metabolic processes which makes it a particularly complex and essential organ to maintain normal physiological activities [25].

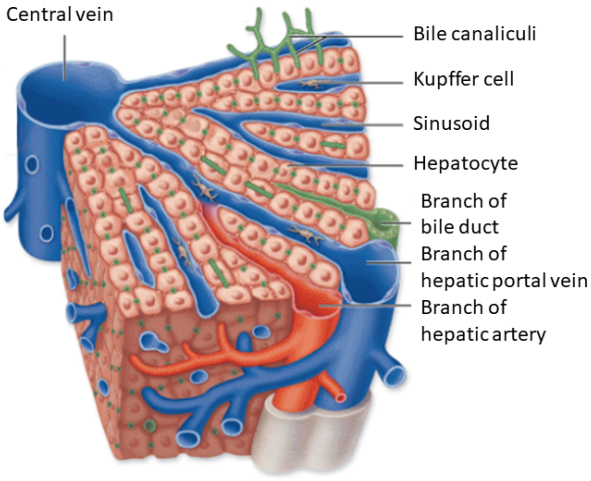

FIGURE 1.5: Reconstitution of a part of an hepatic lobule. Adapted from [23].

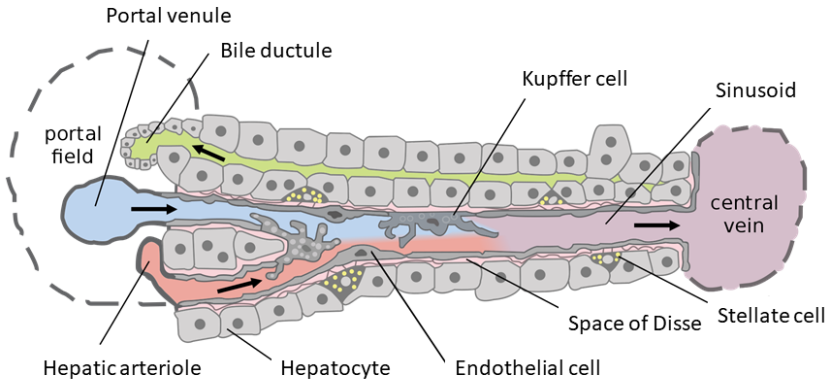

FIGURE 1.6: Schematic representation of the structure of a sinusoid. Adapted from [24].

Major metabolic activities

The liver is involved in different metabolisms including that of carbohydrates, lipids, proteins, amino acids necessary for the human body to function.

It synthesizes glycogen from glucose (glycogenesis) and stores it but can also achieve the reverse process by breaking glycogen into glucose (glycolysis) ensuring a regulation of blood glucose level in the body. In the absence of glycogen, it is able to synthesize glucose from lactate, glycerol or some amino acids (gluconeogenesis).

Concerning lipid metabolism, it plays an important role in cholesterol synthesis but also in production and breakdown of triglycerides, lipogenesis and lipolysis respectively, into glycerol and fatty acids.

It is responsible of a lot of proteins and amino acids synthesis and degradation. For example, it synthesizes the albumin, a blood transport protein, that carries fatty acids, drugs and others molecules to the liver itself.

The liver has many other functions essential for the human body. It plays an important role in the digestive system as it is the only one to synthesize bile, required for the digestion. One step of the red blood cells degradation is performed by the liver. It transforms the bilirubin (glucuronidation), breakdown product of the hemoglobin, which is then excreted into the bile or the blood. During the degradation of amino acids, ammonia, a toxic substance at high concentrations, is produced. It is the liver which transforms it into a harmless metabolite, the urea. It can store vitamins, especially vitamin A which is stored almost only in the liver.

Due to liver zonation, the hepatocytes do not perform functions in the same way all along the lobule. Depending on their position between the periportal zone and the perivenous zone, the cells are specialized in some functions only. This functional zonation is described by an ascending or descending gradient of activity (Figure 1.7) [26].

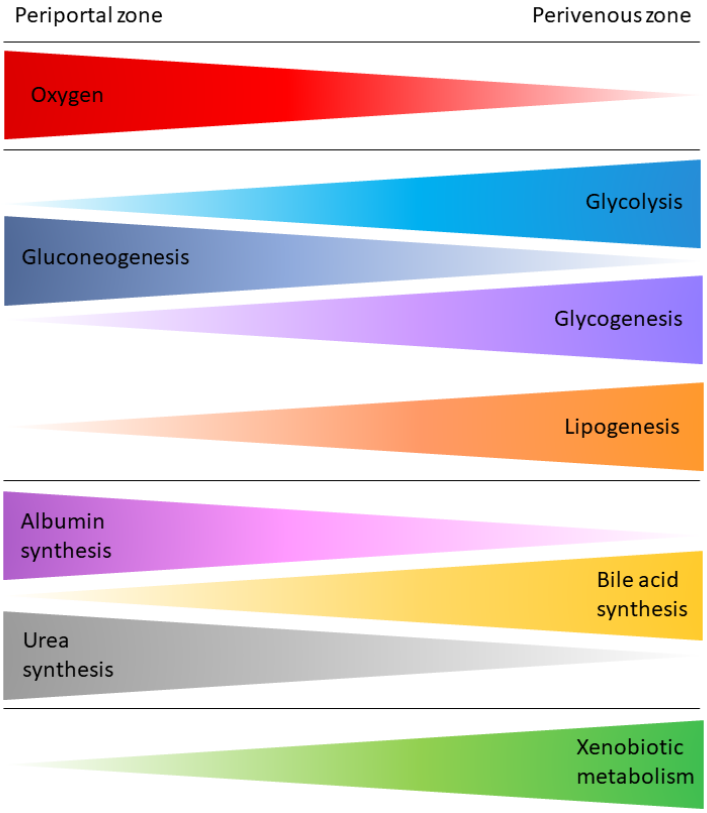

FIGURE 1.7: Liver functions and their zonation in the sinusoid. Adapted from [27].

Xenobiotic activities

In addition to accomplish all these metabolic activities, the liver is the principle organ which achieves xenobiotics'metabolism, corresponding to the breakdown of foreign substances present in the body. This phenomenon is also known as the biotransformation. It is composed of the phase I and II, called the functionalization and the conjugation respectively.

The first one, the functionalization phase, aims at transforming the xenobiotic substances in more hydrophilic molecules. To do so, the main reactions performed by the liver are oxidation, reduction and hydrolysis. They lead to metabolites with commonly hydroxyle (-OH), amine (-NH_2) and carboxyle (-COOH) functional groups. Oxidation is performed in majority and is catalyzed by the cytochrome P450 monooxygenase, also called CYP450. Among them, the CYP3A4 is the most present in the liver. The obtained metabolites can then continue the process of biotransformation.

The conjugation phase aims to transform the substances into soluble substances by the conjugation of charged groups like sulfate, glutathione, glucuronic acid, acetyl or methyl. The substrates are generally the metabolites obtained after the functionalization phase but can also be substances which were already hydrophilic enough and did not have to go through the phase I. These reactions are catalyzed by different enzymes of the transferase group (Table 1.2). The most common reaction is the glucuronidation which conjugates the metabolite with glucuronic acid thanks to the glucuronyltransferase (UGT). Two main other reactions are the sulfatation with the sulfotransferase (SULT) and the glutathione conjugation with the Glutathione S-transferase (GST).

Once the metabolites sufficiently soluble, they are mainly eliminated by passing into the blood and then the kidneys (urea) but can also be eliminated by the bile (faeces), the lungs (exhaled air), saliva...

Enzyme family	**Abbreviation**	**Reaction**
Cytochrome P450	CYP	oxidation
N-Acetyltransferase	NAT	acetylation
UDP-glucuronosyltransferase	UGT	glucuronidation
Glutathione S-transferase	GST	glutathione conjugation
Sulfotransferase	SULT	sulphation

TABLE 1.2: Principle enzymes of phase I and II.

Like the metabolic functions, the xenobiotic activities depend on the different zones of the hepatic lobule. The xenobiotic metabolism is thus higher in the perivenous zone (Fig. 1.7).

A well-known example of this metabolic activity is the biotransformation of the acetaminophen, also known as paracetamol or APAP. It is one of the most commonly used drug for the treatment of pain and fever around the world. Its biotransformation implies several pathways leading to different metabolites (Fig. 1.8). Indeed, after the uptake of the APAP by the hepatocytes, a competition occurs between the phase I and phase II enzymes since the molecule can be directly processed by the transferases. In majority the drug is transformed in inactive metabolites by conjugation with different groups: 52 to 57% of APAP-glucuronide (APAP-GLUC) and 30 to 44% of APAP-sulfate (APAP-SULF) [28]. A minority of APAP, 5 to 10%, is however transformed into an active metabolite, N-acetyl-p-benzoquinone imine (NAPQI), by oxidation with CYP. This metabolite is highly

reactive and is responsible for hepatotoxicity leading to liver necrosis [29]. It is detoxified by its conjugation to glutathione (APAP-GSH). The obtained metabolites are then either excreted in the blood or in the bile. A small part of APAP, less than 5%, is excreted unchanged in the blood.

Although commonly used and presenting a safety profile, APAP is not without danger. In developed countries, it represents the majority of DILI: 75% for the United States, 84% for the United Kingdom and 52% for Germany [14]. Indeed, hepatotoxicity can occur in case of overdose or in case of abusive uptake in at-risk populations. In case of excessive intake of APAP, the available stock of glutathione, necessary for the transformation of NAPQI into APAP-GSH in the phase II, decreases. The NAPQI is thus not transformed anymore, leading to hepatotoxicity.

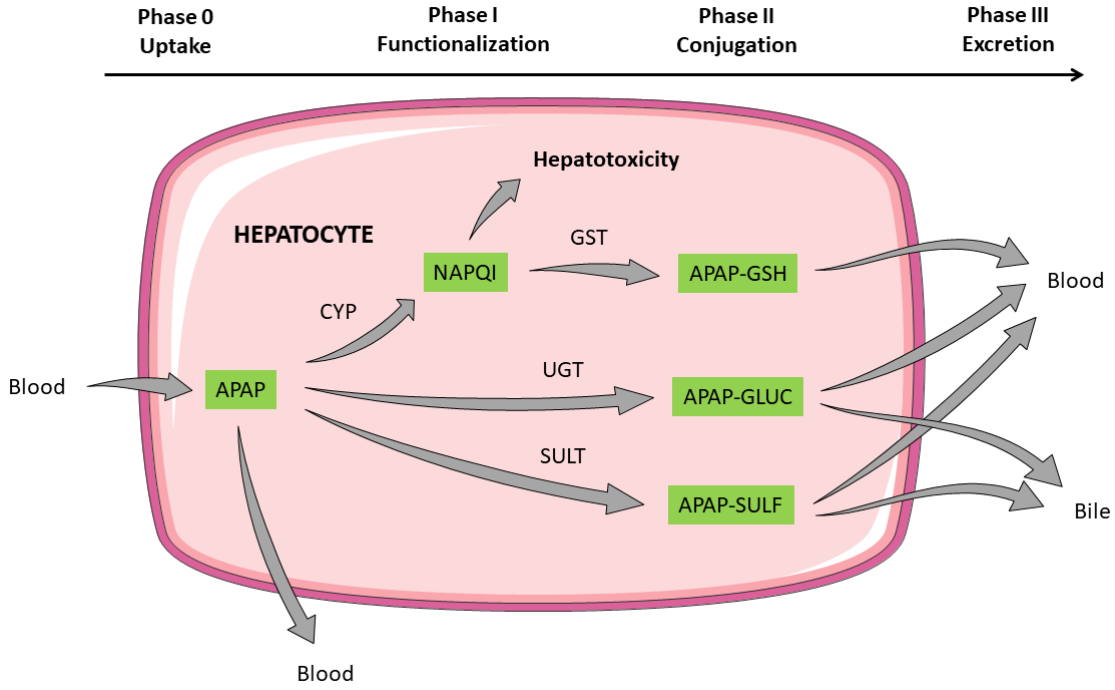

FIGURE 1.8: Schematic representation of APAP metabolism.

In case of a liver damage, the consequences are usually severe due to the loss of liver ability to perform physiological functions. As hepatotoxicity is often the cause of failure to obtain marketing authorization or even development stoppages by the pharmaceutical industries, it thus appears necessary to predict any potential adverse effects of the drug candidates on the liver, and preferably before clinical trials. It is therefore important to have experimental models during the preclinical phase which are able to determine the toxicity and pharmacology of drug candidates that could lead to hepatotoxicity.

1.3 From *in vivo* to *in vitro* models

To perform the different toxicological and pharmacological tests, experimental models are used in laboratories. They can be classified into 3 groups: *in vivo*, *in silico* and *in vitro*.

1.3.1 *In vivo* issues

Animal experiments are traditionally used in the pharmaceutical and chemical industry, or in basic toxicological sciences, to evaluate the effects of a chemical on the organism. In general, the effects observed during these experiments are assumed comparable to the ones observed with Humans. It is expected that biotransformations will be performed in the animal's liver. Thus, systemic or organ toxicity are assessed since the molecule tested and its metabolites are released in the whole blood circulation. However, the current trend is to limit the use of these *in vivo* studies for several reasons.

Due to criticisms and the pressure from public opinion on the welfare of animals these last years, supervision of animal tests has been increased. In this way, about 60 years ago, the principles of the 3Rs were developed by Russel and Burch [30] and still provide today a framework on the use of animals in scientific research [31], [32]:

- Reduction: methods which minimize the number of animals used per experiment. It is mandatory to estimate the number of animals required by statistical analysis, not to perform non-essential experiments, not to conduct experiments that have already be done.
- Refinement: methods which minimize animal suffering and improve welfare. The experimenter have to use non invasive methods if possible, to perform appropriate euthanasia methods. An enrichment of the living environment of animals is also required like the presence of congeners, the possibility to hide or to distract.
- Replacement: methods which avoid or replace the use of animals. If alternatives methods to animal experimentation exist, they must be used. These methods must have been tested and validated beforehand.

In Europe, animal experimentation is regulated and harmonized by several texts. Among them, the European directive 2010/63 published in 2010 imposes the application of the 3R rule, diversifies the categories of protected animals and recommends the use of alternative methods [33].

In France, regulation, governed by the Rural Code, is supplemented by a procedure by an authorization of scientific experience procedure involving animals. The project is studied by an ethics committee: the experimenters must justify their experimental choices, have received a training in animal experimentation, the research establishment must have an approval. If alternative methods exist, they should be used. The

final authorization is delivered by the ministry of research.

In addition to ethical issues, animal models present also scientific limitations. Due to the difference among species, animals may represent poor relevance to human biology: it has been shown that about half of the drugs that caused liver damage during clinical trials did not show any damage in animal models *in vivo* [34]. This is reinforced by the fact that the way animals are housed and handled can affect their physiology and behaviour which could result in distorted data [35]. Moreover, animal experimentation is often costly and time-consuming.

Although the animal experiments present some issues, they are still used to predict and evaluate the toxicity, pharmacology and adverse effects of drugs. Reduction and refinement are today achieved relatively easily by statistical analysis and environment adapted to animals' needs respectively. Replacing animals that is to say *in vivo* experiments in general will be difficult in a near future, but alternative methods are under development and complete now some of the *in vivo* studies. These methods represent a key challenge for the pharmaceutical industry and a part of last years research was devoted to develop and validate them.

1.3.2 Alternative models

The alternative methods to *in vivo* models can be divided in 2 groups: the *in vitro* and the *in silico* ones.

In silico models

In silico systems are based on mathematical and bioinformatics modeling. They rely on current physiological knowledge and toxicity databases but are also continuously enriched by data obtained from *in vivo* and *in vitro* experiments. These models are usually used as a first filter on the drug candidates by predicting their toxicity and their ADME properties [36], [37]. Thus, they represent a strategic challenge for the pharmaceutical industry in particular to reduce the substantial costs of drug development.

One of the used models is the Quantitative Structure-Activity Relationship (QSAR). This type of models establishes molecular relationships between chemical structures. It assumes that molecules with similar chemical properties will have similar biological effects. These relations are mainly used to predict drug efficacy but can also be used in toxicology as they predict the carcinogenicity and mutagenicity of molecules [38]. However, when the structure-activity is complex, the predictivity is poor [39].

Besides QSAR, others models have been developed to study the pharmacology of a molecule in the body. Known as Physiologically based pharmacokinetics (PBPK), these computational models predict the ADME phases. They are usually multi compartment models: an organ, a group of organs or tissues is modelized by a compartment which is

itself linked to other compartments. The connections between compartments follow the physiology and the compartments are regulated by equations respecting the principles of mass transport, fluid dynamics and biochemistry. These models allow predicting the concentrations in the different compartments and therefore the organs that will be most exposed. The advantage of this method is the possibility of extrapolating the results according to the route of administration, exposure duration and doses of the drug. It is also possible to transpose the model to other species or to study the inter-individual differences [40].

The advantages of these *in silico* models are the speed and the low cost procedures. However, their reliability rely on the quality of the data obtained from the experiments on which they are based.

In vitro models

The *in vitro* models correspond to the use of organism's components like tissues, cells or molecules, out of their biological context. The aim of these models is to obtain first biological responses and to extrapolate them to Humans, representing thus a predictive power. Thus, *in vitro* models are more and more used for research but also for drug development and safety. In this way, during the last years, several *in vitro* liver models have been developed to study biotransformation pathways and to predict cell-drug interactions or hepatic toxicity [41]–[43]. Today, some of them are used in preclinical phase, and can present different degrees in complexity regarding both structure and functions.

The simplest *in vitro* models are the so-called liver fractions. They are obtained after centrifugations and can be used to study the biotranformation of drugs. Among them, human liver microsome contains vesicles of endoplasmic reticulum of hepatocytes. It thus contains almost only CYP and UGT enzymes. In the same way, Human liver cytosol contains enzymes but from phase II: NAT, GST and SULT. Human liver S9 fraction is composed of both microsomal and cytosolic fractions. It is therefore useful to study the entire biotransformation pathway by the production of metabolites by phase I or II and also the combination of both.

Another possible *in vitro* model is the cell culture. The use of liver cell lines or primary hepatocytes allow having a view at the cellular level and so more complete than the previous ones. The cell lines are by their nature available in large quantities but lack of some metabolic enzymes. On the contrary, the primary hepatocytes have a strong resemblance with *in vivo* human liver but are difficult to culture.

To have an overall view, liver slices or isolated perfused liver can be used by keeping intact the cellular tissue architecture. The first method is performed thanks to high-precision tissue slicers that allows producing slices of a few hundred micrometers. The perfusion of liver is a more complicated model and performed only with animal livers.

The table 1.3 summarizes the *in vitro* liver-based models. The choice of the method is determined by the question to be answered. It is thus usual to use different *in vitro* models to assess the safety of a drug.

Model system	Advantages	Disadvantages
Human liver microsomes	- Low cost - Simplicity in use - Study of interindividual variations	- Unsuitable for quantitative measurements - Only CYP and UGT enzymes
Human liver cytosol	- Biotransformation study of NAT, SULT and GST enzymes - High enzyme activity - Study of interindividual variations	- No CYP and UGT enzymes
Human liver S9	- Contain phase I and II enzymes - Study of interindividual variations	- Lower enzyme activity than in microsomes and cytosol
2D culture of liver cell lines	- Easy to culture - Stable enzyme expression levels - Unlimited amount of cells available	- Lack of phenotypic characteristics - Low phase I and II enzymes expression level - Difficulty of metabolites detection
2D culture of primary hepatocytes	- Well established and characterized - Cryopreservation possible - Phase I and II enzymes - Drug transporters present - Enzyme inducible	- Isolation complicated and time consuming - Cell damage during isolation - Lack of non hepatocyte cells - Interindividual variation
Liver slices	- Intact cellular tissue architecture and interactions - Morphological studies possible - All cell types	- Inadequate penetration of the medium - Damaged cells on the edges - Short viability time - Expensive equipment
Isolated perfused liver	- Best representation of *in vivo* situation - Possibility to collect and analyze bile - 3D architecture - All cell types	- No human liver available - Labor intensive - Poor reproductibility - Really short functional integrity

TABLE 1.3: Summary of commonly used *in vitro* hepatotoxicity model systems [41]–[43].

Around the world, specific organizations were created to evaluate, validate and

coordinate the implementation of these alternative methods. The European Centre for the Validation of Alternative Methods (ECVAM) in Europe and the Interagency Coordinating Committee on the Validation of Alternative Methods (ICCVAM) in the USA are the organisms that coordinate the evaluation of alternative methods and promote them. Today, several alternative methods are approved and commonly used in preclinical phase, in particular for the eye irritation and the hepatotoxicity [44]. They can be used as partial or complete replacements for animal experiments. If an alternative method exists for the question to be answered, it is mandatory to use it. However, the approved alternative methods remain few, do not concern all organs and are restricted to some tests.

Although some *in vitro* liver models exist and were approved, they have short integrity or they cannot fully perform liver-specific functions, limiting their relevance especially in predictive toxicology. Indeed, the use of hepatocytes *in vitro* presents major limitations: the cells are generally grown on 2D surfaces and in static conditions, which are very far from their physiological context. This results in the partial or total loss of the structure and functions they normally present in the organism, in particular regarding the biotransformation pathways. The limitation of these models implies a limitation of predictive studies for pharmaceutical industries. The toxicity and lack of efficacy of drug candidates are thus detected late, during the clinical phase, resulting in a high attrition rate. It is therefore necessary to develop new *in vitro* models closer to the physiological conditions of the liver. To overcome this, tissue engineering is a promising way. This field aims at developing biological substitutes of tissues or organs for *in vitro* studies or *in vivo* implantation by combining engineering methods and cell culture. It allows getting closer to an environment that mimics the *in vivo* conditions and so to the *in vivo* behavior of cells.

Chapter 2

Current research on tissue engineered liver models

As stated in the first chapter, understanding the physiological and pathological processes in this complex organ is limited with the 2D classical *in vitro* liver models. These knowledge appear nevertheless mandatory to improve drug development strategy and to avoid facing attrition in the latest stages for apparently promising molecules. Considering these limitations, research has recently focused on the design and validation of new *in vitro* liver models involving different cell types and innovative culture methods to get closer to the *in vivo* environment. They rely on tissue engineering, a quite recent interdisciplinary field, as defined by Langer and Vacanti in 1993 " Tissue engineering applies the principles of biology and engineering to the development of functional substitutes". First introduced to replace damaged tissues, tissue engineering is now a recognized tool in cell biology and finds applications in predictive toxicology. Primary cells, cell lines, stem cells but also co-cultures of different liver cell types are used as biological components. Engineering is dedicated to the design of novel cultures methods, 2D planar cultures in sandwiches or micropatterned surfaces, but also 3D cultures as spheroids, in tuned scaffolds, after bioprinting or in perfusion systems. More recently, the advantages in microfluidics and microfabrication led to the design of specific perfused microsystems, called " microchips", also known as "biochips" or "organ on chips", that attempt to mimic the sinusoid architecture of the liver.

2.1 Cells

Three major hepatocytes'sources are currently available for tissue engineered liver: primary cells, cell lines and pluripotent stem cell (embryonic, adult or induced). They present pros and cons depending on the type of model developed and its application (Table 2.1). Morever, hepatocytes can be cultured alone or with non-parenchymal cells to reproduce the complexity of the liver, as seen in the previous chapter.

2.1.1 Primary cells

Primary cells are considered today as the most relevant for *in vitro* models since they come directly from the liver. They can be of human or animal origin.

Primary human hepatocytes (PHH) are usually obtained after human liver biopsies or from non-transplantable organs. The hepatic tissues are treated with collagenase and centrifuged to isolate hepatocytes which can be used fresh or cryopreserved. They contain all the cellular machinery and are therefore considered as the gold standard for xenobiotic metabolism and toxicity studies. They exhibit many liver characteristics such as phase I and II enzyme activities, metabolic activities such as albumin synthesis and ammonia detoxification. In 2D *in vitro* culture, hepatocyte's phenotype cannot be maintained longer than 72 h, which does not make them suitable for mid/long term studies [45], [46]. However, PHH are very sensitive to culture methods and it has been shown that hepatic functions can be maintained for a longer period of time if cultured in a suitable environment. An appropriate media formulation, the use of matrices, the contact with a flow, the growth with other cell types help to reduce the loss of hepatic functions [47]. Despite their important functional features, primary hepatocytes present several limits that cannot be neglected. Once isolated, they rapidly lose their liver-specific functions, phenotype and polarization making them unsuitable for long-term studies. Moreover, their inability to proliferate *in vitro*, associated to a limited availability and high costs have to be taken into account. In addition, the donors' variability and their collection from liver disease patients potentially treated with drugs, result in a large variation of cell responses.

Primary hepatocytes from rats and mice are also employed in the pharmaceutical industry. Like PHH, they exhibit many liver characteristics such as metabolic and xenobiotic activities. Moreover, animal hepatocytes are more easily available and less expensive than PHH. However, due to interspecies differences, the variations in metabolism between humans and animals impact relevance of these *in vitro* liver models as it does *in vivo* [34].

2.1.2 Cell lines

A cell line is a cell population, homogeneous and stable in time, which can infinitely divide making them immortal. They usually come from cancer cells taken from a patient that have subsequently undergone, if necessary, a mutation in the genes involved in the regulation of the cell cycle. They are well characterized, easy to handle and can be grown over extended periods. In addition, they are less expensive and easy available compared to PHH [48]. They preserve some hepatocyte's characteristics but present a lack or very low expression of some metabolic enzymes. The mutations they underwent to become immortal may also have altered some of their functions [49], [50]. Therefore, their use is limited for xenobiotic metabolism studies. In addition, although they divide infinitely, the expression of their genes changes during their successive divisions thus losing some of their characteristics. However, they remain a popular *in vitro* cell model. They provide higher reproducibility of results than those obtained with primary hepatocytes [51]. They are also interesting for a first evaluation of new cell culture devices.

Among the different liver cell lines, HepG2 is one of the most commonly used. It is derived from a human hepatocellular carcinoma and constitutes a well-characterized

hepatocyte cell line. These cells secrete liver plasma proteins such as albumin and can transform many xenobiotic compounds [51]. However, gene expression levels of enzymes, especially phase I, are lower than those of human hepatocytes making them inappropriate for pharmacokinetic studies [52]–[54]. These cells are still widely employed because of their metabolic stability, allowing a good reproducibility of results and long-term culture. One of the subclones of this cell line, called HepG2/C3A, has interesting properties such as high albumin production. HepG2 cell line is therefore not completely representative of PHH but because they are easier to maintain they are frequently used in various studies and offer an approximation of hepatic functions.

Another interesting cell line is HepaRG, a human bipotent progenitor cell line coming from a hepatocholangiocarcinoma. These cells can differentiate toward two different cell phenotypes: hepatocyte-like and cholangiocyte-like cells, using dimethyl sulfoxide (DMSO). These cells present similar characteristics to those of hepatocytes and biliary cells. They have been shown to express phase I and II enzymes and to secrete liver plasma proteins [51], [55]. Therefore they represent a valuable alternative to PHH for drug metabolism and xenobiotic toxicity studies since they retain a correct enzymatic activity while possessing the proliferative capacities of cell lines [56], [57]. However, the use of DMSO and the long culture process are disadvantages that have to be taken into account when developing a new model with these cells.

2.1.3 Stem cells

Stem cell derived hepatocytes represent a new alternative of liver cell source. Stem cells come from embryos, fetuses, umbilical cords or individuals. They are nevertheless difficult to collect and can face ethical issues. Only induced pluripotent stem cells (iPSCs) are mentioned here. They can be obtained from somatic cells following protocols initially described by Yamanaka [58]. Like other pluripotent stem cells, they can be maintained in undifferentiated states or differenciated into several cell types including hepatocytes [59]. Therefore, they could provide a limitless supply of hepatocytes. They present many hepatocytes features like morphology and functions including drug metabolism and albumin secretion. However, it seems that their differentiation into mature hepatocyte-like cells is not complete since they express lower levels of enzyme activity and hepatic gene expression than PHH [60], [61]. Progress in differentiation protocols and cell culture have shown to provide more functional hepatocytes [62]. Therefore, iPSC represent a promising source for toxicity assessment and drug metabolism studies [63]. Nevertheless, the culture of stem cells is expensive, time-consuming and difficult due to their high sensitivity.

2.1.4 Co-cultures

In order to obtain an *in vitro* liver model as close as possible to the *in vivo* situation, addition of NPC to hepatocytes is essential. Although these cell types do not represent the

Cell Type	Advantages	Limitations
Primary hepatocytes (human, rat)	Liver intrinsic characteristics, including phase I and II metabolic enzyme activity, glucose metabolism, ammonia, detoxification	Losing liver specific function; unsuitable for long-term; high cost; donor variation, difficult isolation
Hepatic-derived cell lines (HepG2, HepaRG)	Unlimited lifespan; easily manipulated; stable phenotype; essential for drug metabolism and toxicity response	Drug reaction are inaccurate; low metabolic competence and rapid loss of expression of liver-specific enzymes/transporters
iPSCs derived hepatcocytes	A stable source of hepatocytes; liver organoid; stable functions including albumin secretion, liver-specific gene expression, urea production and metabolic activity	Hardly manipulated; required specific induce factor; high cost; insufficient maturate

TABLE 2.1: Advantages and limitations of cell types used in *in vitro* liver models [64].

functional part of the liver, they play a key role in hepatocyte responses due to the release of an array of inflammatory mediators, growth factors, and reactive oxygen species [65], [66]. It has been shown that co-cultures of liver cells improve functions of hepatocytes, increase their sensitivity to drugs and their longevity [67]. In particular, LSEC have shown to increase and maintain phase I enzyme activity, whether with primary cells or cell lines [68], [69]. Kupffer cells influence hepatocyte function in response to an inflammatory stimulus and can respond to hepatocyte stress and damage from hepatotoxins leading to side effects associated with DILI [70], [71]. Hepatic stellate cells have an important role in cellular communication between hepatocytes and LSEC which impacts on their morphology [72]. Therefore, there are several evidence that the addition of NPC in *in vitro* liver models can improve their structure, function and response, allowing to provide more predictive results to drug metabolism.

2.2 Engineering strategies

To overcome the poor viability and the reduction of major liver functions observed in classical 2D cultures, different approaches have been proposed: 2D culture models in more complex configuration than Petri dish, 3D culture models to reproduce 3D morphology and organization of cells *in vivo* but also perfused systems to mimic the high vascularization of the liver. They allow culturing cells in specific environments that get closer to the *in vivo* conditions. The main approaches are detailed below.

2.2.1 Micropatterning

The photolithography process used in microelectronics industry for microfabrication is interesting for biology since it allows the production of micrometric structures. This method has therefore been adapted to perform cell patterning [73]. A substrate coated with photoresist is irradiated through a stencil-like photomask possessing the geometrical pattern to be transferred. Solvent is then used to wash the unpolymerized photoresist, revealing the pattern on the substrate. Silane chemistry is then performed to allow cell adhesion on the pattern. A similar result can be obtained by soft lithography: the microfabrication process is used to design a patterned soft material, usually polydimethylsiloxane (PDMS), which is then employed as a stamp or mask to pattern a substrate with cell-adhesive proteins (Fig. 2.1) [74], [75]. These methods allow culturing one or two cell types in a specific spatial organization.

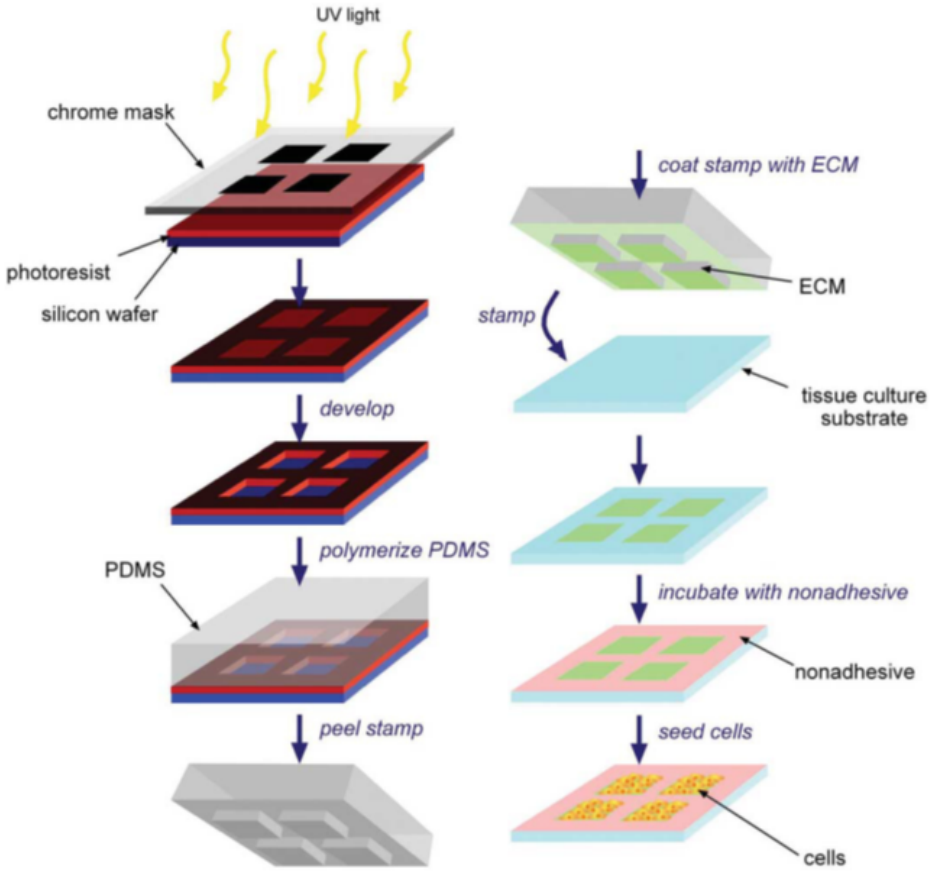

FIGURE 2.1: Schematic of micropatterning process. PDMS stamps are generated by photolithography (left column) and, using these stamps, ECM proteins are printed onto tissue-culture substrates upon which cells are seeded [74].

Micropatterning is mostly used to study cell-cell interactions. Co-cultures of primary hepatocytes with fibroblasts leads to improved hepatocyte functions, such as albumin and urea synthesis, compared to hepatocytes cultured alone and depend on the

configuration of the micropatterned areas and on the cells ratio [76]–[78]. Hepatocytes retain also phase I and II metabolism, canalicular transport and sensitivity to hepatotoxic compounds for several weeks [79]. In the same way, co-culture of primary hepatocytes and Kupffer cells improves hepatic cell functionalities [80]. IPSCs derived hepatocytes can also be used in micropatterned cell cultures and show results similar to PHH [81].

Micropatterned cell culture allows miniaturizing tissues, controlling cell-cell interactions and improving hepatocyte functionality. Moreover, it offers the possibility to study drug metabolism [82]. Despite these interesting features, the micropatterning method quickly finds its limits. The cells are patterned on flat surfaces leading to 2D monolayers formation that is far from the *in vivo* conditions. Moreover, the precise seeding of the second cell type is difficult as some cells could adhere on the first cell type.

2.2.2 Sandwich and layer-by-layer

The sandwich configuration consists in culturing cells, usually primary hepatocytes, between two layers of gel composed of proteins from the ECM such as collagen or Matrigel^{TM}. This method mimics the general organization of cells that are in rows in the hepatic lobules and thus allows reducing cytoskeletal changes and stabilizing cell-cell contacts.

This technique results in improved hepatocytes characteristics: it has been shown that sandwich cultures promote the development of bile canaliculi and the polygonal shape usually observed *in vivo* with cellular polarization [83], [84]. Moreover, it keeps hepatocytes functionality: phase I and II enzymes are preserved and respond to drugs induction for several weeks [85], [86]. It also enables to maintain polarized cells with functional basolateral and apical domains that mediate cell uptake and biliary efflux [45], [87]. For hepatocytes and endothelial cells co-cultures, two sandwiches, one above the other, can be made. This configuration reproduces the physical separation between the two cell types normally performed by the space of Disse [88] (Fig. 2.2 **A**).

To go further, a similar approach, known as layer-by-layer, has been developed consisting in stacking layers of cells and matrix alternately. To do so, thermally responsive polymers, such as poly(N-isopropylacrylamide), are used: they are hydrophobic at 37 °C allowing cell adhesion and growth but become hydrophilic at 20 °C permitting the detachment of cell sheets when confluence is reached [89], [90]. Patterned cell sheets are created on thermally responsive surface, detached by decreasing the temperature and transferred on another monolayer with a gelatin-coated manipulator [91] (Fig. 2.2 **B**). In the same way as sandwich cultures, hepatocyte specific functions were improved with this method.

The characteristics of sandwich culture make it an interesting model for hepatotoxicity and hepatobiliary drug transport studies [92]. Moreover, layer-by-layer technique offer the possibility to perform co-cultures and to assemble as many layers as desired. However, cell functions are only stable for short duration, therefore long-term hepatotoxicity assessments is generally limited and expression of the genes responsible for many liver-specific functions decreases over time [93]. In addition, hepatocytes are sensitive

to variation of ECM layers leading to variation in outcomes and the number of layers is limited by oxygen and nutrients diffusion.

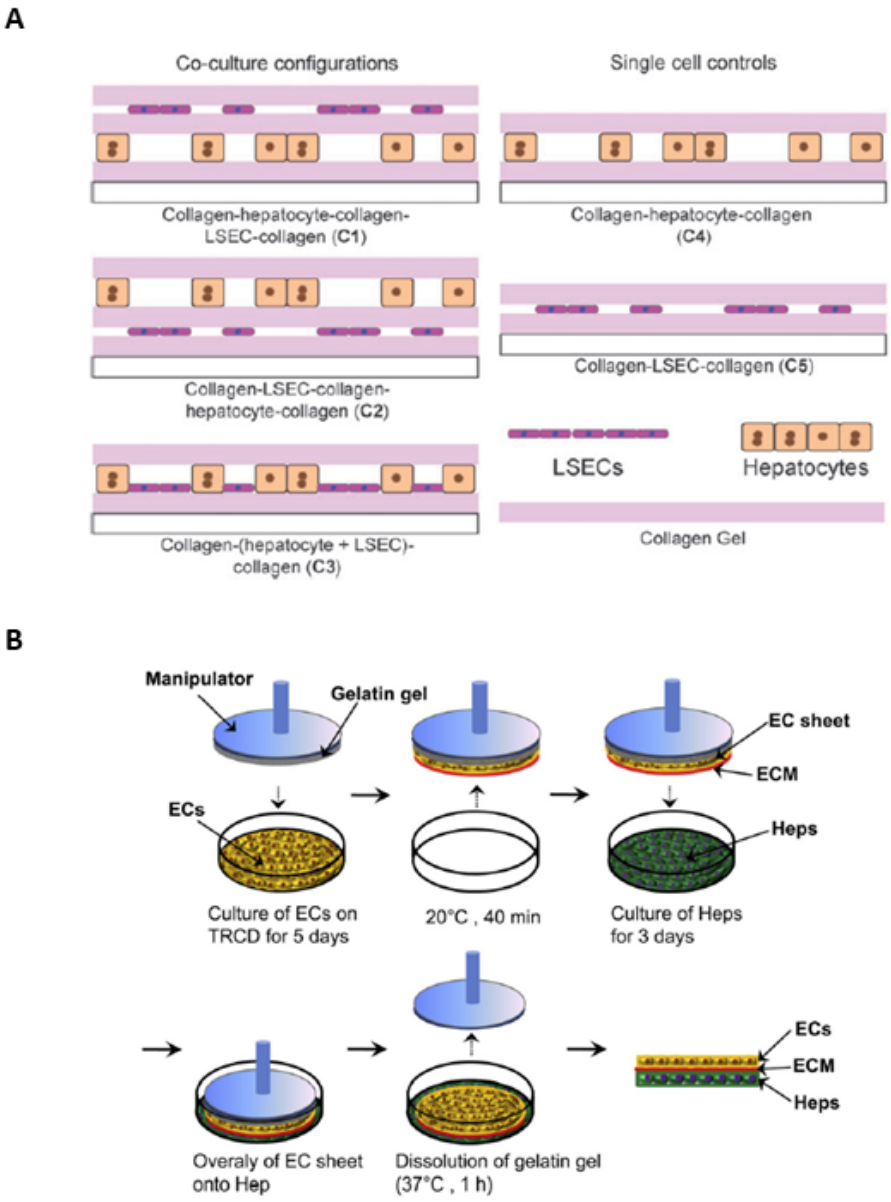

FIGURE 2.2: Schematic illustrations of sandwich and layer-by-layer cell culture method. (**A**) Hepatocytes and liver sinusoidal endothelial cells (LSEC) coculture configurations in sandwich collagen gel [88]. (**B**) Hepatocytes (Heps) and endothelial cells (ECs) layer-by-layer procedure with temperature responsive culture dish (TRCD) [91].

2.2.3 Spheroids and beads

The hepatic cells can be cultured as aggregates, called also spheroids, with a size of about 200 μm in diameter. They can be generated using primary cells, cell lines or stem cell derived hepatocyte-like cells. Different methods such as hanging drop or culture plastic wares with non adhesive surface have been developed to aggregate cells [94], [95]. The hanging drop technique consists in depositing drops of medium containing hepatic cells onto the underside of the lid of a Petri dish. When the lid is inverted, the drops stay by surface tension and gravity concentrates the cells forming thus spheroids. Spheroids can also be formed by seeding cells in wells made of non adhesive plastic or coated with agarose films or hydrophobic polymers. As they cannot attach on the surface, cells spontaneously form spheroids after a few days. This technique can be performed under static or rotating conditions.

The culture in spheroids exhibits several beneficial features. It promotes cell-cell interactions leading to morphological characteristics of well differentiated hepatocytes. Cell polarity and structures similar to bile canaliculi can be observed [96], [97]. Besides maintaining cellular phenotypes, spheroid culture improves viability, especially for PHH, and functionality compared to classical cultures in monolayers or suspensions. The phase I and II enzymes of xenobiotic metabolism are maintained for culture periods of several weeks [98]. When cultured in dynamic conditions like in bioreactors, nutrient and oxygen exchanges are optimized improving liver-specific-functions [99]. Therefore, spheroid culture is a promising method for *in vitro* liver model to study liver functions but also drug biotransformation and DILI.

Hepatocyte culture in aggregates can also be carried out in beads. For this, cells are encapsulated in matrices that allow oxygen and nutrients to pass through, such as alginate. Within these beads, cells form aggregates enhancing viability and functionality in the same way as spheroids described previously [100], [101]. One of the advantages of this method is the possibility to cryopreserve encapsulated hepatocytes for several months and preserve their hepatic functions once unfrozen [102], [103]. This method is particularly interesting for cell transplantation [104].

Although spheroids exhibit several beneficial features, their size is difficult to homogenize and has to be limited: necrosis can occur in the center of spheroids bigger than 200 μm due to lack of oxygen and nutrients. Moreover, although their organization allows them to retain part of their phenotype, it is non-representative of the *in vivo* one since cells are randomly distributed [94].

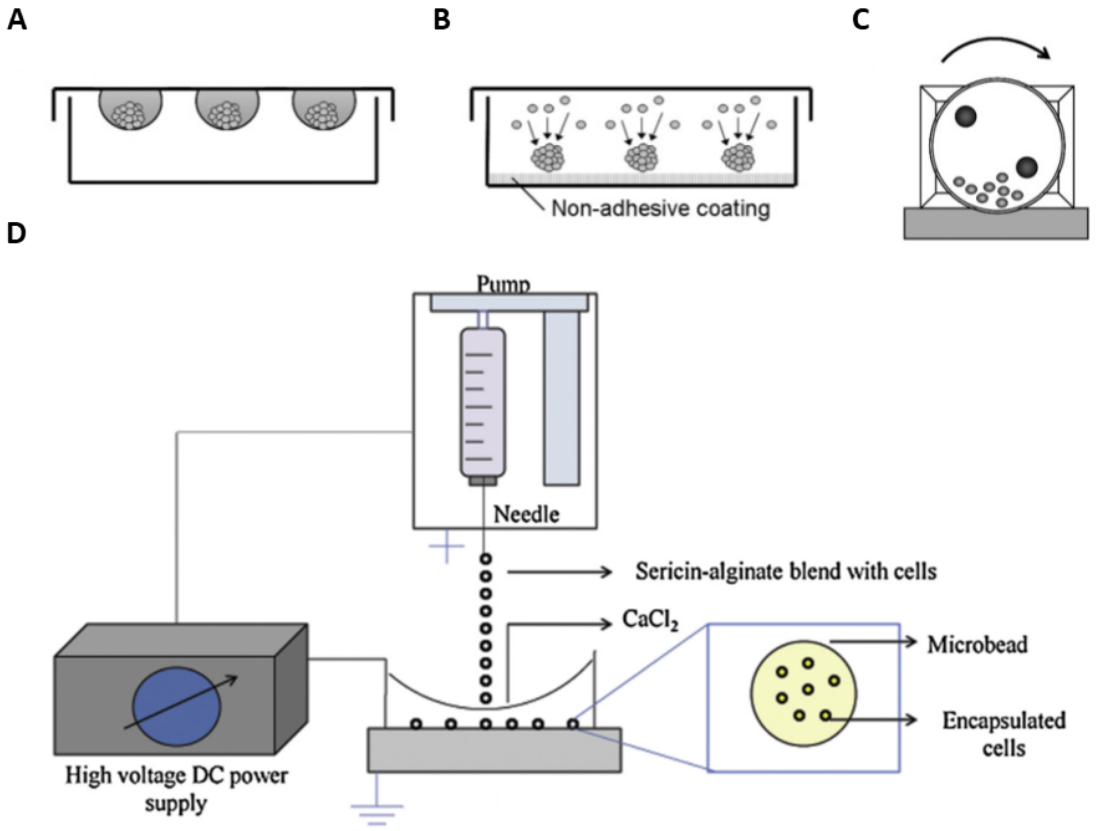

FIGURE 2.3: Schematic of spheroids generation methods. (**A**) Hanging drop, (**B**) cell culture on non-adhesive surface, (**C**) rotary cell culture system and (**D**) cell encapsulation in alginate beads. Adapted from [94], [100].

2.2.4 Polymer based scaffolds

In a similar way as beads, scaffold-based models were developed to provide structural support to cells. More than a passive scaffold, these structures attempt to mimic the ECM and thus can play a major role in cell phenotype which depends on the microenvironment [105].

Scaffold-based systems consist in seeding cells on 3D matrix composed of natural or synthetic materials. On the one hand, natural substrates such as collagen, fibrin or hyaluronic acid ensure biocompatibility and cell-matrix interactions. On the other hand, synthetic ones such as poly(vinyl alcohol) or poly(ethylene glycol) offer more reproducibility between batches since they are synthesized. They are rather inert but can be coated or functionalized with ECM proteins. These polymers are cross-linked to form hydrogels, a 3D network that enables high water content, that are mainly used in tissue engineering as they mimic the mechanical properties of soft tissues [106]–[108]. PHH or hepatic cell lines cultured in scaffolds composed of one or several polymers sustain their metabolism such as albumin synthesis, urea secretion, CYP activity [109], [110]. However, cultures are limited by medium diffusion since hydrogels exhibit nanoporous structure which does not foster medium circulation.

Macroporous hydrogels have thus been developed in response to such limitation: they exhibit interconnected porous network and large pore size. Different methods can be used to obtain them such as freeze-drying, porogens leaching, gas foaming and cryogelling (Fig. 2.4) [111]. Freeze-drying process consists in successive freezing and drying stages of already cross-linked hydrogel. The formation of pores can also be made during the polymer cross-linking by the presence of particles, gas or ice crystals that are eliminated after. The most common used methods are freeze-drying and cryogelling since they avoid the need for porogen removal and their pore size is tunable by freezing temperature [112], [113]. Similar results to those of hydrogels were observed [114]–[116]. Moreover, macroporous hydrogels allow uniform spatial cell distribution and cell migration.

Despite the advantages of scaffold-based culture, it lacks of reproducibility since the methods used create pores with random shape and spatial distribution. In addition, the bulk and local mechanical properties have important impact on cell behaviour and thus must be measured and tuned.

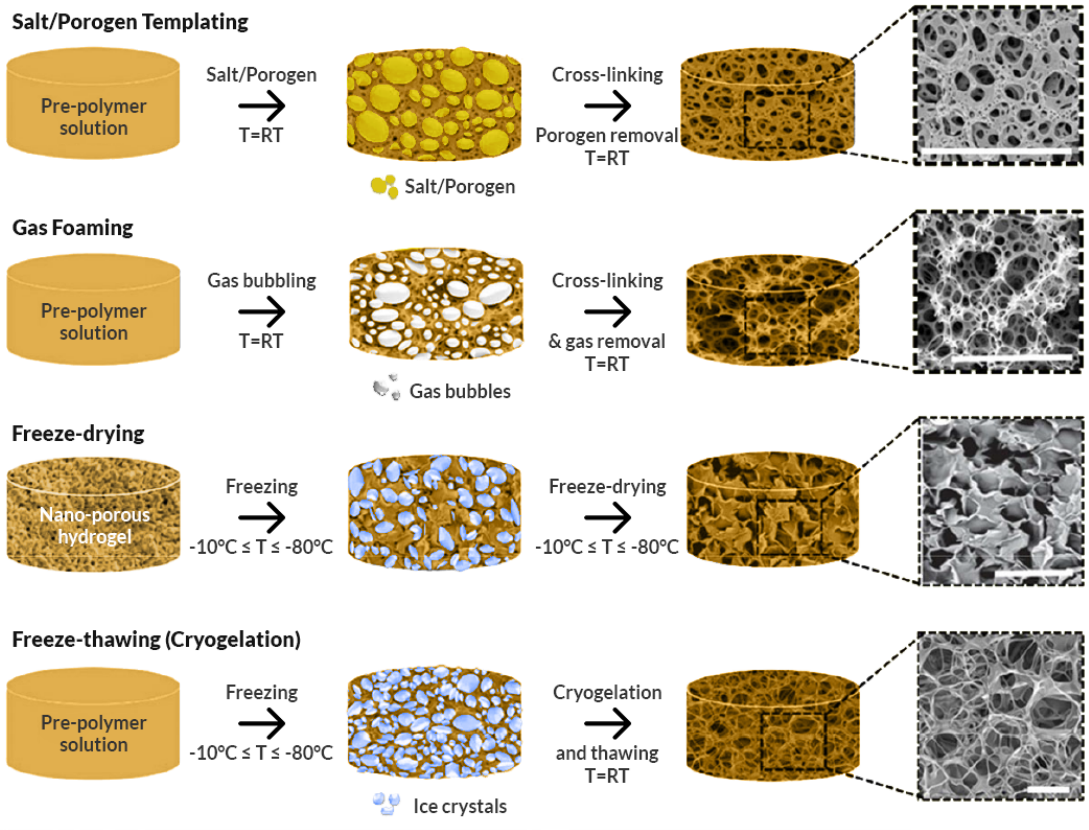

FIGURE 2.4: Various techniques and their respective successive steps for the fabrication of macroporous hydrogels. Scale bar = 100 μm. Adapted from [111].

2.2.5 Bioprinting

The development of 3D printing technology had led to a new cell culture method: the bioprinting. This process consists in the fabrication of 3D structures using precise layer-by-layer deposition of biological materials, called bioink, with spatial control thanks to computer-aided manufacturing. It allows 3D cell culture within complex 3D biomimetic architectures. This technology is particularly interesting for organs with repetitive structures such as the liver [117].

The bioink is composed of cells and biomaterials. Natural polymers such as alginate, hyaluronic acid or gelatin are commonly used in liver bioimpression but synthetic ones are also used as they offer more tunable mechanical properties such as polyethylene glycol [118]. They can also be used in different combinations to respond to needs. Indeed, the bioink must meet several criteria including biocompatibility, liver-close structural and mechanical properties but also printability [119]. The main methods used in 3D bioprinting are inkjet, extrusion and laser-assisted bioprinting [120]–[122] (Fig. 2.5). The first one produces bioink droplets by thermal or acoustic mechanism whereas the extrusion method consists in producing continuous bioink filament by pressure systems. The last one is more complex as the bioink is deposited after laser pulse on bioink layer.

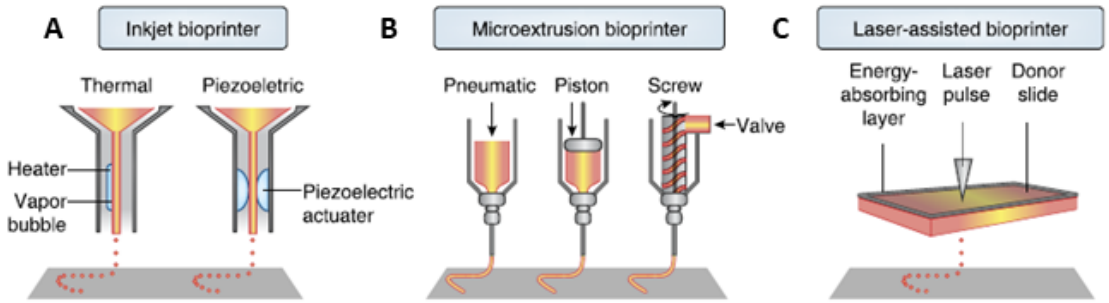

FIGURE 2.5: Bioprinting techniques. (**A**) Inkjet, (**B**) microextrusion and (**C**) laser-assisted bioprinting [120].

Different studies showed that 3D bioprinting improves functions and long-term culture of primary hepatocytes. Albumin expression as well as drug-induced enzyme activity were found to be higher over several weeks in bioprinted cultures than 2D cultures [123], [124]. Moreover, iPSCs have been successfully printed during their differentiation process into hepatocytes and were found to be viable and express hepatic markers for several weeks [125]. When printed with non-parenchymal cells, phenotypic and functional enhancements have been observed in particular morphological organization, product secretion and liver-specific gene expression [126].

In addition to enhanced cellular response, 3D bioprinting is a promising technology thanks to correct spatial resolution, reproducibility and design flexibility. It allows printing structures with high complexity, approximating thus tissue composition, both in cell types and architecture. However, it requires a high amount of cells, which should be able to survive under shear stress caused by the bioprinting process. Moreover, it

is difficult to obtain mechanical properties of printed liver consistent with the ones of the native liver. In addition, in order to overcome size limitations, sufficient vascularization must be ensured for long-term viability. Such technology is still at its premises, and would request additional work on the above mentioned elements before producing complex organs or tissues.

2.2.6 Perfusion systems

Although the previous methods allow the maintenance of hepatic phenotypes and functionality, they fail in ensuring perfusion of the culture medium. As a result, the poor diffusion-based oxygen supply limits the size of the engineered tissue. Hemodynamics and shear stress have been shown to have important effects on hepatic functions [127], [128]. In addition, pharmacokinetics studies request to deliver the dose of substances following specific concentrations profiles. Therefore, systems providing perfusion, known as bioreactors, have been developed to support liver function [129] but also to provide continuously nutrients and oxygen to cells.

Among the various bioreactors, membrane-based and entrapment-based systems are commonly used. The first one is composed of hollow fibers made of semipermeable membranes which acts both as a selective barrier for biological molecule and as a scaffold for cell attachment. The hepatocytes can be located either in the lumen or in the extraluminal space, cell culture medium flowing in the cell-free space (Fig. 2.6). The entrapment-based system consists in encapsulating spheroids in semi-permeable beads which are then inserted in a column and exposed to perfusion. Both of these bioreactors promote cell viability and function [130], [131]. Primary hepatocytes are generally used but can be replaced by IPS cells which exhibit cell maturation and maintain hepatocytes features such as cell morphology but also phase I and II enzymes and functional genes comparable to PHH [132], [133]. Although these bioreactors are today mainly intended as extracorporeal supply for acute liver failure patients, they can also become relevant *in vitro* models when scaled down [134].

The development of microfabrication and microfluidic technologies at the end of the 20th century has provided another perfusion system to culture cells called microchips or biochips. A silicon substrate mold is etched by photolithography to obtain microstructures such as microchannels and recovered by a liquid polymer. Once the polymer cross-linked, it is demolded and laminated with another piece of polymer or glass slide to generate a closed microchip which is then perfused. Polydimethylsiloxane (PDMS) is the most commonly used polymer as it gathers several advantages: biocompatibility, optical transparency, high oxygen permeability and low cost. An interesting feature of microchips is the wide possibilities of microstructuration, therefore different designs are deployed such as microchannels [135] or microchambers [136], [137] with tangential flow. More complex designs mimicking the sinusoidal organization have also been studied [138]. Primary hepatocytes cultured in these models have shown not only the maintaining of viability and functions but also the correlation between *in vitro* and *in vivo* toxicity data demonstrating the potential use of these devices for drug testing [138], [139].

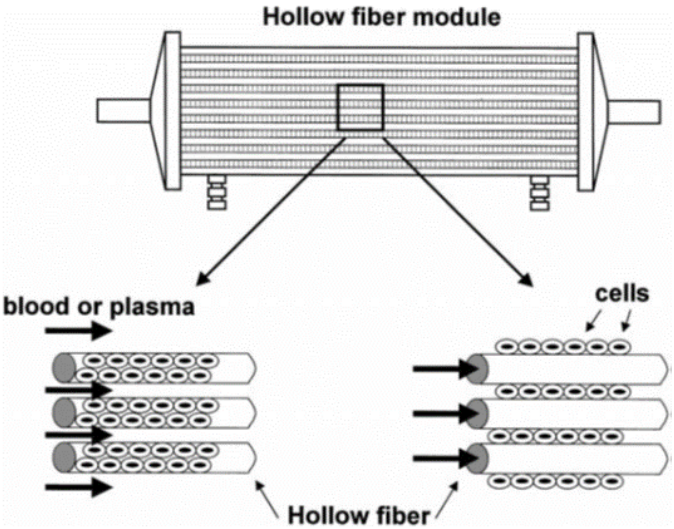

FIGURE 2.6: Schematic representation of hollow fiber [131].

In addition to flow environment, microchips represent an essential step in research thanks to their several advantages: low cost, well defined microenvironment with controlled geometry, adjustable flow rate, use of minimal cells and reagents. Moreover, the promising results obtained for cell cultures within microchips have led to a significant amount of research. The microchips have been enhanced and a new approach has emerged: the organ-on-chip.

The different cell culture strategies described here are summarized in the following table 2.2.

2.3 Liver on chip

Cell culture in microchips has shown overall enhancement in hepatocyte viability and functionality. Thus, more complex microfluidics systems have been built and combined with some of the promising cell culture methods previously described to develop liver-on-chip. These models can bring together some *in vivo* tissue structures, functions, biochemical cues and mechanical environment. Among the large variety of microchips developed up to now, only the most representative ones are described below.

2.3.1 Liver on chip sandwich and layer-by-layer

Sandwich cultures can be combined with a perfusion system in order to add flow to the spatial organization in hepatic rows.

Sandwich culture can be integrated in microchips where a laminar flow immediately overlay the cells [140]. The results show that primary hepatocytes are more sensitive and consistent over time than in static culture. To get closer to the *in vivo* conditions where the hepatocytes are not in direct contact with the blood circulation, microfluidic

Strategies	Advantages	Disadvantages
Micropatterning	- Co-cultures with spatial organization - Improvement of hepatocyte functions - Study of cell-cell interactions	- 2D cultures - Cell seeding precision
Sandwich and layer-by-layer	- Co-cultures assembly - Improvement of hepatocyte functions - Study of hepatobiliary drug transport	- Short duration of cell functions - Impact of ECM layers variations on cells
Spheroids and beads	- 3D cell organization - Cell-cell interactions - Improvement of hepatocyte viability and functions - Maintenance of cell phenotype	- Spheroid size limitation and variations - Random distribution
Polymer based scaffold	- 3D structural support - Improvement of hepatocyte functions	- Lack of reproducibility - Impact of mechanical properties on cells
Bioprinting	- 3D organization - Improvement of hepatocyte functions - Reproducibility - Design flexibility	- High amount of cells - Shear stress during printing - Size limitations if no vascularization - Difficulty to control mechanical properties
Perfusion systems	- Continuous oxygen and nutrients supply - Cell viability and function promotion	- Non specific binding of molecules to materials - Perfusion systems required

TABLE 2.2: Summary of engineering strategies to develop *in vitro* liver models.

devices with membrane have been developed. The microchips are composed of two compartments separated by a porous membrane: the lower one with the cell sandwich and the upper one where the culture medium circulates [141] (Fig. 2.7). Moreover, endothelial cells can be seeded in the top of the membrane to mimic the liver sinusoid [142]. The cultures are maintained for several weeks and the hepatocytes cultured under flow exhibit higher albumin synthesis, urea secretion and CYP activity compared to static cultures. Moreover, hepatocytes show a well-connected cellular network with formation of bile canaliculi. In addition to medium cell culture flow, mimicking the blood circulation, some microchips are equipped with a second channel under the cell culture area and in

the opposite direction to mimic the bile flow [143].

Culturing cell sandwich in microchip allows performing culture under flow which increases the hepatic cell function and extend the cell viability over time. The membrane protect the cells from shear stress but at high flow rate, reduced albumin and urea secretion have been observed [141].

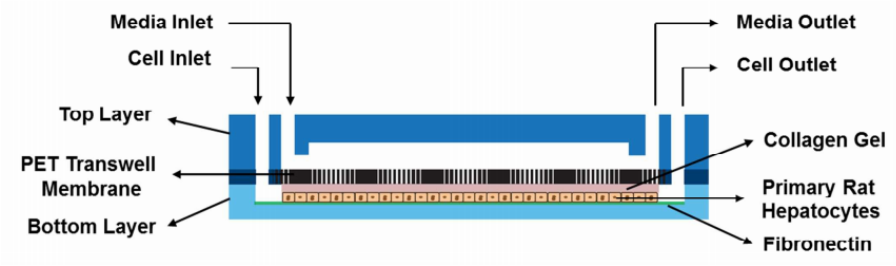

FIGURE 2.7: Cross-sectional view of microfluidic device with hepatocytes in sandwich configuration [141].

2.3.2 Liver on chip with 3D spheroids

Since spheroids are interesting structures to maintain hepatocytes *in vitro*, culturing them in microchips have been implemented. This requests to adapt the microchip design, to avoid them to be swept out of the device with the flow.

To culture spheroids already formed in microchip, they are generally introduced in specific chambers or microchannels that are continuously perfused. However, spheroid retrieval and transfer in microchip is laborious, it is therefore preferable to form the spheroids directly in the microchip. Such method is not widely used except for some co-cultures of different organs such as liver spheroids with pancreatic microtissues [144].

The formation of spheroids inside microchips is easy and is mainly performed with emulsion-based techniques and microwells or U-shaped microstructures (Fig. 2.8) [145]. The first technique consists in encapsulating cells in oil or hydrogel by generating emulsion droplets which are then trapped in wells for culture. Another method is the introduction of a cell suspension in a microchip containing wells. After several minutes, cells deposit on wells bottom and the excess of cells is rinsed out of the microchip by the flow. The trapped cells create spheroids that keep growing with a continuous supply of culture medium. In the same way, a U-shape microstructure can also be used to trap the suspended cells.

Hepatocyte spheroid culture in microchip present a high cell viability in dynamic conditions in microchip compared to static conditions after several days of culture [146]. Moreover, they exhibit more hepatocyte-specific characteristics according to gene expression profiles in dynamic conditions [147].

In addition to improved hepatic functions, spheroid-based liver on chip provides size control. However, the capacity to retrieve the cultured spheroids is limited or even

impossible: a high flow rates can be applied but can affect cell viability. Moreover, it is not adapted to high-throughput screening as a large number of microwells is needed.

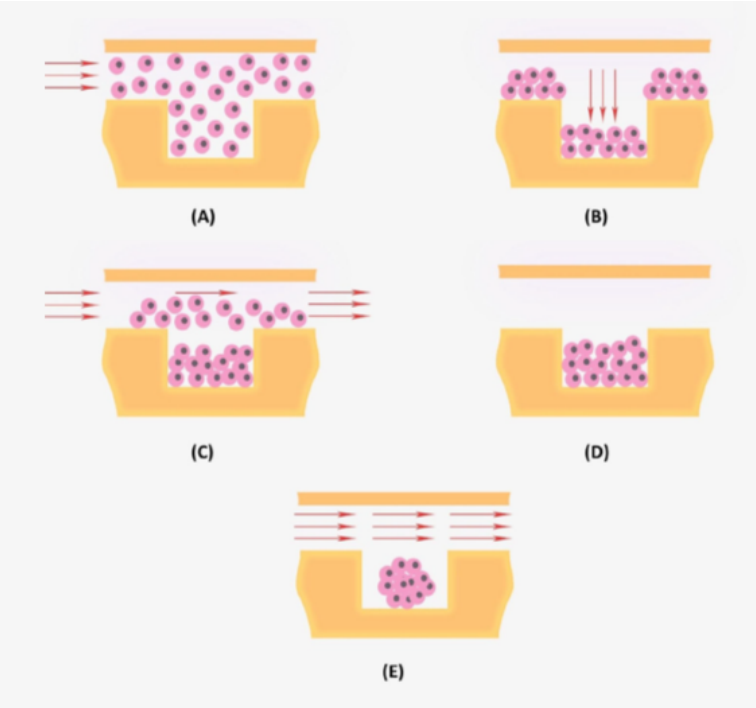

FIGURE 2.8: Spheroid formation process in a microwell-based microchip: (**A**) Introduction of a cell suspension. (**B**) Cell deposition. (**C**) Culture medium flows through the microchip. (**D**) Spheroid formation (**E**) Spheroid culture under a perfusing flow [145].

2.3.3 Liver on chip 3D bioprinting

Liver on chip based bioprinting gather the previous approaches as it is possible to print any culture design, whether sandwich, patterns or scaffolds [148]. Using adapted bioink compositions, it is possible to print in microchip tissue constructs composed of several cell types and substrates which are heterogeneous, a key characteristic difficult to obtain in microfluidic systems.

Bioprinting cell structure directly on microchips is the most commonly used method. Once printed the cell structure is covered by PDMS layer to close the microchip [149] (Fig. 2.9). Some bioreactors can also be developed to keep a direct access to cells [150]. Cell viability and metabolic functions were maintained several weeks in perfusion culture and these systems have shown to be reliable for drug toxicity evaluation.

To go further, the microchip can be printed in the same way as cells in one-step fabrication [151]. Bioprinting the microchip along with cells allows perfect fitting and therefore avoids any leaks or non-perfused areas. It has been shown that albumin and urea liver functions were significantly enhanced on the liver on chip.

Combining microchips with 3D cell culture methods represents a new advance in engineered liver models. However, it seems that one strategy has not been yet tried without using bioprinting method: scaffold based liver on chip.

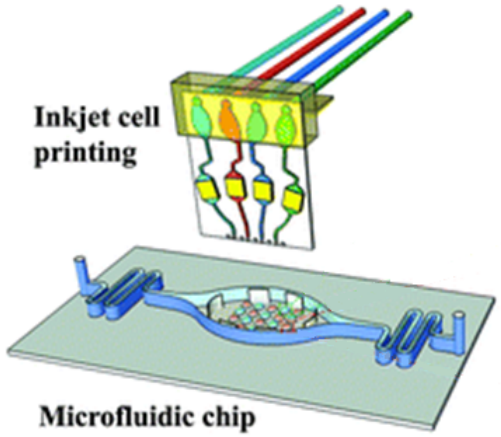

FIGURE 2.9: Inkjet bioprinting in a microchip [149].

The different liver on chips described here are summarized in the following table 2.3.

Strategies	Advantages	Disadvantages
Liver on chip sandwich and layer-by-layer	- Structure close to a sinusoid - Extended viability and functions compared to classic sandwich	- Few cells - Not adapted to high throughput
Liver on chip 3D spheroids	- Size control - Extended viability and functions compared to classic spheroids	- Not adapted to high throughput
Liver on chip 3D bioprinting	- Capacity to construct complex 3D structures - Possibility to use various cell types and biomaterials - Reliable for drug toxicity evaluation	- Printing accuracy - Properties of printed biomaterials limited

TABLE 2.3: Summary of liver on chip models.

2.4 Thesis project: a new generation of liver on chip

The two main approaches used in tissue engineering, 3D cell culture and perfused cell culture, have improved cells' functions of *in vitro* liver. In the BMBI laboratory, these approaches have also been explored. On the one hand, our lab pioneered the culture of hepatic cells in microchips, based on the previous achievements of Eric Leclerc in Fujii and

Sakai Lab (LIMMS/CNRS-IIS UMI 2820). With cell lines and primary cells, we demonstrated that genomic, proteomic and metabolomic responses were enhanced in terms of biotransformation compared to standard culture [152], [153]. On the other hand, the culture of liver cells in aggregates within alginate beads resulted also in an improvement of their functions [154]–[156].

Although these cell culture methods improved hepatic activities, they are still not satisfactory since cell functions remain partial. In order to accumulate the benefits of the 3D and perfused cell culture, new methods combining these two approaches should be explored. To our knowledge, such studies do not seem to have been done, except for the culture of spheroids in microchips. Therefore, the thesis project consists in developing a new *in vitro* liver model combining 3D cell culture and perfused cell culture to get closer to *in vivo* conditions. This model should improve the reliability of cell responses and therefore be used in pharmacology to predict any toxicity or lack of efficacy of drug candidates. Using the knowledge and skills present in the laboratory, we decided to use the microchip developed in our team in which an alginate cryogel is integrated.

2.4.1 Microchip used

The microchip is made in polydimethylsiloxane (PDMS), a silicon widely used for microfluidic devices and in particular those used for biomedical applications [157]. Indeed, this polymer is cheap, optically clear which allows microscopic observations, biocompatible and gas permeable ensuring cell gas exchanges. Although PDMS is inert, it is easy to coat with proteins to create interactions with cells. Moreover, a wide variety of microchip design can be created thanks to the easy PDMS molding process.

A first design of the microchip was made in 2004 and the final one was patented in 2010 [158]. The microchip is composed of 2 faces, corresponding to 2 different wafers. The lower face is microstructured at the inlet and outlet with microchannels to distribute homogeneously the cell culture medium, and microstructured between them with microchambers separated by microchannels to allow cell culture. It is composed of 15 rows composed themselves of 9 microchambers. The corresponding dimensions are shown in the figure 2.10. The upper face is not microstructured. The total height inside the microchip is around 200 μm, 100 μm depth for each face, the cell culture surface around 2 cm^2 and the volume about 40 μL. This design allows a uniform distribution of the cell culture medium, a reduction of the shear rate on the cells and a homogeneous distribution of the cells in the micro-chambers.

The microchip was used for hepatic cell cultures and showed encouraging results. First experiments with HepG2 showed, in addition to good attachment and proliferation, higher cell metabolism rates such as albumin production, glucose and glutamine consumption than in static condition [137], [159]. Moreover, transcriptomic analysis demonstrated that phase I and II enzymes were up-regulated [160]. The response to different drugs were also studied like acetaminophen [152], [161]. In the same way, investigations

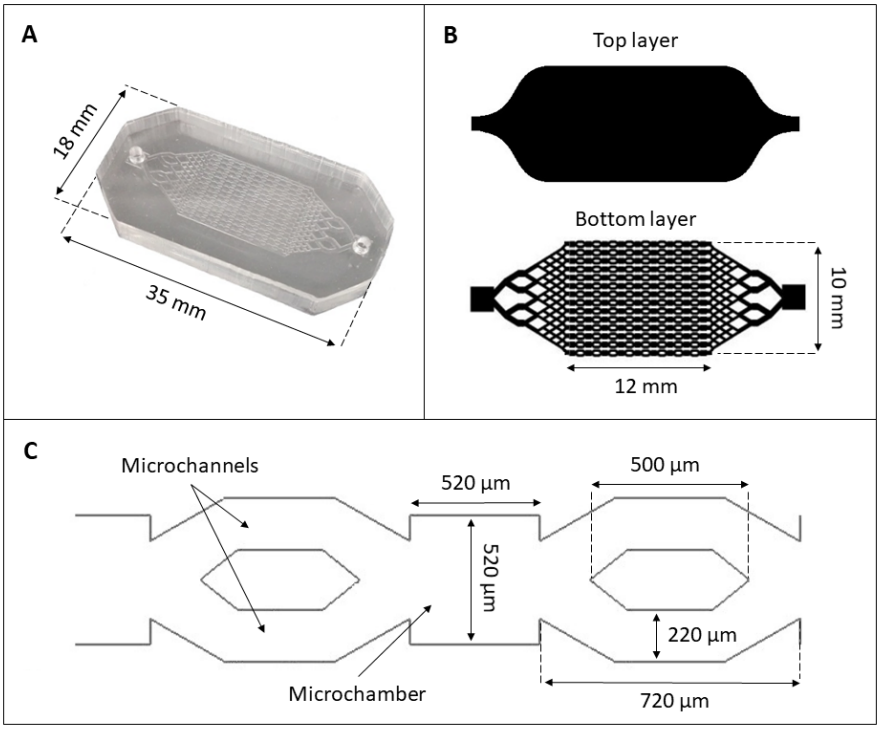

FIGURE 2.10: Microfluidic device. (**A**) Photo of a microchip. (**B**) Photomasks used to fabricate top and bottom layer molds. (**C**) Geometry and dimensions of the microstructured bottom layer.

on primary rat and human hepatocytes were performed. Studies on the biotransformation of different drugs and on the expression levels of genes involved in xenobiotic activity highlighted the higher functionality of cells [162]–[165].

2.4.2 Alginate cryogel as 3D scaffold

Alginate, a polysaccharide from brown algae, is widely used since several years in biomedical applications thanks to its physicochemical properties, biocompatibility and ease of gelation [166]–[168]. Composed of β-D-mannuronate (M) and α-L-guluronate (G) monomers, this copolymer is frequently ionically cross-linked with cations like Ca^{2+}. However, this type of bonds results in alginate gels with mechanical properties difficult to control. To overcome this, we performed a covalent cross-linking with chemical agents to obtain alginate hydrogels. However, the hydrogels usually exhibit a nanoporous structure but is not satisfactory for cell culture. Indeed, it is better to use scaffold with large pores to promote cell infiltration and to increase surface area for cell attachment. Different techniques have thus been developed to create macroporous hydrogels like gas foaming, freeze-drying or porogen leaching. In the project, we used a recent technique called cryopolymerization to obtain macroporous hydrogels.

The covalent cross-linking of alginate hydrogels was performed with the adipic acid dihydrazide (AAD), a symmetrical molecule with primary amines at each end, and

the 1-Ethyl-3-(3-dimethylaminopropyl) carbodiimide (EDC), a commonly used activation agent of carboxylic groups. The chemical reaction that occurs between alginate and the AAD and EDC cross-linkers is described in figure 2.11. In summary, the carboxylic group of alginate monomers M and G are first activated by EDC (O-acylisourea). This molecule can then react in 3 different pathways producing desired and undesired products. The reaction with AAD leads to the creation of amide bonds by the coupling of the primary amines of AAD to the activated carboxylic groups of alginate monomers, resulting to the desired product alginate amide. In the same way, the reaction with alginate monomers leads to alginate amide by passing through an intermediate product, the acid anhydride. The undesired reaction is the rearrangement of the O-acylisourea that leads to the stable N-acylurea and not to alginate amide. To obtain a covalently cross-linked alginate gel, the AAD must be bound to alginate by its two amine groups located at its extremities.

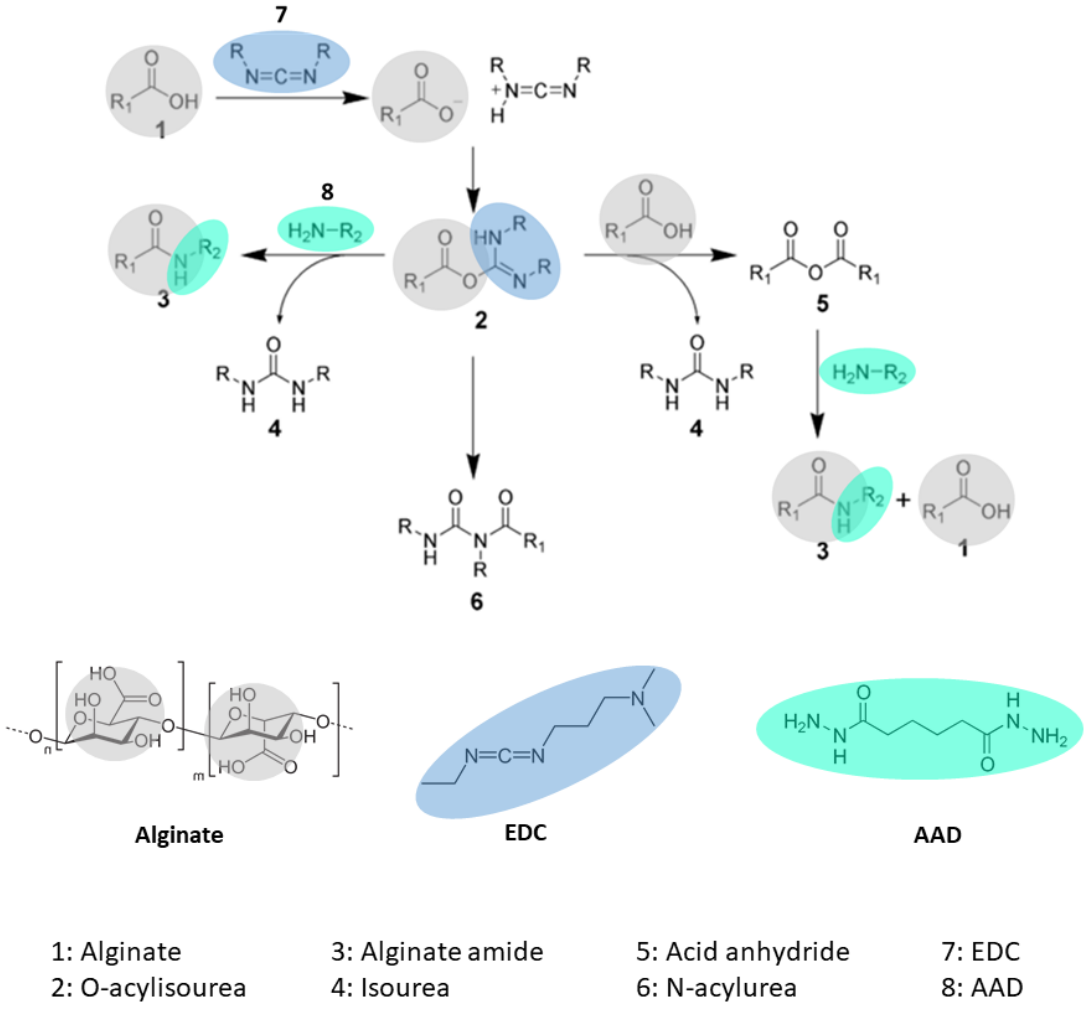

FIGURE 2.11: Schematic representation of alginate covalent cross-linking with AAD and EDC agents.

The macroporous structure of alginate scaffold was created by cryopolymerization. The materials obtained by this technique, called cryogels, represent a great interest

for biomedical applications thanks to their physical and chemical stability, their interconnected macroporous structure and ease of formation compared to other macropore forming techniques [111], [169]–[172]. An overview of the process is described in the figure 2.12. The alginate solution containing the cross-linkers is placed at subzero temperature. During the freezing, a phases separation occurs: the chemical agents are in an unfrozen state and the aqueous phase is frozen in the form of ice crystals. The alginate polymerization occurs in the unfrozen state, around the ice crystals, that act as porogens. The melting of the ice crystals at ambient temperature gives then rise to macropores. The size of the pores depends thus of the size of the ice crystals. At very low temperatures the ice crystals are small because they do not have time to grow resulting in small pore size. On the contrary, at low temperatures near zero, cristals have time to grow resulting in higher pore size.

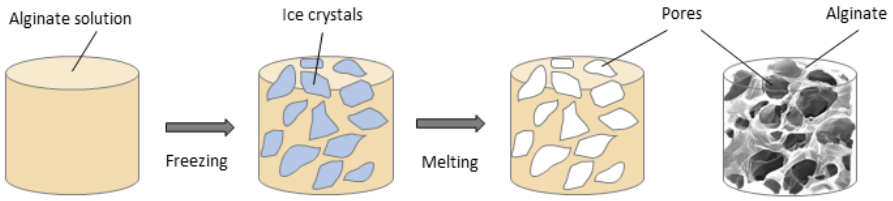

FIGURE 2.12: Overview of the cryopolymerization process to obtain alginate cryogel. Adapted from [173].

2.4.3 Objectives

This project aims at developing an alginate cryogel integrated microchip as a new *in vitro* liver model. It should approach the healthy but also the pathological (cirrhosis, metastasis) liver conditions to be used in pharmacology. This represents an important issue for the pharmaceutical industry which lacks reliable models to study toxicity and efficacy during the preclinical phase.

The theoretical design of the alginate cryogel integrated microchip is represented in figure 2.13. In order to develop such a model, some specifications must be fulfilled:

- Scaffold should present interconnected pores whose size is in the range of 100 μm to limit hydraulic resistance and allow cell seeding

- Perfusion should be possible with limited resistance to flow to avoid pressure build up in the microfluidic device

- The scaffold's mechanical properties should be tunable to mimic a healthy or pathological liver tissue

- Cell anchorage and reorganization in the microchip should be ensured by the material itself or an adequate coating/functionalization.

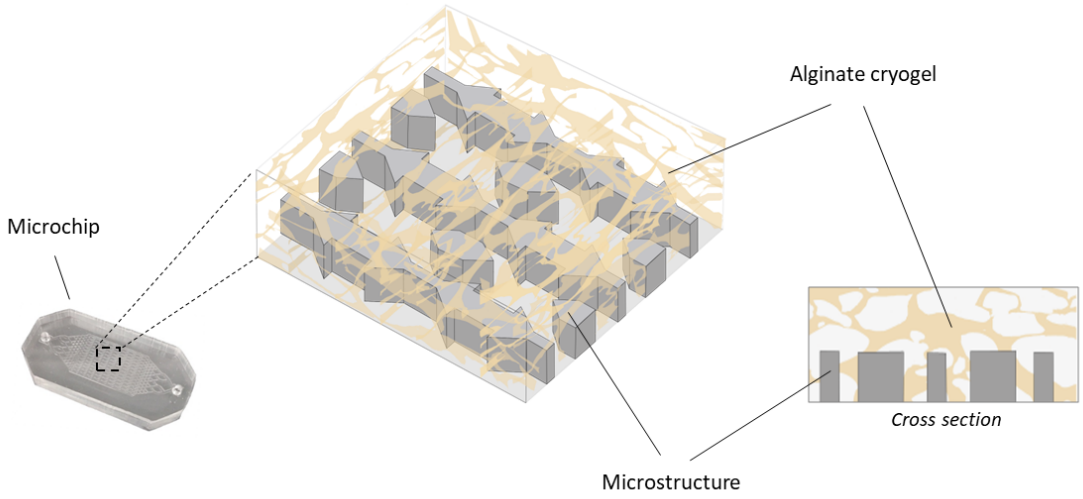

FIGURE 2.13: Illustration of the alginate cryogel integrated microchip.

To reach these aims, the project is divided into different steps corresponding to the following chapters:

- **Alginate cryogel integrated microchip for liver tissue engineering: implementation and physical characterization**
  Covalent alginate cryogel is first prepared and characterized out of the microsystem. The effects of freezing temperature on mechanical properties, pores size and morphology are studied. In particular, the parameters to obtain interconnected and macro size pores are defined in order to let the flow going through when placed in the microfluidic device. The alginate cryogel is then integrated inside the microchip where it is characterized regarding its structure and resistance to flow. Finally, in order to culture cells inside the device, two possible ways are investigated.

- **Proof of concept: human liver cancer cell line HepG2/C3A culture in alginate cryogel integrated microchip**
  HepG2/C3A, a well recognized and widely employed cell line, is chosen to start the biological study. First, microscopic observations and cell viability are performed. Metabolic activities are then studied by measurement of glucose and albumin quantities. The xenobiotic activity is also assessed by the biotransformation of APAP. The results are compared to cell culture in the cryogel-free microchip. Finally, the possibility to remove the alginate cryogel during the cell culture was tested.

- **Towards a complex liver model: primary human hepatocytes and co-cultures**
  In order to explore the different possibilities offered by this novel of liver on chip, preliminary experiments were performed. First, primary human hepatocytes were cultured: cell viability and metabolic activities were studied. Then, co-cultures were performed: HepG2/C3A with HUVEC in order to reproduce the liver sinusoid and HepG2/C3A with MDA-MB-231, a breast cancer cell line, in order to study extravasation and metastases mechanism.

This thesis is part of the university hospital research project Innovations for Liver Tissue Engineering (iLite - PI Prof. JC Duclos-Vallée) which aims at producing "mini livers". The option of combining 3D scaffold and microfluidics is one of the different methods that have been considered in this large project. This work is also funded by the "Comité de l'Oise de la Ligue contre le Cancer", in view of developing novel approach to study the impact of cytotoxic drugs on liver tissues.

Chapter 3

Materials and methods

3.1 Materials

Acid adipic dihydrazide (AAD), alginate lyase, bovine serum albumin (BSA), 1-Ethyl-3-(3-dimethylaminopropyl)carbodiimide (EDC), fluoresceinamine isomer I, 2-(N-morpholino) ethanesulfonic acid (MES), acetaminophen (APAP), paracetamol beta-D-glucuronide (APAP-GLU), paracetamol sulfate potassium salt (APAP-SULF), sodium bicarbonate were purchased from Sigma-Aldrich. Alginate manucol LKX was purchased from FMC Biopolymer. G_4RGDSP was purchased from Peptide 2.0 (Table 3.1).

Product	CAS Number
AAD	1071-93-8
Alginate Manucol LKX	9005-32-7
Alginate Lyase	9024-15-1
BSA	9048-46-8
EDC	25952-53-8
Fluoresceinamine, isomer I	3326-34-9
G_4RGDSP	/
MES	4432-31-9
APAP	103-90-2
APAP-GLU	16110-10-4
APAP-SULF	32113-41-0
Sodium Bicarbonate	144-55-8

TABLE 3.1: References of chemical products.

Alexa Fluor 488 Phalloidin, DAPI, Donkey anti-Mouse IgG (H+L) secondary antibody, Alexa Fluor 488 conjugate, Vybrant^{TM} DiI Cell-Labelling Solution, Vybrant^{TM} DiO Cell-Labelling Solution were purchased from Invitrogen. MEM Eagle w: EBSS, w/o: L-Glutamine, w: 2.2 g/L $NaHCO_3$, Penicillin-Streptomycin, Stable Glutamine (200 mM), HEPES Buffer 1 M, were purchased from PAN BIOTECH. MEM Non-Essential Amino Acids Solution (100X), PBS, pH 7.4 (1X) [-]$CaCl_2$ [-]$MgCl_2$, Sodium Pyruvate 100 mM (100X), Trypsin EDTA 0,25% (1X) were purchased from Gibco. HBM (Hepatocyte Basal Medium with UltraGlutamine-1), HCM SingleQuots were purchased from Lonza. Anti-collagen I antibody (mouse) was purchased from abcam. Collagen I, rat tail was purchased from Corning. ViaQuant^{TM} Far-Red Fixable Dead Cell Stain Kit was purchased from Genecopoeia. Human Albumin ELISA Quantitation set was purchased from Bethyl

Laboratories. LDH CytoTox 96 Non-Radioactive Cytotoxicity Assay was purchased from Promega. Glucose (GOD-POD) kit was purchased from Thermo Scientific.

Pump tubing, 2-stop, PharMed®BPT, 0.89 mm ID, Masterflex® Adapter Fittings were purchased from Cole-Parmer. Tubing PTFE, 0.8 mm ID x 1.6 mm OD was purchased from Fisher Scientific. Peristaltic pump IPC-N 24 was purchased from ISMATEC.

3.2 Alginate cryogels

3.2.1 Synthesis

Alginate powder (Alginate Manucol LKX, FMC Biopolymer) at (G/M) ratio of (30-40/60-70) was dissolved in 2-(N-Morpholino) ethanesulfonic acid (MES) solution (50 mM, pH 6) at 1 and 2% (w/v) overnight with gently continuous stirring. After dissolution, for 1 mL of 1% alginate solution, 1.2 mg of AAD was added and mixed with a vortex following by 2.7 mg of EDC for a (AAD:EDC) ratio of (1:1). Different alginate concentrations and (AAD:EDC) ratios were used (Table 3.2). Immediately after mixing, the solution was distributed in cylindrical molds (8 mm diameter, 6 mm height) or within microchips and stored at subzero temperature (-20 °C, -50 °C, -80 °C) overnight. The alginate cryogels were then thawed at room temperature and washed 3 times in MilliQ H_2O to remove any unreacted chemicals. They were incubated in a sodium carbonate solution (0.1 mM, pH 8.2) for 20 min to promote hydrolysis of EDC-activated carboxylic groups. Finally, the samples were washed 3 times with MilliQ H_2O.

Sample names	Alginate (w/v)	AAD (mg)	EDC (mg)
1% (1:1)	1%	12	27
1% (1:2)	1%	12	54
1% (1:3)	1%	12	81
2% (2:2)	2%	24	54

TABLE 3.2: Summary of alginate concentrations and (AAD:EDC) ratios used for alginate cryogel preparation.

3.2.2 Mechanical properties

Cylindrical samples of alginate cryogels (8 mm diameter, 6 mm height) were used to measure the mechanical properties by uniaxial compression test. First, the samples were incubated in PBS solution at 37 °C overnight. Using a mechanical testing system (Synergie 400, MTS system) with a 2 N load cell, the samples were then compressed in PBS solution at a rate of 3 mm/min up to 67% of deformation. The Young's modulus was then obtained by measuring the slope of the stress-strain curve in the first 10% deformation.

3.2.3 Physical properties

Cylindrical samples of alginate cryogels (8 mm diameter, 6 mm height) were used to measure the degree of pore connectivity (DC) and the swelling ratio (Q_M). The samples were

hydrated in PBS at 37 °C overnight. Then the hydrated mass (m_h) and the dehydrated mass (m_w), obtained after wicking the samples on absorbent paper, were measured. The samples were then washed with water and lyophilized to measure the dried mass (m_d) (Fig. 3.1). The DC and Q_M were finally calculated as follows:

$$DC = (m_h\text{-}m_w)/m_h \times 100$$

$$Q_M = (m_h\text{-}m_d)/m_d$$

The DC represents the volume of interconnected pores, expressed as a percentage of the total volume. The Q_M represents the quantity of total water absorbed, expressed as a number of times that the sample can take its weight in water.

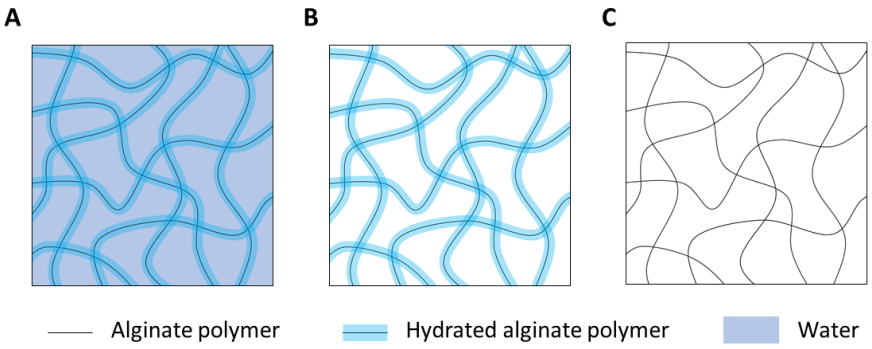

FIGURE 3.1: Schematic representation of alginate cryogel structure. (**A**) Hydrated, (**B**) Dehydrated and (**C**) Dried alginate cryogel.

3.2.4 Microstructure analysis

Cylindrical samples of alginate cryogels (8 mm diameter, 6 mm height) were prepared. The samples were first lyophilized (Alpha 1-2 LDplus, CHRIST) and then observed using scanning electron microscopy (SEM) (XL 30-ESEM FEG, Philips, The Netherlands). The pore size was measured from the SEM images using the software ImageJ.

3.2.5 Aminofluorescein functionalization

A solution of 1 mL of MES solution (50 mM, pH 6), 12 μL aminofluorescein (1 mM) and 2.7 mg of EDC were mixed and injected inside the alginate cryogel-integrated microchips. After overnight incubation, the samples were washed with PBS and finally observed under confocal microscopy (Zeiss LSM 710).

3.2.6 RGD functionalization

Alginate powder (Alginate Manucol LKX, FMC Biopolymer) at (G/M) ratio of (30-40/60-70) was dissolved in MES buffer (50 mM, pH 6) at 1% (wt/v) overnight with gently continuous stirring. After dissolution, 40 mg of sulfo-N-Hydroxysuccinimide (NHS) and

60 mg of EDC were mixed for 1 mL of 1% alginate solution. Then, 25 mg of amine-terminated G_4RGDSP were added and the solution was kept under continuous stirring overnight to let the reaction proceed. The resulting G_4RGDSP grafted alginate was first purified by precipitation in acetone and then dried in a vacuum oven overnight. The polymer was purified a second time by several washes with water.

3.2.7 Collagen coating

A collagen type I from rat tail (Corning Life Science) at 0.3 mg/mL was injected in the alginate cryogel and incubated for 2 h at 37 °C. The alginate cryogel was then washed with PBS.

3.2.8 Collagen staining

The collagen was labeled by immunofluorescence. The sample was first incubated in a mouse anti collagen I antibody solution (1/500, abcam) for 2 h at room temperature. After washing with PBS, the cryogel was then incubated in an anti-mouse Alexa Fluor 488 conjugated solution (1/500, ThermoFisher) for 2 h at room temperature. Finally, the sample was washed with PBS and observed using epifluorescence microscopy.

3.3 Microchip

3.3.1 Fabrication

The step of mold fabrication was performed by the "Laboratoire d'analyse et d'architecture des systèmes" in Toulouse. The microstructure of the microchip was first designed on computer and transferred on a specific paper used as a photomask. To create the mold, a thin slice of silicon, called wafer, was coated with a photosensitive resin thanks to a spin coater. After heating at 95 °C for 30 min, photolitography was performed: the wafer was exposed to ultraviolet rays through the photomask allowing the exposed resin to cross-link. The non cross-linked resin was then removed with a developer bath. Finally, the obtained molds were dried with nitrogen.

The polydimethylsiloxane (PDMS) (SYLGARD 184 kit, Dow Corning) was mixed with a cross-linking agent at 10:1 (w/w) and poured on the molds, 10 mg and 5 mg for the top and bottom layers respectively. After degassing PDMS under vacuum bell, the molds were heated in an oven at 70 °C for 2 h. Once the PDMS cross-linked, layers were unmolded. The top layer was then perforated with a 2 mm puncher to create the inlet and the outlet of the microchip. The two replica were then sealed together after an air plasma treatment for 1 min. Finally, the microchip was cut with a custom made puncher to standardize its shape.

At this step, the microchips can be filled with alginate solution to obtain the cryogel. After cross-linking, the excess of cryogel located in the inlet and outlet holes were removed with tweezers.

Finally, silicone tubes with a polypropylene connector (Luer, diameter 1.6 mm, Cole Farmer) were inserted in the inlet and outlet holes. They were sealed to the microchip with PDMS. The microsystem was then placed in the oven at 70 °C for the cryogel-free microchips and in the incubator at 37 °C overnight for the alginate cryogel-integrated microchips to prevent the cryogel from drying out.

3.3.2 Hydrodynamic characterization

The resistance to flow of the microchip was characterized by a setup composed of a pressure controller (MFCS^{TM}-EZ, Fluigent) and a flowmeter (Flow Unit type M model, Fluigent) (Fig. 3.2). The pressure P required at the inlet of the microchip to reach the desired flow rate Q at the outlet was measured.

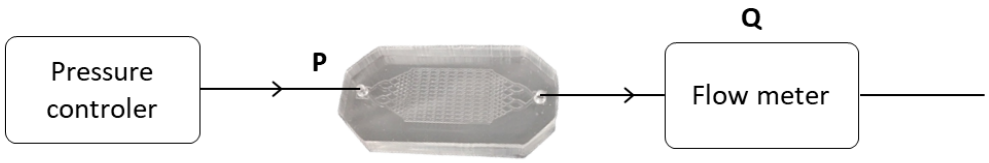

FIGURE 3.2: Scheme of the hydrodynamic measurement set up.

3.4 Cell culture

3.4.1 HepG2/C3A

The HepG2/C3A is a clonal derivative of HepG2, a human hepatocyte cell line coming from a hepatocellular carcinoma. They come from ATCC (reference CRL-10741).

The HepG2/C3A cells were cultured at 37 °C in a 5% CO_2 supplied incubator in a T75 culture flask. The culture medium consisted of Minimum Essential Medium (MEM, Gibco) completed with 10% fetal bovine serum (FBS, Gibco), 2 mM L-Glutamine (PAN BIOTECH), 0.1 mM nonessential amino acids (Gibco), 1 mM sodium pyruvate (Gibco), 1% HEPES buffer (PAN BIOTECH) and 100 units/mL penicillin-streptomycin (PAN BIOTECH). The medium was changed every two days. At confluence, the cells were detached with 0.25% trypsin EDTA (Gibco) for 10 min and seeded at 20 000 cells/cm^2.

3.4.2 Primary human hepatocytes

The PHH used are cryopreserved cells. They come from Biopredic (reference HEP701LN).

The PHH were not cultured in culture flask T75 but directly in the microchips at 37 °C in a 5% CO_2 supplied incubator. The culture medium consisted of hepatocyte basal medium (HBM^{TM} Basal Medium, Lonza) completed with hepatocyte culture medium supplements (HCM^{TM} Kit SingleQuots^{TM} Kit, Lonza) containing 2% FBS, ascorbic acid, albumin, free fatty acids, hydrocortisone, recombinant human Epidermal Growth Factor

(rh EGF), transferrin, insulin, gentamicin and amphotericin. After the adhesion phase, corresponding to the first 24 h after seeding, the medium was replaced by serum free medium.

3.4.3 HUVEC

The HUVEC is a cell line of endothelial cells from the umbilical cord. They come from ATCC (reference CRL-1730).

The HUVEC were cultured at 37 °C in a 5% CO_2 supplied incubator in a T75 culture flask. The culture medium consisted of endothelial basal medium (EBM^{TM}-2 Endothelial Cell Growth Basal Medium, Lonza) completed with endothelial cells supplements (EGM^{TM}-2 Endothelial SingleQuots^{TM} Kit, Lonza) containing 2% FBS, ascorbic acid, heparin, Insulin-like Growth Factor (IGF), hydrocortisone, human Epidermal Growth Factor (hEGF), recombinant human Fibroblast Growth Factor (rh FGF), Vascular Endothelial Growth Factor (VEGF), gentamicin and amphotericin. The medium was changed every two days. At 70-80% of confluence, the cells were detached with 0.25% trypsin EDTA (Gibco) for 10 min and seeded at 20 000 cells/cm^2.

3.4.4 MDA-MB-231

The MDA-MB-231 is a human breast cell line coming from an adenocarcinoma. They come from ATCC (reference HTB-26) and have been transfected with Green Fluorescent Protein (GFP) by the pSUPER neo.GFP vector in the INSERM U908 laboratory at Lille.

The MDA-MB-231 cells (ATCC, reference HTB-26) were cultured at 37 °C in a 5% CO_2 supplied incubator in a T75 culture flask. The culture medium was the same as the HepG2/C3A medium which consisted of Minimum Essential Medium (MEM, Gibco) completed with 10% fetal bovine serum (FBS, Gibco), 2 mM L-Glutamine (PAN BIOTECH), 0.1 mM nonessential amino acids (Gibco), 1 mM sodium pyruvate (Gibco), 1% HEPES buffer (PAN BIOTECH) and 100 units/mL penicillin-streptomycin (PAN BIOTECH). The medium was changed every two days. At confluence, the cells were detached with 0.25% trypsin EDTA (Gibco) for 10 min and seeded at 20 000 cells/cm^2.

3.5 Cell culture in alginate cryogel-integrated microchip

To avoid any high pressure inside the microchip, which could cause alginate cryogels tears, all the solution injections were gently performed with a 200 μL micropipette.

3.5.1 Perfusion devices: IDCCM and bubble trap

Bubble trap system

The bubble trap system (MEDICOLAB) was a cylindrical glass reservoir (volume of 2 mL). It was composed of a plug on the top and of two holes: an inlet at the mid-height and an outlet at the bottom (Fig. 3.3 **A**). The bubble trap system was connected to a

microchip and to the peristaltic pump with tubings and connectors (Fig. 3.3 **B**). The culture medium flowed from the top to the bottom to avoid any air bubbles in the microchip. Each microchip was independently connected to one bubble trap with its proper microfluidic circuit. To maintain this system in an upright position, it was placed in a homemade PDMS support.

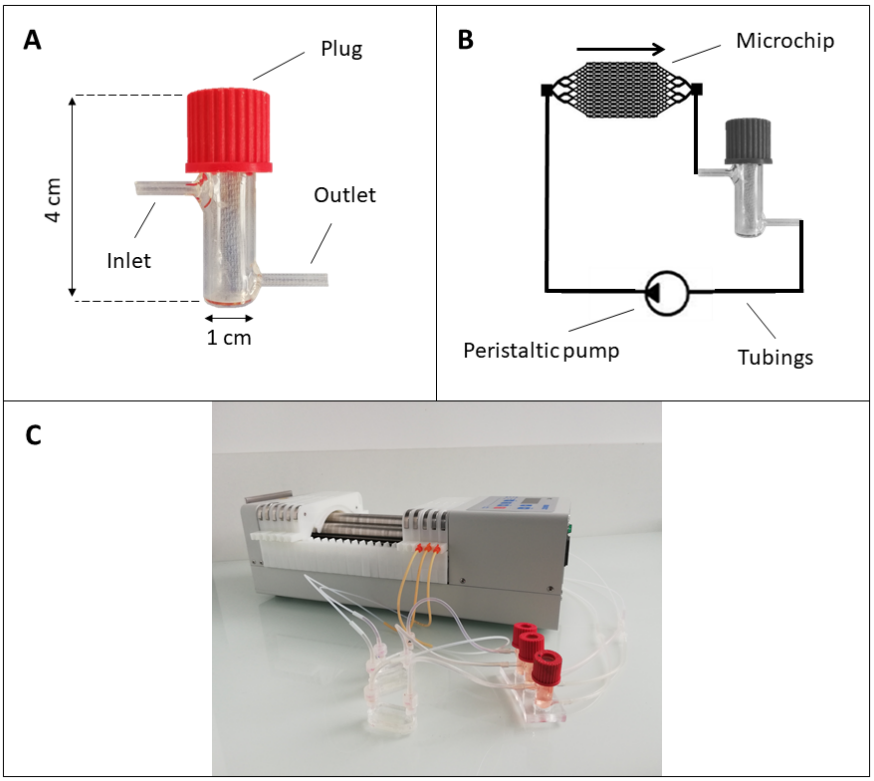

FIGURE 3.3: Bubble trap system. (**A**) Photo of the device. (**B**) Schematic representation of the microfluidic circuit.

IDCCM device

The device Integrated Dynamic Cell Cultures in Microsystems, called IDCCM, was developed in the laboratory and patented in 2011 [174], [175]. It was a manufactured polycarbonate box, the size of a 24-well plate, composed of a top layer and a bottom layer separated by a silicon seal (Fig. 3.4 **A**). The bottom layer was composed of 24 holes allowing to connect the microchips on one side and of 24 wells, one over each hole, on the other side. Each microchip was connected to 2 wells (volume of 2 mL per well) thanks to connectors. Up to 12 microchips could be used simultaneously and independently with one IDCCM device. The top layer was composed of 24 holes to connect the tubes. The box was tightly maintained closed by a metal clamping system (Fig. 3.4 **B**). The microchip perfusion was ensured by a peristaltic pump integrated to the microfuidic circuit (Fig. 3.4 **C**). Thanks to a plexiglass support, the IDCCM device could be placed on the peristaltic pump (Fig. 3.4 **D**).

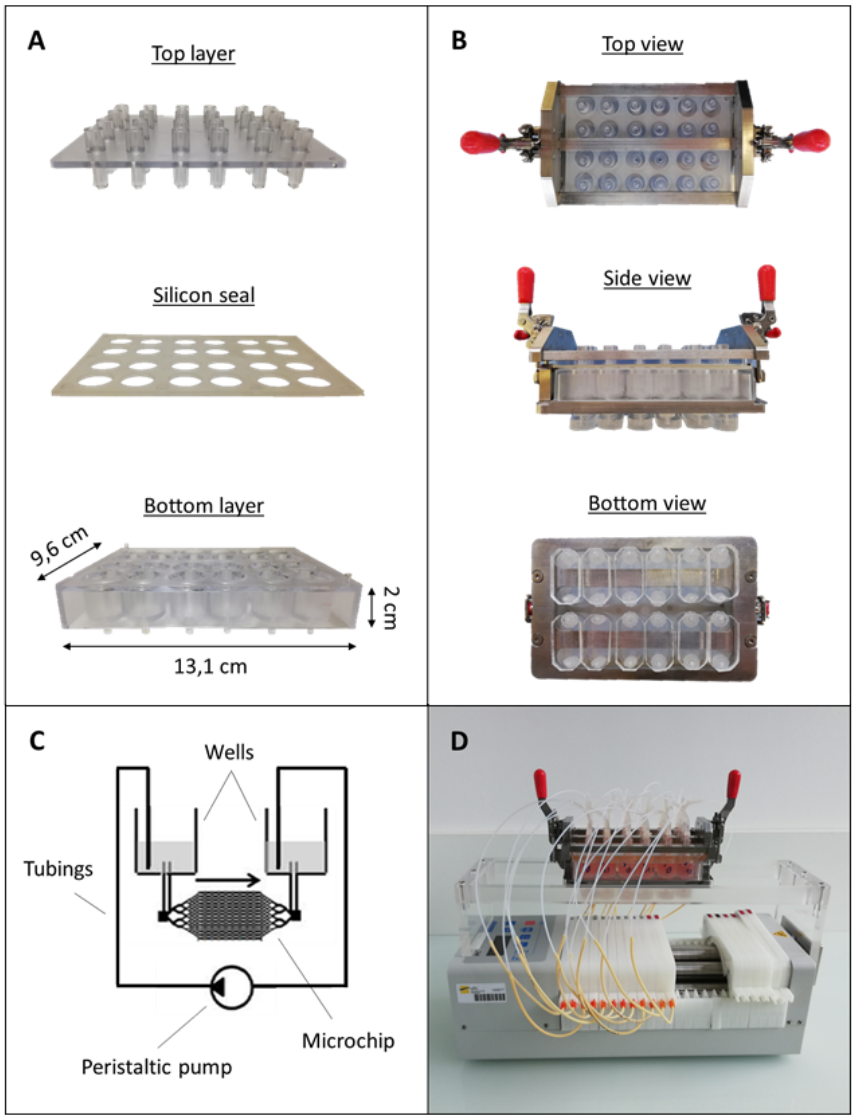

FIGURE 3.4: IDCCM device. (**A**) Photos of the IDCCM components. (**B**) Photos of the IDCCM device connected to 12 microchips and closed with the metal clamping system. (**C**) Schematic representation of the microfluidic circuit. (**D**) Photo of the whole IDDCM device.

An evaporation of cell culture medium was observed with the IDCCM device and the bubble trap system. This phenomenon is well known in microfluidics because of the very small volumes used [176]. It was already observed in the previous study of Dr. Baudoin [177] with the bubble trap system. It was estimated to 300 μL/24h. To take into account this evaporation, all volumes of the medium samples were measured.

3.5.2 HepG2/C3A culture

The culture was performed with the IDCCM device connected to 12 microchips: 6 1% (1:1) alginate cryogel-integrated microchips and 6 cryogel-free microchips. The experiment was performed during 6 days (Fig. 3.5).

At day 0, prior to use, the microchips were sterilized using 70% ethanol for 15 min. After washing with PBS, the microchips were coated with collagen I and then washed with cell culture medium. The HepG2/C3A were detached from the culture flask with 0.25% trypsin EDTA (Gibco) for 10 min and seeded in the microchips at a density of 500 000 cells/biochip (10 million cells/mL). The microchips were placed in a 5% CO_2 incubator at 37 °C overnight to allow cell adhesion.

At day 1, the 12 microchips were plugged to the IDCCM device which was then connected to a peristaltic pump (ISMATEC, ISM 939) with PharMed BPT tubings of 0.89 mm inner diameter (Cole Parmer). The wells of the IDCCM device were filled with 2 mL of cell culture medium (4 mL per microchip). The whole device was placed in the incubator at 37 °C with 5% CO_2 under perfusion at 10 μL/min.

At day 2, 4 and 6, the culture medium was changed. Each culture medium sample was collected and stored at -20 °C for further analysis (glucose and albumin quantifications). Moreover, cell viability assays and SEM observations were performed.

The xenobiotic activity was assessed by APAP biotransformation. At day 2, 4 and 6 the cells were exposed to APAP (100 μM). After 24h of exposure, the culture medium was collected and the APAP metabolites were quantified by mass spectrometry.

After use, the IDCCM device and tubings were washed with SDS at 2% (Sigma) for 1 h and then washed with deionized water. Once analyzed, the microchips were discarded.

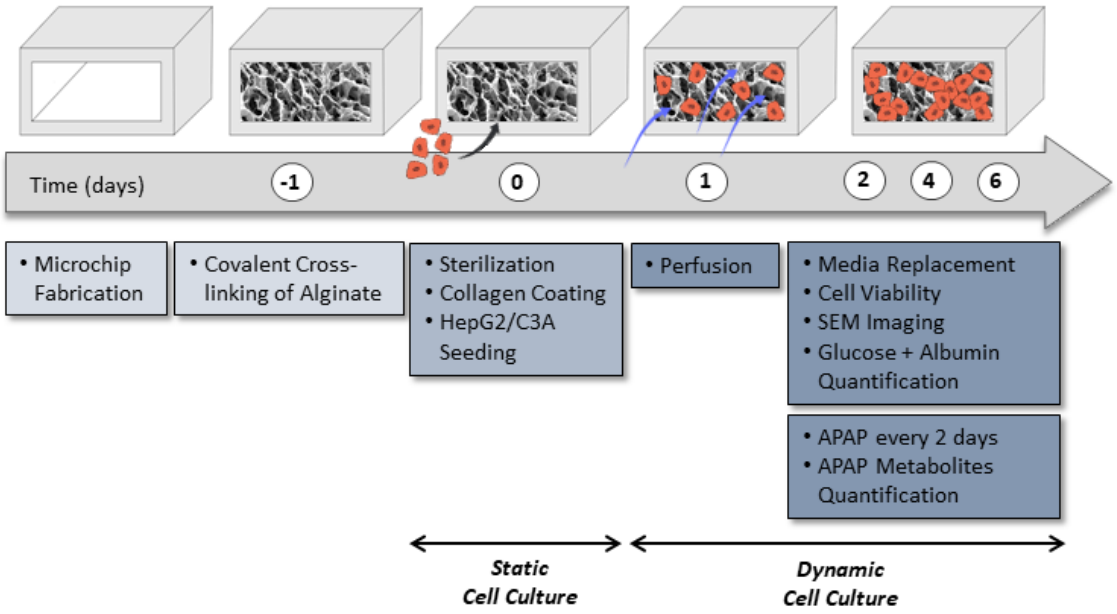

FIGURE 3.5: Experimental steps of HepG2/C3A cell culture in the alginate cryogel-integrated microchip.

3.5.3 PHH culture

The culture was performed with the IDCCM device with 1% (1:1) alginate cryogel-integrated microchips. The experiment lasted 15 days (Fig. 3.6 **A**).

At day 0, prior to use, the alginate cryogel-integrated microchips were sterilized using 70% ethanol for 15 min. After washing with PBS, the microchips were coated with collagen I and then washed with cell culture medium. The PHH were thawed and seeded in the microchips at a density of 500 000 cells/biochip (10 million cells/mL). They were placed in a 5% CO_2 incubator at 37 °C overnight to allow cell adhesion.

At day 1, the 24 microchips were plugged to IDCCM devices that were then connected to peristaltic pumps (ISMATEC, ISM 939) with PharMed BPT tubings of 0.89 mm inner diameter (Cole Parmer). The wells of the IDCCM devices were filled with 2 mL of cell culture medium (4 mL per microchip). The whole devices were placed in the incubator at 37 °C with 5% CO_2 and perfused at 10 μL/min.

At day 2, and every odd-numbered day thereafter, the culture medium was changed by APAP free culture medium. From day 4, and every even-numbered day thereafter, the cell culture medium was changed by culture medium with APAP (15 μM). Each culture medium sample was collected and stored at -20 °C for further analysis (albumin and LDH quantifications).

At day 7 and 15, cell viability assays were performed.

After use, the IDCCM devices and tubings were washed with SDS at 2% (Sigma) for 1 h and then washed with deionized water. Once analyzed, the microchips were discarded.

3.5.4 HepG2/C3A and HUVEC co-culture

The culture was performed with the bubble trap system with 1% (1:1) alginate cryogel-integrated microchips. The co-culture was performed during 5 days with the HepG2/C3A medium culture (Fig. 3.6 **B**). Two options were performed.

Option 1: sequential seedings

At day 0, prior to use, the microchips were sterilized using 70% ethanol for 15 min. After washing with PBS, the microchips were coated with collagen I and then washed with cell culture medium. The HepG2/C3A were detached from the culture flask with 0.25% trypsin EDTA (Gibco) for 10 min and seeded in the microchips at a density of 500 000 cells/biochip (10 million cells/mL). The microchips were placed in a 5% CO_2 incubator at 37 °C overnight to allow cell adhesion.

At day 1, each microchip was connected to a bubble trap system, connected to a peristaltic pump (ISMATEC, ISM 939) with PharMed BPT tubings of 0.89 mm inner diameter (Cole Parmer). The bubble trap systems were filled with 2 mL of cell culture medium. The whole microfluidic circuit was placed in the incubator at 37 °C with 5% CO_2 and perfused at 10 μL/min.

Once the HepG2/C3A cells occupied the cryogel, they were labeled with DiO (Vybrant DiO Cell-Labelling Solution, ThermoFisher) by following the manufacturer's instructions. The medium was replaced by a solution of alginate lyase to remove the cryogel. Then, HUVEC were detached from the culture flask with 0.25% trypsin EDTA (Gibco) for 10 min and labeled with DiI (Vybrant DiI Cell-Labelling Solution, ThermoFisher) by following the manufacturer's instructions. They were seeded at 700 000 cells/biochip.

After 5 days of co-culture in dynamic conditions, the microchip were observed under confocal microscopy.

Option 2: simultaneous seedings

At day 0, prior to use, the microchips were sterilized using 70% ethanol for 15 min. After washing with PBS, the microchips were coated with collagen I and then washed with cell culture medium. HUVEC and HepG2/C3A were detached from their culture flasks with 0.25% trypsin EDTA (Gibco) for 10 min and labeled with DiO (Vybrant DiO Cell-Labelling Solution, ThermoFisher) and DiI (Vybrant DiI Cell-Labelling Solution, ThermoFisher) respectively by following the manufacturer's instructions. They were seeded at a ratio of 2:1 HepG2/C3A:HUVEC (1million:500 000) cells/biochip.

After 5 days of co-culture in dynamic conditions, the microchip were observed under confocal microscopy.

After use, the bubble trap system and tubings were washed with SDS at 2% (Sigma) for 1 h and then washed with deionized water. Once analyzed, the microchips were discarded.

3.5.5 HepG2/C3A and MDA-MB-231 co-culture

The culture was first performed in well plates and then in 1% (1:1) alginate cryogel-integrated microchips. The experiment was performed during 6 days in well plates and 4 days in microchips (Fig. 3.7).

Concerning the well plate experiments, at day 0, HepG2/C3A were detached from the culture flask with 0.25% trypsin EDTA (Gibco) for 10 min and seeded in the wells at a density of 20 000 and 200 000 cells/cm^2.

At day 1, MDA-MB-231 were detached from the culture flask with 0.25% trypsin EDTA (Gibco) for 10 min and seeded in the wells at a density of 1 000 cells/cm^2.

At day 2, 4 and 6, the culture medium was changed and cell viability assays were performed. Cell counting of the different cell types was then carried out with a Malassez'hemocytometer after 0.25% trypsin EDTA treatment for 10 min.

Concerning the microchip experiments, at day 0, prior to use, the microchips were sterilized using 70% ethanol for 15 min. After washing with PBS, the microchip were coated with collagen I and then washed with cell culture medium. The HepG2/C3A were detached from the culture flask with 0.25% trypsin EDTA (Gibco) for 10 min and

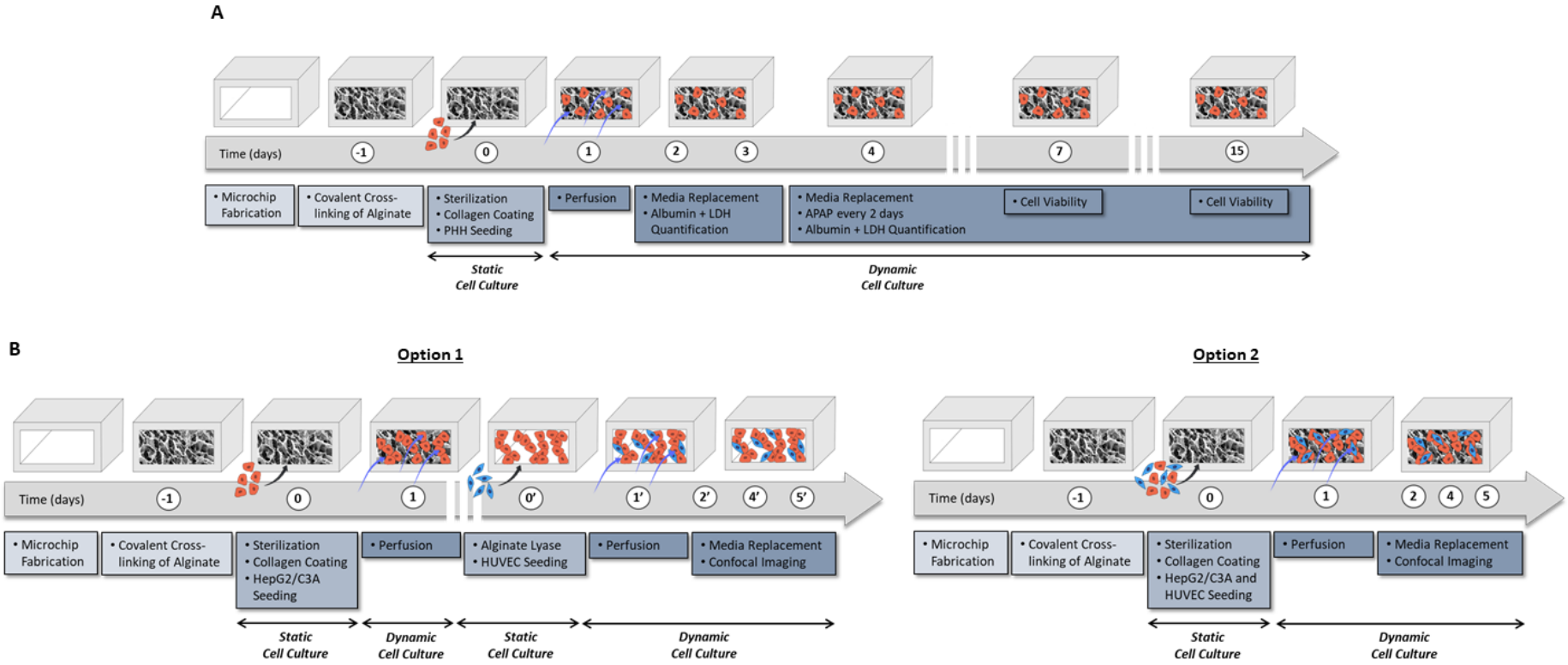

FIGURE 3.6: Experimental steps of cell cultures in the alginate cryogel-integrated microchip. (**A**) PHH cell culture. (**B**) HepG2/C3A and HUVEC co-culture.

seeded in the microchips at a density of 1 million cells/biochip (20 million cells/mL). The microchips were placed in a 5% CO_2 incubator at 37 °C overnight to allow cell adhesion.

At day 1, MDA-MB-231 were detached from the culture flask with 0.25% trypsin EDTA (Gibco) for 10 min and seeded in the microchip at a density of 1 000 cells/microchip.

At day 2 and 4, cell culture medium was changed and cell viability assays were performed.

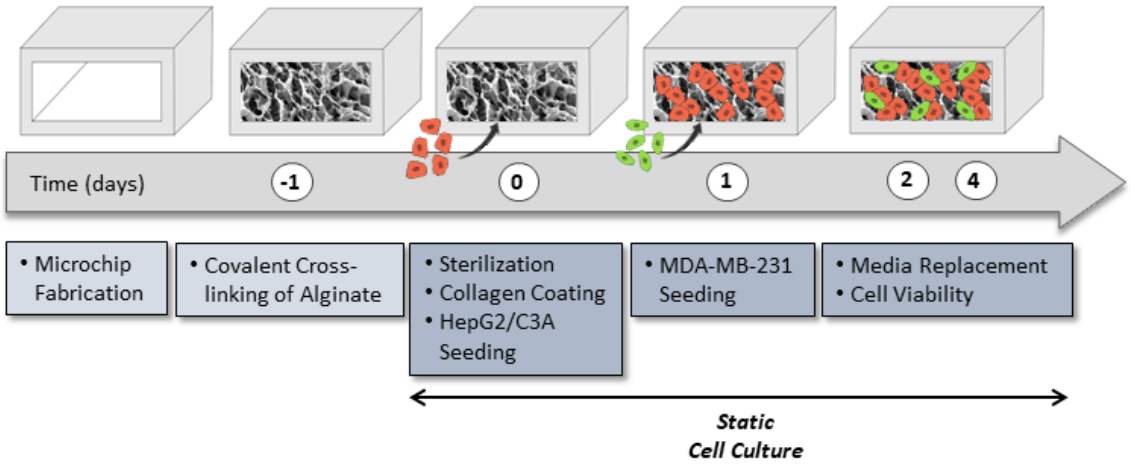

FIGURE 3.7: Experimental steps of HepG2/C3A and MDA-MD-231 co-culture in the alginate cryogel-integrated microchip.

3.5.6 Alginate lyase

To remove the alginate cryogel, alginate lyase (Sigma) was first diluted in culture medium at 10 mg/mL. The culture medium in the bubble traps or in the wells of the IDCCM device was then replaced by the alginate lyase solution. The systems were then placed in the incubator at 37 °C for 1 h under perfusion at 10 μL/min. After breaking down of the alginate cryogel, the solution was replaced by culture medium.

3.6 Cell culture analysis: imaging

3.6.1 Cell viability

The microchips were first washed with PBS and then incubated with a Via Quant^{TM} Far-Red Fixable Dead Cell Stain Kit (GeneCopoeia) for 30 min at room temperature. After washing with PBS, the samples were fixed in a 4% paraformaldehyde (PFA) solution (VWR) for 10 min at room temperature. Samples were then permeabilized with a 0.1% TritonX-100 solution for 5 min and blocked with a 1% Bovine Serum Albumin solution (Sigma) for 30 min. Actin and nuclei staining were performed using Alexa Fluor 488 Phalloidin (1/1000, Thermofisher) and DAPI (1/200, Sigma) respectively. The samples

were finally washed with PBS before visualization using confocal microscopy (Zeiss LSM 710).

3.6.2 Confocal and epifluorescence microscopy

Microchips were observed using either confocal (Zeiss LSM 710) or epifluorescence (Leica DMI6000 B) microscopy in the days following their staining. Single images or stacks of 200 μm were performed (Fig. 3.8). The fluorescent dyes used are listed in table 3.3.

Name	Abs/Em (nm)	Color	Target
DAPI	358461	Blue	Nucleus
Alexa Fluor 488 Phalloïdin	495/518	Green	Cytoskeleton
Far-Red	650/665	Red	Dead cell
Fluorescein	490/520	Green	Alginate
Vybrant DiO Cell-Labelling	484/501	Green	HepG2C3A
Vybrant DiI Cell-Labelling	549/565	Red	HUVEC

TABLE 3.3: Fluorescent dyes used in imaging.

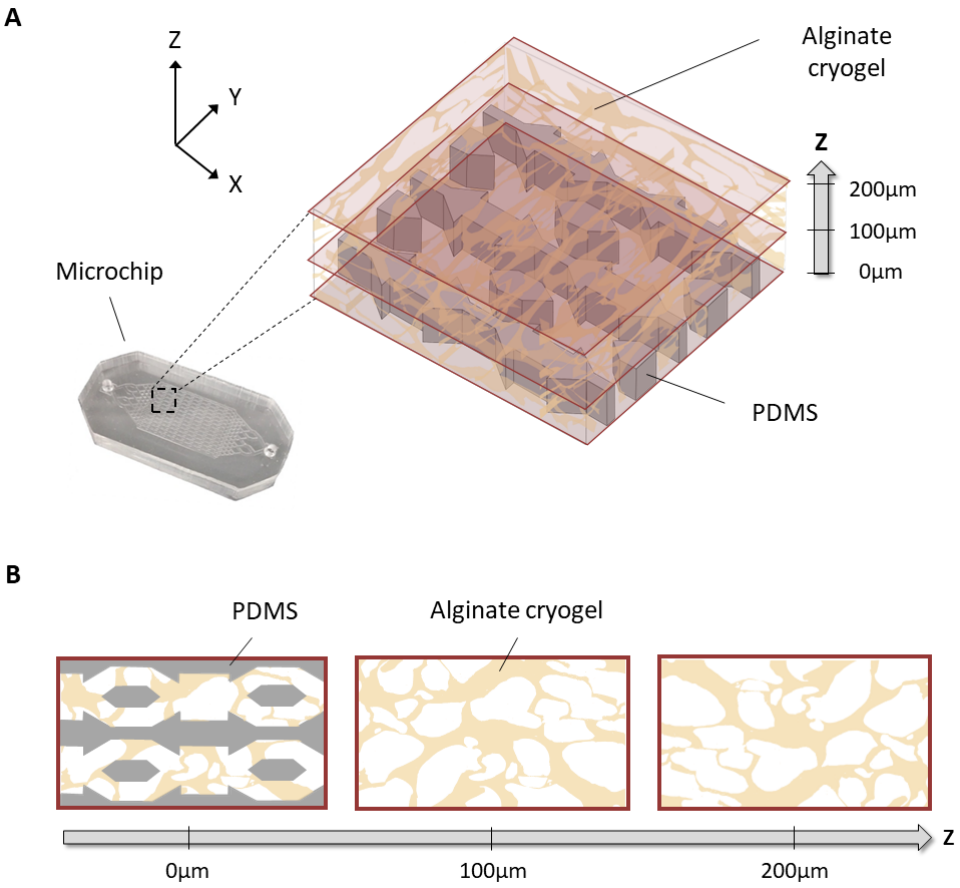

FIGURE 3.8: Confocal microscopy imaging. (**A**) Representation of a microchip view under confocal microscopy (**B**) Top view representation of confocal images.

3.6.3 Scanning electron microscopy

The microchips were first washed with PBS. Cell were then fixed with a 4% PFA solution for 10 min at room temperature. After PBS washing, small slices of microchips were cut with a scalpel. The slices were observed on the transverse view using SEM (XL 30-ESEM FEG, Philips, The Netherlands) (Fig. 3.9).

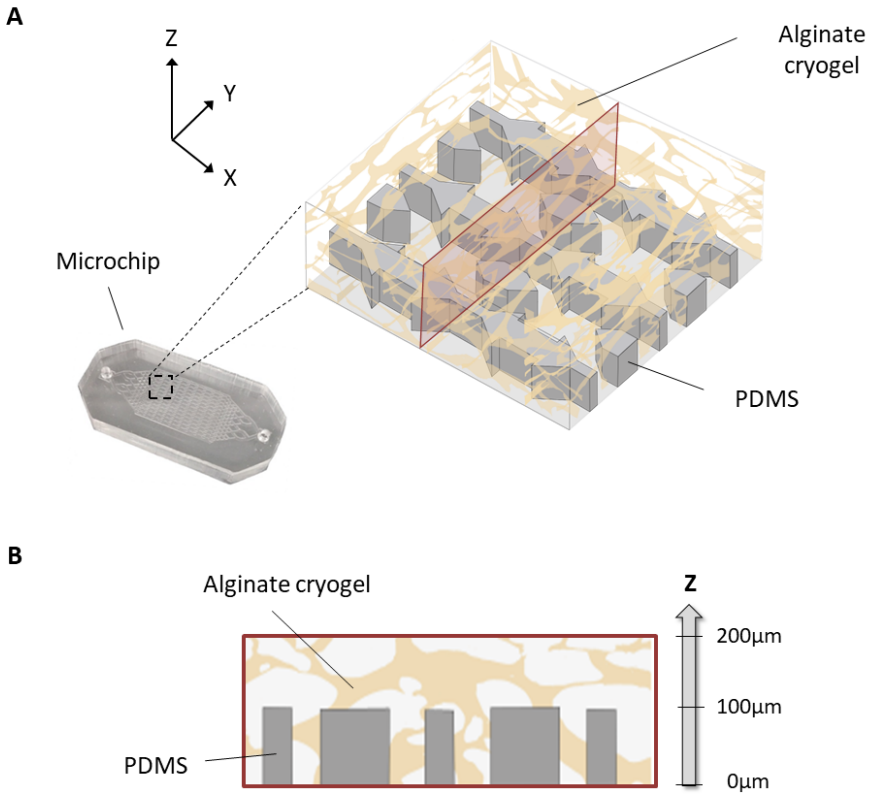

FIGURE 3.9: SEM imaging. (**A**) Representation of the microchip slice cutout for SEM imaging (**B**) Cross-sectional representation of a microchip slice to be observed by SEM.

3.7 Cell culture analysis: quantification

3.7.1 Albumin

Albumin was quantified in the medium samples using an ELISA sandwich technique (Human Albumin ELISA kit, Bethyl Laboratories). First, the 96-well plate was coated with 100 μL of a goat anti human albumin antibody diluted (1/100) in a carbonate buffer (0.05 M, pH 9.6) for 1 h at room temperature. After five washing with a washing solution (50 mM Tris, 0.14 M NaCl, 0.05% tween, pH 8, Sigma), 200 μL of a blocking solution (50 mM Tris, 0.14 M NaCl, 1% BSA, pH 8, Sigma) was added to each well. After an incubation of 30 min at room temperature, the wells were washed with the washing solution five times. The samples and the standards diluted in a 0.1% tween solution were then prepared. 100 μL were added to each well and incubated for 1 h at room temperature.

After five washing, 100 μL of a HRP conjugated goat anti human albumin antibody solution diluted (1/50 000) was incubated for 1 h at room temperature. After five washing, the peroxidase was revealed with 100 μL of a citrate buffer (0.05 M, pH 7.4) completed with o-Phenylenediamine dihydrochloride (OPD) and H_2O_2. After 5 to 15 min protected from light at room temperature, the reaction was stopped with 100 μL of sulfuric acid (0.18 M). The absorbance was then measured with a microplate reader at 492 nm (Spark 10M, TECAN).

3.7.2 Glucose

Glucose was quantified in the medium samples using two successive enzymatic reactions performed by a chemistry analyzer (INDIKO, ThermoFisher) with the GOD-POD system glucose reagents kit (ThermoFisher). The glucose was first transformed in glucono-delta-lactone and hydrogen peroxide by the glucose oxidase (GOD). Then, in presence of peroxidase (POD), the hydrogen peroxide reacted with 4-aminoantipyrine and phenol to form a red quinone imine. The absorbance of the obtained colored solution was measured at 510 nm.

3.7.3 Lactate dehydrogenase

Lactate Dehydrogenase (LDH) was quantified in the medium samples using the Cytotox96 kit (Promega). Culture medium samples were placed in a 96 well plate, 50 μL per well. Then, 50 μL of the Reagent Solution containing lactate, nicotinamide adenine dinucleotide (NAD+) and iodonitrotetrazolium (INT), were added to each well and incubated at room temperature for 30 min. LDH catalysed the reduction of NAD+ to NADH in the presence of lactate. INT was then reduced into formazan, a red dye, thanks to the presence of NADH. The reaction was stopped by 50 μL of the Stop Solution. The formazan concentration that is proportional to the LDH one was finally measured with a microplate reader at 492 nm (Spark 10M, TECAN).

3.7.4 APAP metabolites

The resulting metabolites of APAP biotransformation, APAP-GLUC and APAP-SULF, were quantified by mass spectrometer. An Agilent QQQ 6460 mass spectrometer with a jet stream electrospray ion source and an Agilent 1200 series fast resolution LC system (Wilmington, DE) were employed to detect APAP and its metabolites in the culture medium samples. MassHunter software was used for system control, data acquisition, and data processing. LC separation was performed on an Agilent poroshel C18 reverse phase column (100 mm x 4.6 mm i.d., 2.6 μm particle size) with a gradient program at a flow rate of 1 mL/min. The mobile phase A consisted of 100% HPLC grade water with 0.1% formic acid and mobile phase B consisted of 100% HPLC grade acetonitrile. The gradient started with 2% solvent B, held at 2% B for 1 min before being increased to 20% B then increased to 95% in 1 min and was then held at 95% B for 2 additional minutes. The column was re-equilibrated with 2% B for 3 min. Total run time was 12 min with a

10 μL injection volume. The mass spectrometer was operated in positive and negative jet stream ESI modes. Nitrogen was used as a nebulizer, turbo (heater) gas, curtain, and collision-activated dissociation gas. The capillary voltage was +3800 V and +3500 B. The ion source gas temperatures were 350 °C with flows of 12 L/min. Jetstream gas temperatures were 350 °C with flows of 12 L/min. APAP and metabolits were measured by selective reaction monitoring (SRM). Figure 3.10 lists the optimal mass spectrometric settings (frag mentor and collision energy) for each quantifying and qualifying transition. The calibration curve was performed with internal calibration using 0.5 μm APAP-D4 in acetonitrile. The samples are prepared by taking 20 μL of medium and adding 80 μL of the internal standard solution to the actenotrile in a 1 mL glass vial, then centrifuged for 5 min at 13500 rpm before being transferred from a vial with a 200 μL glass insert.

Scan Segments

Cpd Name	ISTD?	Prec Ion	MS1 Res	Prod Ion	MS2 Res	Dwell	Frag (V)	CE (V)	Cell Acc (V)	Polarity
APAP D4	Yes	156	Unit/Enh (6490)	114	Unit/Enh (6490)	20	80	8	7	Positive
APAP	No	152.07	Unit/Enh (6490)	110.1	Unit/Enh (6490)	20	80	12	7	Positive
APAP	No	152.07	Unit/Enh (6490)	65.1	Unit/Enh (6490)	20	80	32	7	Positive
APAP SULF	No	230.1	Unit/Enh (6490)	150	Unit/Enh (6490)	10	120	12	7	Negative
APAP SULF	No	230.1	Unit/Enh (6490)	107	Unit/Enh (6490)	10	120	20	7	Negative

FIGURE 3.10: Mass spectrometric settings.

3.8 Statistical analyses

Group data are presented as mean +/-SE. The data analysis were performed with one-way or two-way ANOVA using the GraphPad Prism 5 statistical software. Values of $p < 0.05$ were considered statistically significant.

Chapter 4

Alginate cryogel integrated microchip for liver tissue engineering: characterization

The first part of this work concerns the study of the biomaterial, i.e. the alginate cryogel, that we propose to implement in the microfluidic device. As seen in chapter 2, the scaffold used as a 3D extracellular matrix plays an important role for 3D cellular organization. Starting from alginate material that is currently used in the laboratory for hepatic cell microencapsulation into microporous beads, we aim at producing a cryogel whose macroporosity would promote a 3D cell structure. As cells/scaffold interactions impact cells' behaviour and functions, it is essential to characterize the cryogel itself, considering both the macroscopic and microscopic levels.

First, the physical properties and microscopic structure of alginate cryogel are evaluated. The scaffold is then integrated into the microchip where its perfusion is studied from a hydrodynamic point of view. Finally, in order to achieve further cell cultures in the cryogel-integrated microchip, two methods, coating and functionalization, are explored to ensure cell adhesion.

4.1 Alginate cryogel characterization

In this part, we choose to perform all the characterizations on cylindrical samples of alginate cryogels. Indeed, after implementation in the microchip, some of the scaffold's properties are not accessible anymore. The effects of three major parameters on cryogels properties are studied: temperature of polymerization, alginate concentration and cross-linking ratio. The aim is to understand these parameters on the biomaterial's mechanical and physical properties and to select the best conditions for cell culture in the microchip.

4.1.1 Cryopolymerization: choice of the freezing temperature

Cross-linking alginate at subzero temperatures ($T < 0\ ^{\circ}C$), a mechanism known as cryopolymerization, allow the fabrication of ice-templated cryogels. Once the cross-linking reaction complete, the biomaterial is brought to room temperature, leading to the melting

of the crystals, therefore creating pores. As shown in the bibliography study, these cryogels present remarkable and tunable properties, including an interconnected and macroporous network. Among the different reaction parameters, the cryopolymerization temperature is an important one that determines the size of the ice crystals and consequently the size of the pores. At very low temperatures, the ice crystals do not have time to grow and remain small leading to a scaffold with small pores. On the contrary, at temperatures close to 0 °C, a structure with larger pores is achieved as the ice crystals have time to develop. Thus, different cryopolymerization temperatures (-20 °C, -50 °C, -80 °C) are tested to tune pore size. Cylindrical samples are prepared with a 1% (w/v) alginate concentration, in the presence of a cross-linking agent ratio AAD:EDC of 1:1. They are kept overnight at sub-zero temperature to let the reaction proceed. After cross-linking, the resulting cryogels are thawed at room temperature.

The resulting alginate cryogel cylinders are shown in figure 4.1. The samples cross-linked at -20 °C present a well defined cylindrical shape. In contrast, those cross-linked at -50 °C and -80 °C cannot maintain their shape and collapse under their weight. In this case, polymerization is likely not to be complete. Extending the cross-linking time to a few days does not change the results. The cryopolymerization temperature is thus set at -20 °C for further studies.

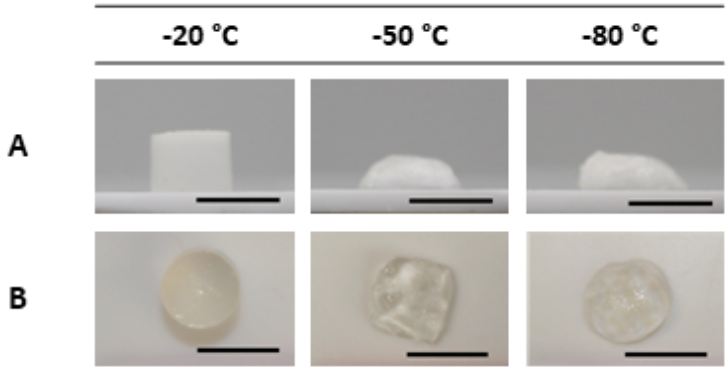

FIGURE 4.1: Photographs of cylindrical 1% (w/v) (1:1) alginate-based cryogels cross-linked at various subzero temperatures. (**A**) Side view. (**B**) Top view. (1:1) represents the (AAD:EDC) cross-linkers ratio. Scale bar = 10 mm.

4.1.2 Mechanical properties

The mechanical properties of the liver differ according to its physiological state. The Young's modulus (YM) of a healthy liver is below 4 kPa and increases in case of fibrosis [178], [179]. The more advanced the fibrosis, the higher the YM, ranging from 8 kPa to 15 kPa (Fig. 4.2). In order to mimic as closely as possible the liver physiological microenvironment, the scaffold should exhibit mechanical properties close to those measured *in vivo*. Depending on the physiological state to be reproduced, the scaffold YM need thus to be adjusted. It is therefore interesting to design cryogels with tunable mechanical

properties. For this purpose, two parameters can be tuned: alginate concentration and AAD:EDC cross-linkers ratio.

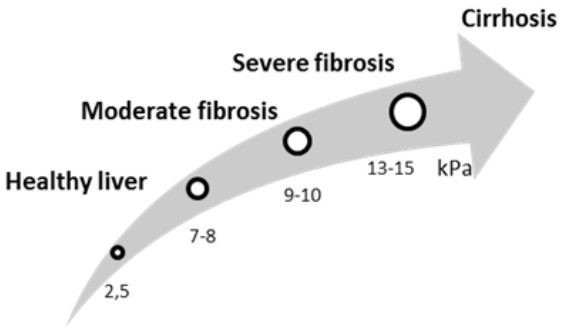

FIGURE 4.2: Evolution of the liver Young's modulus depending on its physiological state.

The alginate concentration cannot vary over a large range since the viscosity of alginate solutions rapidly increases rapidly with concentration. A too high viscosity hampers the homogeneity of the final solution that contains the cross-linkers and results in an inhomogeneous cryopolymerization that should be avoided. This limitation has been observed for solutions above 2% alginate (w/v). Therefore, two alginate concentrations are studied here: 1% and 2% (w/v).

Concerning the cross-linkers, we use AAD in excess, so that only EDC amount leads to cross-linking changes. Increasing EDC quantity increases the number of covalent bonds between the alginate chains and leads therefore to higher cross-linking. Although the variation of the (AAD:EDC) ratio does not change the protocol, it has been observed that the cross-linking occurs more quickly with the quantity of EDC increases. Three different (AAD:EDC) ratios are studied here: (1:1), (1:2) and (1:3).

Compression tests are performed on cylindrical alginate cryogels. Plotting the stress-strain curves reveals two types of mechanical behaviour shown in figure 4.3. The type "A" curve is observed for the 1% (1:1) (w/v) and 2% (w/v) (2:2) alginate samples. It corresponds to a typical stress-strain curve of porous scaffold with a linear elastic region (1) followed by a plastic one (2) and finally a densification phase (3) [180]–[182]. The type "B" curve, where the breaking point is reached, is observed for the 1% (w/v) (1:2) and (1:3) alginate samples.

The resulting YM obtained from the stress-strain curves are shown in figure 4.4. Cryogel at 1% (w/v) (1:1) displays lower mechanical properties than 2% (w/v) (2:2) cryogels, with YM of 1.5 $\pm$ 0.6 kPa vs. 6.8 $\pm$ 2.4 kPa, respectively. Similarly, increasing the amount of cross-linking agent increased the YM with much more significance. The 1% (w/v) (1:2) cryogel has a YM of 16.4 $\pm$ 4.1 kPa, more than 10 times higher than 1% (w/v) (1:1) alginate samples. Alginate at 1% (w/v) (1:3) is even stiffer with a YM of 29.4 $\pm$ 3.6

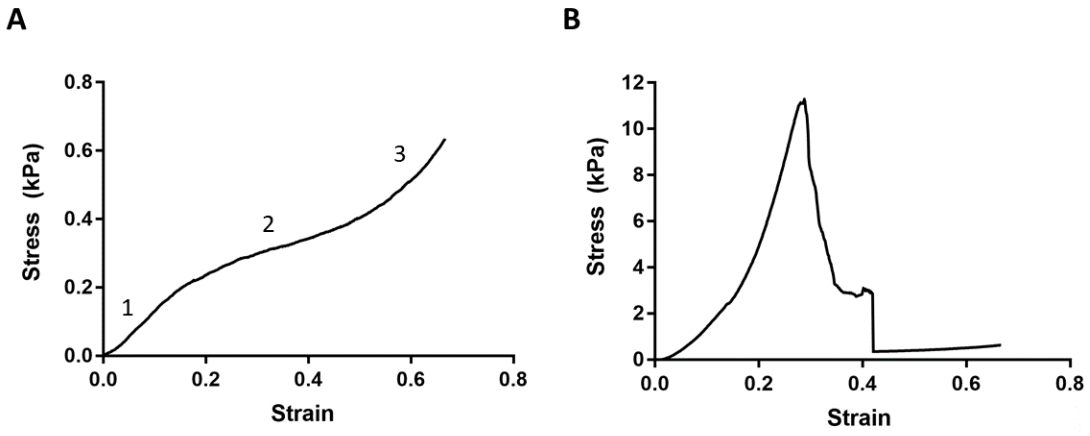

FIGURE 4.3: Stress strain curves obtained by compression test on cylindrical alginate cryogels. (**A**) Typical curve obtained for 1% (1:1) and 2% (2:2) samples with 1: elastic region, 2: plastic region, 3: densification. (**B**) Typical curve obtained for 1% (1:2) and 1% (1:3) samples.

kPa. Therefore, increasing either alginate concentration or AAD:EDC ratio results in an increase of the alginate cryogel's mechanical properties. The YM obtained are in a very wide range, showing that it is possible to adjust the mechanical properties. Moreover, the YM of the alginate cryogels at 1% (w/v) (1:1) and 2% (w/v) (2:2) are similar to that of a healthy liver tissue while alginate cryogel at 1% (w/v) (1:2) is in the range of a cirrhotic liver tissue. The alginate cryogel at 1% (w/v) (1:3) is too rigid to be compared to any liver states. To mimic the other states of the liver, it seems recommended to slightly vary the EDC content.

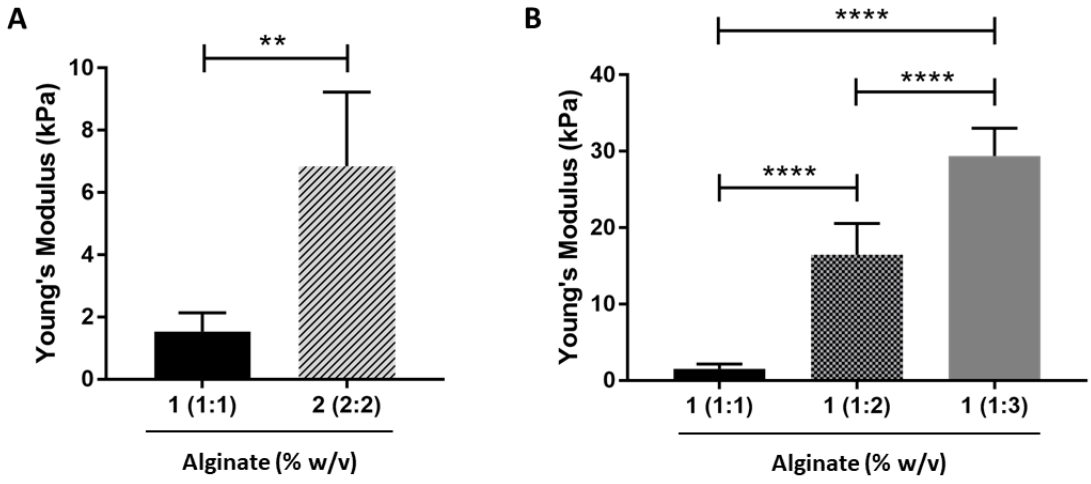

FIGURE 4.4: Young's modulus of alginate cryogels measured by compression test. (**A**) Variation of alginate concentration. (**B**) Variation of (AAD:EDC) ratio. (1:1), (1:2), (1:3) and (2:2) represent the (AAD:EDC) cross-linkers ratio. Values represent mean and SD (n=8). Data were analyzed using one-way ANOVA: ** $p < 0.01$, **** $p < 0.0001$ (n=8).

4.1.3 Degree of connectivity and swelling ratio

It is important for the cryogels to maintain the main property of hydrogels, i.e. the high water uptake capacity. The high water content is a key parameter for cell to ensure a large cell culture medium volume compared to that of the material and help to reduce dead volumes thanks to diffusion.

In order to characterize the samples, two properties are studied: the degree of pore connectivity (DC), corresponding to the volume of interconnected pores and the swelling ratio (Q_M), corresponding to the water uptake. They are measured by weighing cylindrical alginate cryogels in hydrated, dehydrated and dried states (Fig. 4.5). The obtained values for the DC and the Q_M are shown in figure 4.6 and 4.7 respectively.

FIGURE 4.5: Photographs of cylindrical alginate cryogels in hydrated, dehydrated and dried states. Scale bar = 5 mm.

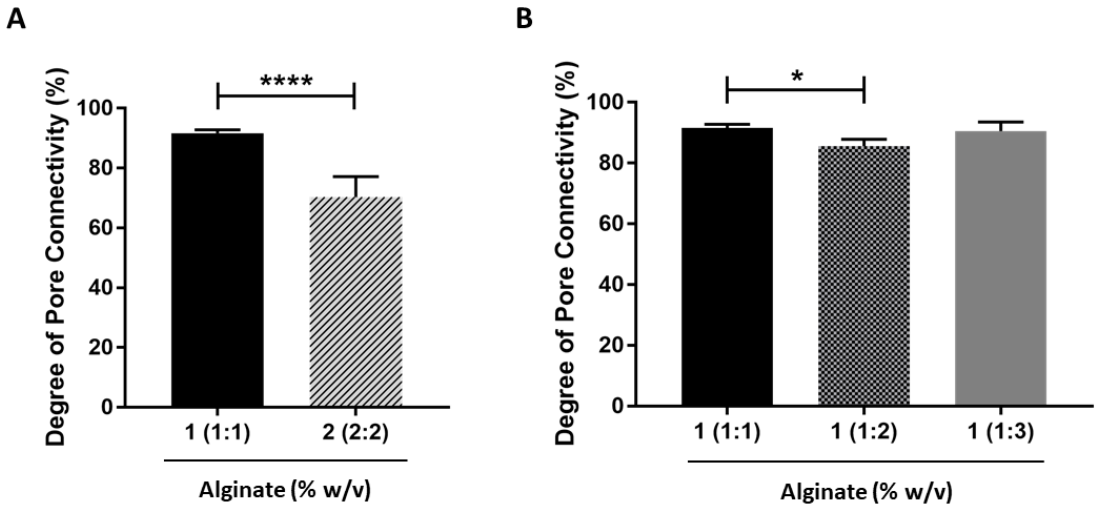

FIGURE 4.6: Degree of pore connectivity of alginate cryogels. (**A**) Variation of alginate concentration. (**B**) Variation of AAD:EDC ratio. (1:1), (1:2), (1:3) and (2:2) represent the (AAD:EDC) cross-linkers ratio. Values represent mean and SD (n=8). Data were analyzed using one-way ANOVA: * $p < 0.05$, **** $p < 0.0001$ (n=8).

The DC are higher than 70% for all the samples. However, the DC of 2% alginate cryogel is lower than the one of 1%, 70% $\pm$ 7% and 92% $\pm$ 1% respectively. Thus, alginate cryogels have a high DC and increasing the concentration of alginate appears to increase

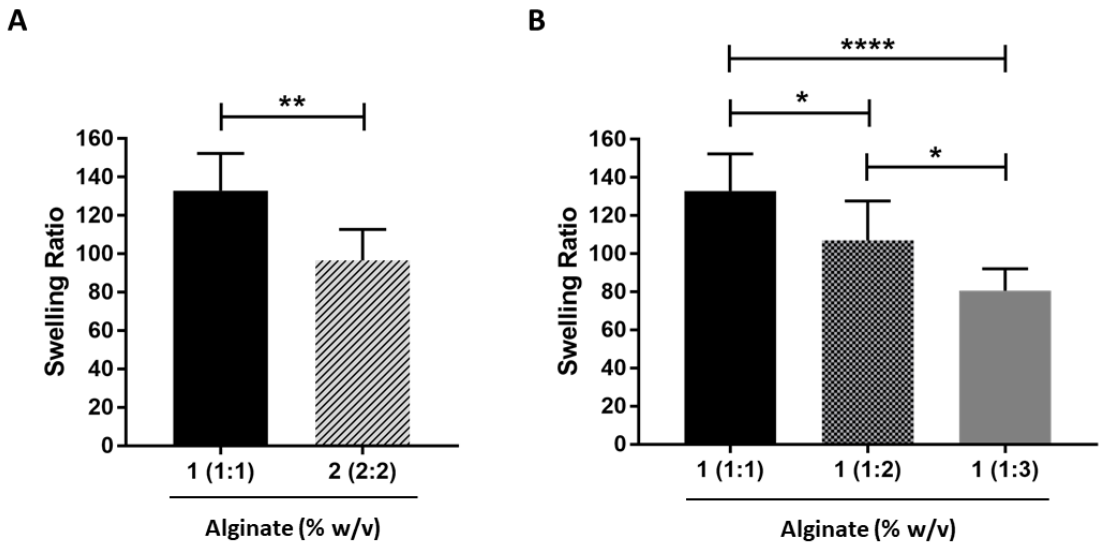

FIGURE 4.7: Swelling ratio of cylindrical alginate cryogels. (**A**) Variation of alginate concentration. (**B**) Variation of (AAD:EDC) ratio. (1:1), (1:2), (1:3) and (2:2) represent the (AAD:EDC) cross-linkers ratio. Values represent mean and SD (n=8). Data were analyzed using one-way ANOVA: * $p < 0.05$, ** $p < 0.01$, **** $p < 0.0001$ (n=8).

the DC. However, increasing the (AAD:EDC) ratio does not seem to influence this property. The obtained values for the three different (AAD:EDC) ratios are quite similar as they are all between 85% and 92%.

Regarding the Q_M, 1% alginate cryogel exhibits a ratio of 133 $\pm$ 20, which is higher than 97 $\pm$ 16 for 2% alginate cryogel. In the same way, 1% (1:1) alginate cryogel has a higher Q_M than 1% (1:2) and 1% (1:3) alginate cryogel: 133 $\pm$ 20, 107 $\pm$ 21 and 81 $\pm$ 12 respectively. Thus, increasing the alginate concentration or the (AAD:EDC) ratio decreases the water uptake of the cryogels.

The variations of the DC and the Q_M values show that the physical properties of the alginate cryogels change according to the alginate concentration and cross-linking. A modification in the macroscopic properties is probably due to a microscopic change. It is thus important to study the samples at this level in order to propose a multiscale analysis.

4.1.4 Morphology

In order to perform 3D cell cultures, the alginate cryogels must exhibit a porous structure. Moreover, the pores should be of macro-sized and interconnected to allow the cell dispersion within the scaffold but also the supply of nutrients and the removal of waste.

To study the structure of the alginate cryogels, the samples are observed under scanning electron microscopic (SEM) (Fig. 4.8). SEM images of 1% (w/v) (1:1) and 2% (w/v) (2:2) alginate cryogels show highly porous structures. Large and interconnected pores with irregular shapes are observed. However, this structure is not present for 1% (w/v) (1:2) and (1:3) alginate cryogels. Both conditions do not seem to create

pores. Therefore, increasing the (AAD:EDC) ratio causes the loss of the porous structure whereas increasing the alginate concentration does not seem to change it. These observations confirm and explain the previous results obtained during the mechanical characterizations: the 1% (w/v) (1:2) and (1:3) alginate cryogels have a stress-train curve different from that typically observed for porous scaffolds, which appeared to lack in these cases.

Although the variation of (AAD:EDC) ratio was an interesting way to modulate the mechanical properties of the scaffold, it does not allow maintaining a macroporous structure, in the conditions we have investigated. Therefore, the 1% (w/v) (1:2) and (1:3) alginate cryogels are not selected for the next steps of the project.

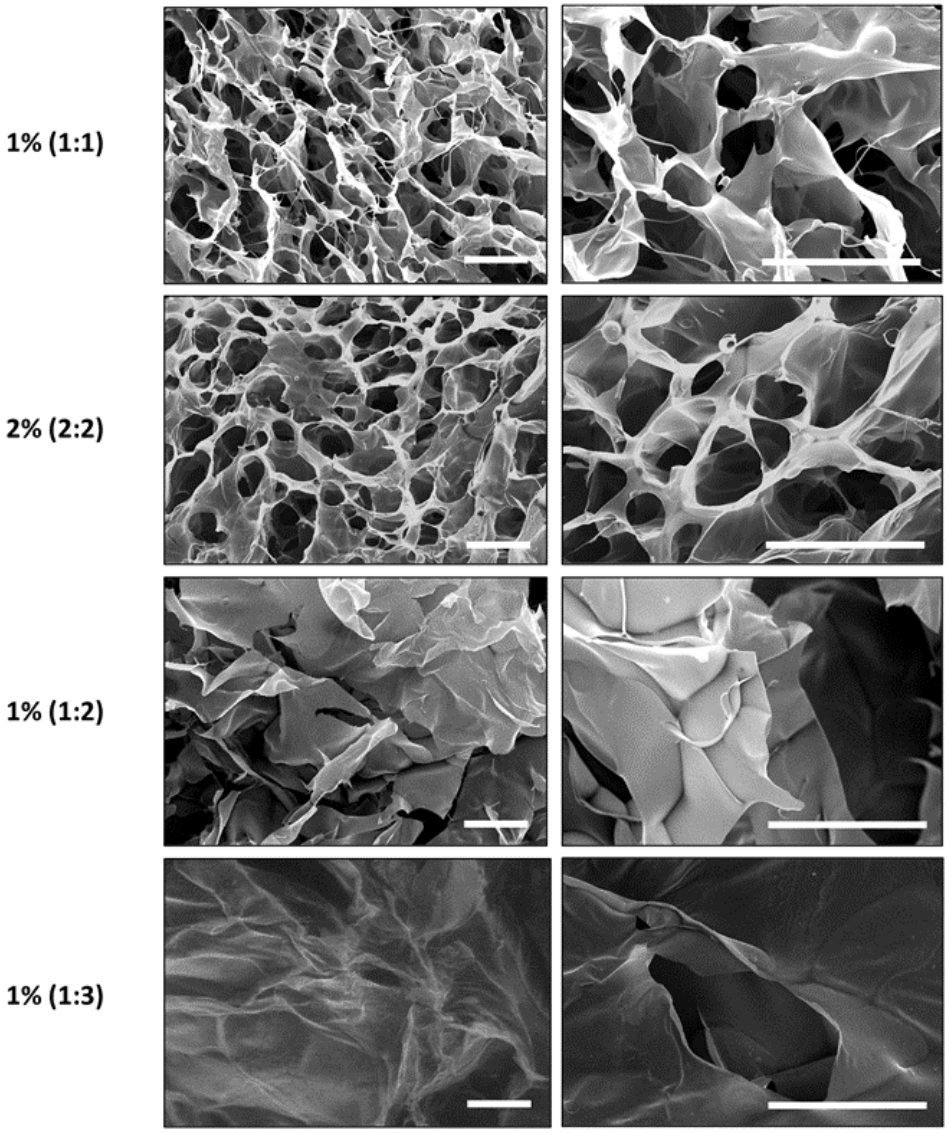

FIGURE 4.8: SEM images of alginate cryogels depending on the alginate concentration and on the (AAD:EDC) ratio. Scale bar = 200 μm.

To study the microstructure in more details and to determine if there is any difference between the 1% and 2% (w/v) alginate cryogels, the pore size is measured for sample (Fig. 4.9). The size of the pores is quite heterogeneous: it ranges from 20 μm up to 340 μm for both alginate concentrations. However, the distributions seem to follow a Gaussian curve centered around 100 μm. The mean pore size is 95 $\pm$ 48 μm and 109 $\pm$ 64 μm for 1% and 2% alginate respectively, corresponding to macropores. Besides, the difference between the pore sizes is not significant meaning that the alginate concentration does not influence this feature.

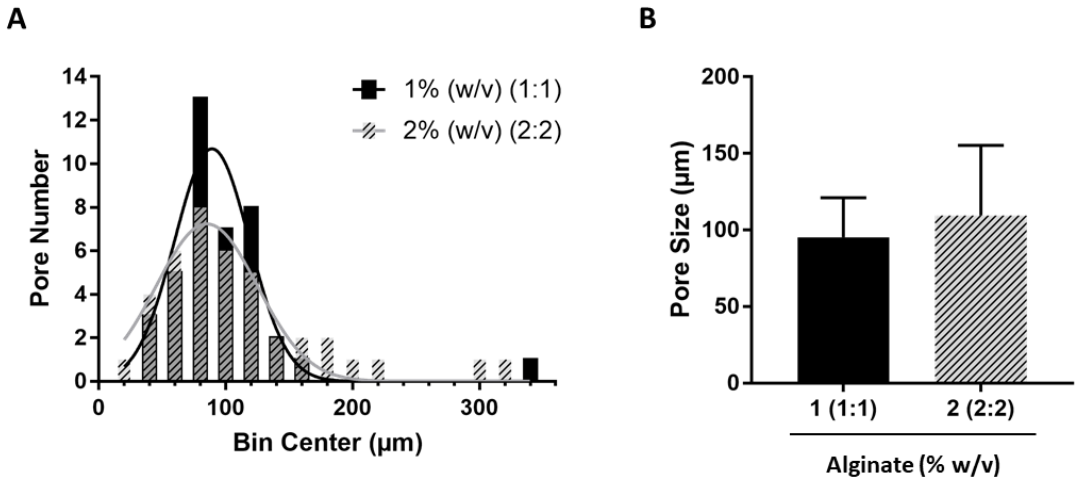

FIGURE 4.9: Pore characterization of alginate cryogels. (**A**) Pore size distribution and (**B**) average pore size of alginate-based cryogels. (1:1) and (2:2) represent the (AAD:EDC) cross-linkers ratio. Values represent mean and SD (n=4, N=10).

4.2 Implementation of alginate cryogel in the microchip

In this part, we study if the selected conditions, i.e. 1% (w/v) (1:1) and 2% (w/v) (2:2), are still suitable when the alginate cryogel is integrated within the microchip.

To obtain such a cryogel-integrated microchip, the alginate and cross-linking agents solution is injected in the microchip and the same cryopolymerization process is applied *in situ*.

4.2.1 General characterization

After cryopolymerization, the microchip is observed under optical microscope (Fig. 4.10). The microsystem 3D structure is visible and easily recognizable with its squares and arrows. The alginate cryogel is also easily visible corresponding to the filaments. They are well distributed, occupying all the available space, from the inlet to the outlet. However, it is difficult with this method to be sure that the alginate cryogel occupies the microchip from the bottom to the top, including the space available between the microstructures.

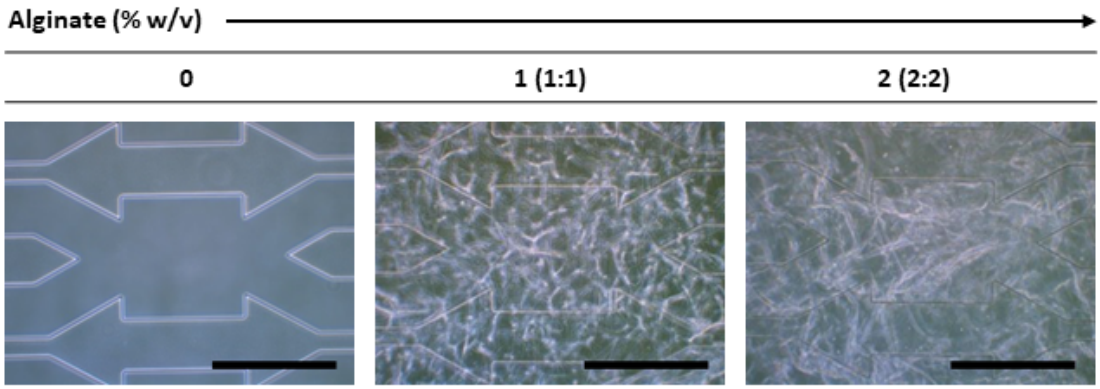

FIGURE 4.10: Microscopic observation of cryogel-free and alginate-based cryogel-integrated microchips. (1:1) and (2:2) represent the (AAD:EDC) cross-linkers ratio. Scale bar = 300 μm.

In order to observe the alginate cryogel across the whole height of the microchip, alginate is tagged with aminofluorescein after its cross-linking. The samples are then observed under confocal microscopy performing stacks from the bottom (0 μm) to the top (200 μm) of the microchip (Fig. 4.11). From 0 μm to 100 μm, corresponding to the lower face (microstructured), the porous structure of the alginate cryogel can be observed ensuring its location inbetween the microstructures of the microchip, here in a square. From 100 μm to 200 μm, corresponding to the upper face (not microstructured), the alginate cryogel is also present with a porous structure. Thus, the alginate cryogel occupies the entire height of the microchip including the space between the microstructures and maintains a macroporous structure when formed *in situ*.

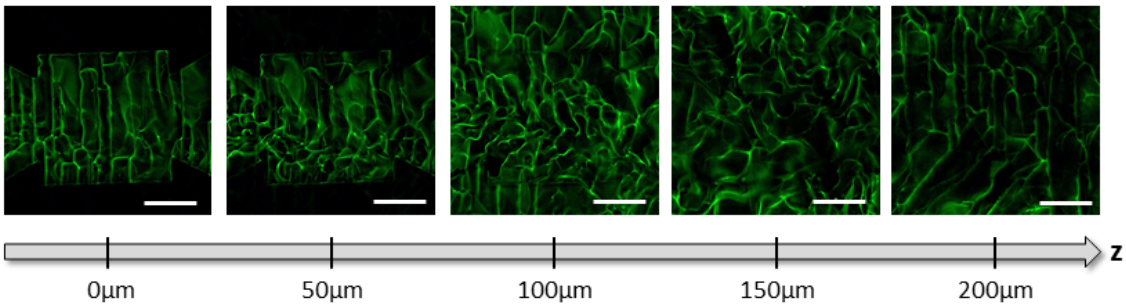

FIGURE 4.11: Confocal images of fluorescently-labeled 1% (w/v) (1:1) alginate-based cryogel-integrated microchips at various depths. (1:1) represents the (AAD:EDC) cross-linkers ratio. Scale bar = 150 μm.

4.2.2 Hydrodynamic characterization

The alginate cryogel occupies the whole volume of the microchip. Although the pores are large and interconnected, the presence of the cryogel can lead to an inhomogeneous perfusion and an excessive pressure on cells. To investigate the additional resistance to flow that might be induced by this structure filling spaces that are classically free, the

pressure applied at the inlet of the microchip to reach the target flow at the outlet is monitored in an open loop circuit (Fig. 4.12). The flow rate varies from 5 μL to 30 μL, corresponding to the range usually applied for cell culture in this microfluidic system [162], [183].

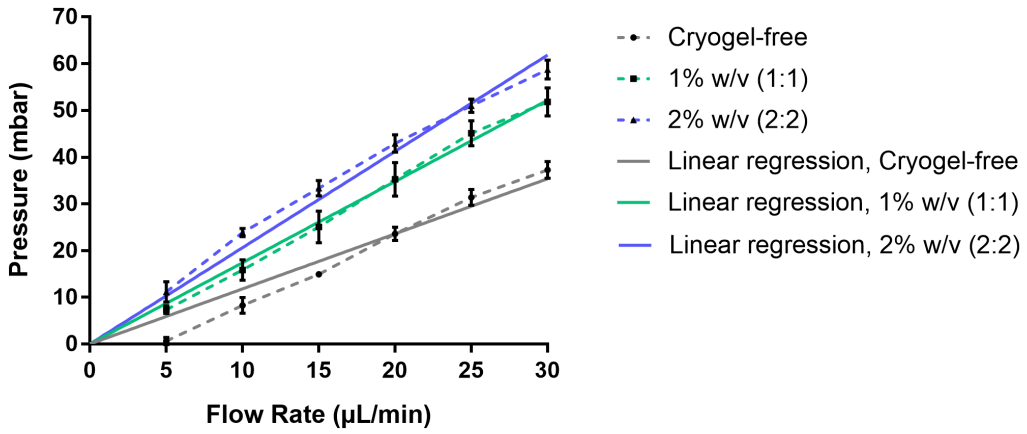

FIGURE 4.12: Hydrodynamic characterization of cryogel-free and alginate-based cryogel-integrated microchips (n = 3).

We propose to use Darcy's law to describe the fluid flow through the porous cryogel structure which is in the microchip. According to this law, the flow rate Q is proportional to the difference of pressure Δp, between the inlet and the outlet of the microchip, as defined by the following equation:

$$Q = \frac{kA}{\mu L}\Delta p$$

with Q the flow rate, k the permeability of the medium, A the cross-sectional area, μ the dynamic viscosity of the fluid, L the length of the samples and Δp the pressure drop. A linear regression passing through the origins can therefore be calculated for each operating condition. The design of the microchip itself resulted in a very poor resistance to flow, under the tested flow rates. The Darcy's law fits well with the experimental data (linear regression of Fig. 4.12). The calculated slopes are 2.06, 1.74 and 1.18 mbar/μL.min for 2% (2:2), 1% (1:1) alginate cryogel-integrated and cryogel-free microchips respectively. These slopes are inversely proportional to the permeability of the corresponding alginate cryogel which is the only variable as the cross-sectional area, the dynamic viscosity and the length remain unchanged.

The inlet pressures measured for cryogel-free microchips are lower than those measured for cryogel-integrated microchips. Therefore, integrating the cryogel within the microfluidic device results in an increase of resistance to flow. Besides, we can observe that the permeability is lower for 2% (w/v) (2:2) than for 1% (w/v) (1:1) alginate cryogel-integrated microchips. The permeability of the cryogel appears thus to be related to alginate concentration: the higher the alginate concentration, the lower the hydraulic

permeability. However, this additional resistance remains acceptable within the workable flow rates used for cell culture: at 10 μL/min, the pressure needed is 15.8 mbar and 23.9 mbar for 1% (w/v) (1:1) alginate cryogel and 2% (w/v) (2:2) alginate cryogel respectively.

In order to perform cell culture, the condition with the lowest inlet pressure is preferred to ensure a correct microfluidic circulation and to avoid excess pressure on the cells. The 1% (w/v) (1:1) alginate cryogel is thus selected as it exhibits the lowest resistance to flow. Moreover, as seen in the previous sections, this cryogel presents all the characteristics of a macroporous hydrogel. In the next steps of the study, all the alginate cryogel-integrated microchip are realized with the 1% (w/v) (1:1) condition.

4.3 Modification of alginate cryogel for cell culture

The composition and charge of the alginate do not promote cell adhesion. It is therefore essential, as for any non adherent surface, to add proteins or peptides allowing the cell adhesion on the scaffold. In doing so, we investigate two methods in the following sections: the cryogel functionalization with the arginine, glycine and aspartate (RGD) peptide and the cryogel coating with collagen.

4.3.1 RGD functionalization

The RGD peptide is an amino acid sequence that mediates cell binding. It is found in different proteins of the ECM such as fibronectin or laminin [184], [185]. It can thus be used to allow cells attachment to a scaffold. We choose to functionalize alginate before its cross-linking with the G_4RGDSP peptide, as described in chapter 3. The RGD grafted alginate was then cryopolymerized inside the microchip to obtain the cryogel. Thereafter, HepG2/C3A were seeded at 1 million cells/microchip and cultured for 4 days to study the cryogel/cells interaction. They are observed under epifluorescent microscope (Fig. 4.13).

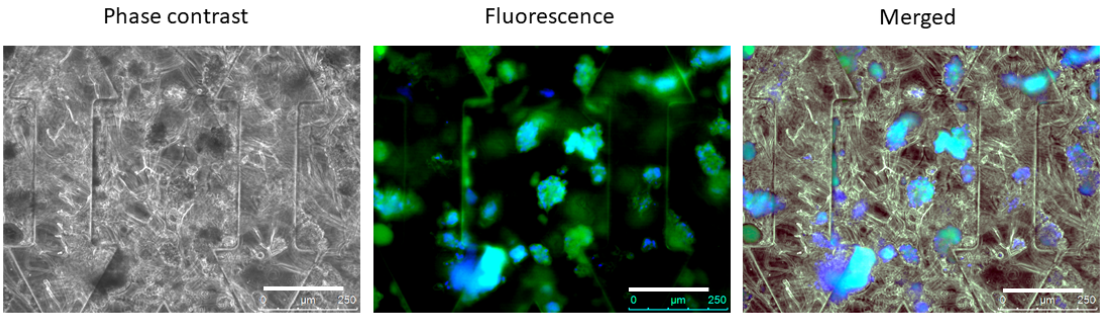

FIGURE 4.13: Observation of HepG2/C3A cultured in RGD grafted alginate cryogel-integrated microchip at day 4 using fluorescence microscopy. Cytoskeleton (green) and nucleus (blue). Scale bar = 200 μm.

After injection, the cells appear individually distributed in the microchip. However, at day 4, aggregates can be distinguished. Only a few cells are likely to adhere on the alginate cryogel and then proliferate or attach to the others forming thus aggregates. The cells that did not bind to the scaffold are probably flushed out of the microsystem with the flow.

The RGD quantity grafted to the alginate is rather low, about 2.3% (w/w), as this peptide is expensive. This could explain the small number of cells that successfully adhere on the scaffold. Moreover, the cross-linking is performed after the functionalization, the RGD sequence may thus be inaccessible to the cells depending on its configuration during the alginate cross-linking. This probably further decreases the number of available peptides for cell binding.

4.3.2 Collagen coating

The alginate cryogel was coated with collagen type I after its cross-linking inside the microchip to allow cell adhesion. Consequently, HepG2/C3A were seeded at 1 million cells/microchip and cultured for 4 days to study the cryogel/cells interaction. They were observed under epifluorescent microscope (Fig. 4.14).

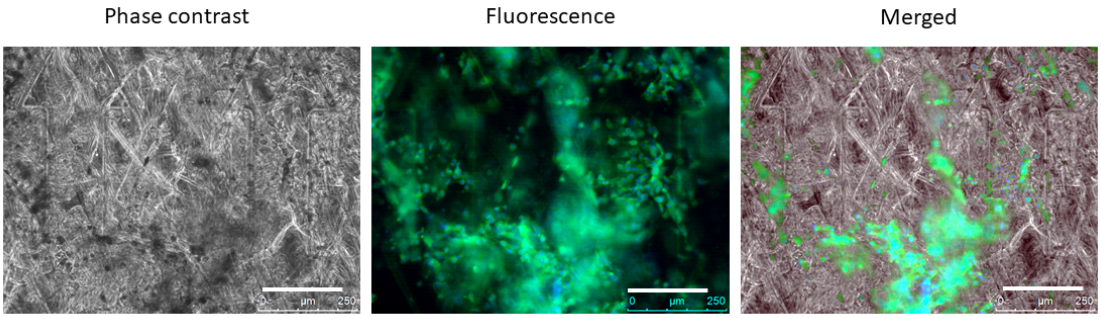

FIGURE 4.14: Observation of HepG2/C3A cultured in collagen coated alginate cryogel-integrated microchip at day 4 using fluorescence microscopy. Cytoskeleton (green) and nucleus (blue). Scale bar = 200 μm.

After injection, the cells are individually distributed in the microchip. At day 4, several individual cells are still present in the alginate cryogel. It seems that the majority of them are bound to the scaffold as they did not go away with the flow.

The amount of cells that successfully bound to the alginate cryogel suggests a high quantity of collagen available for the cells. Moreover, as the coating is performed after the cryogel cross-linking, the collagen adsorbed on the alginate remains accessible. The collagen was stained to observe the coating as shown in figure 4.15. The coating seems to be quite homogeneous on the alginate cryogel.

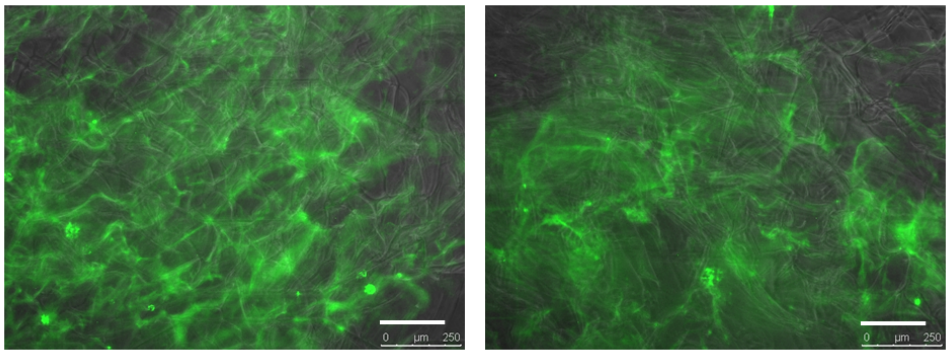

FIGURE 4.15: Collagen coated alginate cryogel-integrated microchip observed using fluorescence microscopy. Immunostaining: collagen (green). Scale bar = 200 μm.

These results demonstrate that RGD functionalization fosters the aggregation of cells into spheroids whereas collagen coating results in a homogeneous cell growth. This is probably due to a larger amount of binding sites available on the collagen-coated alginate cryogel compared to the RGD functionalized one. Since the collagen coating allows a homogeneous cell growth, it has been chosen for the following of the study.

4.4 Discussion and conclusion

Previous studies have shown that 3D organization of liver cell, either in soft gels or as spheroids, improve their long-term culture and functions compared to conventional cultures, as seen in chapter 2. The same positive effects have been observed when cells are submitted to moderate flow in microchips. Combining these approaches, 3D spheroids and medium perfusion, gave rise to a novel culture concept, namely spheroids-on-chip.

Here, our aim is to introduce another innovative culture concept, through the perfusion of a gel in a microchip. To the best of our knowledge, it is the first attempt to design, fabricate and validate such a system, combining 3D scaffold and medium perfusion. This new culture concept could meet the expectations of the pharmaceutical industry, regarding both the amount of cells to use and the maintenance of biological functions.

Based on the literature and our expertise, we choose alginate as material for the scaffold. Alginate can be cross-linked to form hydrogels, hydrophilic polymeric networks capable of absorbing large amounts of water or biological fluids. Such hydrogel scaffolds are non-toxic and have been widely used for soft tissue reconstruction [106], [107]. However, hydrogels are typically mesoporous, leading to an unfavorable microenvironment that entraps and constrains encapsulated cells, and ultimately preventing their cellular organization in 3D. To overcome this limitation, we propose to perform its cross-linking at subzero temperatures (T < 0 °C), a mechanism known as cryopolymerization, allowing the fabrication of ice-templated scaffold. The alginate hydrogels used in biomedical applications are mainly ionically cross-linked. Their properties can be modified by

changing the alginate concentration but also the cation used for its gelation and its concentration [186]. However, these hydrogels are unstable in time. To avoid this, a chemical cross-linking with AAD and EDC is proposed in our study, following protocols described in chapter 2 and 3. Operating conditions should be adjusted to obtain the most adapted alginate scaffold for implementation in microsystems.

In this part, we thus first focus on the effect of the temperature, the alginate concentration and the amount of cross-linking agents on the physical and mechanical properties of the porous scaffold. Table 4.1 summarizes this study.

Alginate Concentration	1% (w/v)	1% (w/v)	1% (w/v)	2% (w/v)
AAD:EDC ratio	1:1	1:2	1:3	2:2
YM (kPa)	1.5 ± 0.6	16.4 ± 4.1	29.4 ± 3.6	6.8 ± 2.4
DC (%)	92 ± 1	82 ± 2	90 ± 3	70 ± 7
Q_M	133 ± 20	107 ± 21	81 ± 12	97 ± 16
Mean Pore Size (μm)	95 ± 48	ND	ND	109 ± 64
Hydraulic Resistance (mbar/μL.min)	1.74	ND	ND	2.06

TABLE 4.1: Summary of alginate cryogel properties. ND: No Data.

In view of adjusting the pore size, the first parameter to play with is the freezing temperature so as to modify the size of ice crystals. Unfortunately, the alginate cryogels prepared at -50 °C and -80 °C collapse unlike those obtained at -20 °C. The kinetics of the reaction with the EDC is probably the limiting factor: the lower the temperature, the slower the reaction is. At -50 °C and -80 °C, the reaction is so slow that cross-linking is not complete, even after a few days. We therefore set the freezing temperature at -20 °C in agreement with literature data where cryogelation with EDC is classicaly performed in the range of -10 °C to -20 °C.

We then focus on alginate concentration and cross-linkers ratio, in link with realistic operating conditions such as alginate viscosity and reaction kinetic. We first measure the mechanical properties of the cryogels. This parameter is important to mimic various physiological and physiopathological states of the liver, as already explained, but also because the substrate stiffness has an impact on liver cell response [187], [188]. As expected, the YM of the cryogel increases with alginate concentration [189]. Interestingly, changing the AAD:EDC ratio (increasing the amount of EDC) affects much more the scaffold stiffness. Henderson et al. observe the same trends with hyaluronic acid cryogels cross-linked with EDC but to a lesser extent (YM from 1 to 10 kPa) [190]. Using 4 couples of parameters allow us to tune the cryogel YM from 1 to 30 kPa, which are relevant to mimic healthy and cirrotic liver tissue. To get YM corresponding to fibrosis, we suggest to vary the AAD:EDC between 1 and 2, rather than changing the alginate concentration. Increasing the alginate concentration over 2% is not recommended because of the high solution viscosity that is then difficult to homogenize and inject in the microchip.

We also check that the basic characteristics of cryogel are maintained. On the one hand, the Q_M decreases with alginate concentration and amount of crosslinking agent

EDC, but remains high, meaning that the cryogel keeps its water/culture medium uptake properties. Similar results have been observed with hyaluronic acid cryogels cross-linked with EDC: the more densely cross-linked gels show less swelling in the same way as more concentrated polymer gels [190]. On the other hand, the DC also decreases with alginate concentration but is not affected by the AAD:EDC ratio. Concerning the microstructure of cryogels, the porosity is essential not only for the nutrients diffusion and waste removal but also for the future integration of the scaffold within a microchip. Large and interconnected pores are required to let the flow go through. We observe that an increase in cross-linkers results in a change of morphology and especially a loss of porosity. Therefore, the 1% (w/v) (1:2) and 1% (w/v) (1:3) alginate cryogel are finally excluded. The interconnected structure and pore size of 1% (w/v) (1:1) and 2% (w/v) (2:2) alginate cryogels, ranging from 20 μm to 340 μm, correspond to scaffolds used for liver tissue engineering. Tripathi et al. synthesized at sub-zero temperature an agarose-chitosan scaffold whose pore size is in the range of 10 μm to 120 μm [191]. In the same way, Glicklis et al. developed a physically cross-linked alginate sponges by the freeze-drying method that display a highly porous structure with interconnected pores and pore sizes ranging between 100 μm to 150 μm [115]. One can also cite the work of the group of Kumar. Different composition of cryogels are studied, such as agarose-alginate with a macroporous interconnected structure and pore size of 122 m [192]. However, these cryogels present low Q_M and high mechanical stiffness, up to 73 kPa, making them less suitable for liver tissue engineering.

To summarize these results, an increase in alginate concentration maintains the porous structure but the mechanical properties remain limited; on the contrary, an increase in cross-linking agents significantly increases the mechanical properties but to the detriment of the structure's porosity, which is lost. Based on these results, it seems that a compromise between alginate concentration and cross-linkers ratio must be found to reach adapted mechanical properties while maintaining cryogel features. The parameters selected for cryogel preparation were 1% and 2% alginate concentration with proportional AAD:EDC ratio, i.e. 1:1 and 2:2 respectively. These cryogels have a macroporous structure and their mechanical properties correspond to a healthy liver. However, we did not succeed to find parameters consistent with diseased liver tissue while maintaining a macroporous structure. To achieve this, alginate concentrations between 1% and 2% (w/v) should be tested with AAD:EDC ratio between 1:1 and 1:2. As the ranges are very narrow, a high degree of precision is required. Another possibility could be the combination between two polymers, such as alginate with agarose, a polymer forming rigid structures [192].

After characterizing and selecting the cryogels, we work on their integration in the microchip used in the laboratory. The cryogel appears to fill completely the microchip. As the system is subsequently perfused, it is essential to characterize the resistance of cryogels to flow. Under working flow rates, i.e. from 0 μL/min to 30 μL/min, we observed that increasing alginate concentration increases the flow resistance of the cryogel.

Tripathi et al. confirm that the cryogel's permeability decreases as the polymer concentration increases [192]. To reduce the resistance to flow, the design of the microchip could be changed. Indeed, the current design is only 200 μm high with microstructures up to mid-height. Preliminary investigations with unstructured microchip are not successful as tearing of the alginate cryogel is sometimes observed. Therefore, it seems that at least few microstructures are needed to act as anchor points for the cryogel and thus prevent it from tearing during perfusion.

In order to culture cells in the cryogel-integrated microchip, we finally explore two methods to get the cells to adhere to the alginate, an inert polymer. The functionalization with RGD peptide leads to a spheroid cell growth whereas collagen coating leads to a homogeneous cell growth.

The spheroids culture is the most widespread in the literature and the formation of spheroids achieved here is comparable to some studies. Yan et al. cultured primary hepatocytes on polystyrene porous fibrous scaffold grafted with galactose and RGD. The cell infiltrated the structure more than 100 μm and aggregated into 3D clusters after a few days [193]. It may be noted that the culture of spheroids is feasible in porous scaffolds without any peptide grafting. Rat hepatocytes seeded in porous alginate scaffold aggregated within 24 h and reached an average diameter in the range of the structure's pore size [115]. However, spheroids in these studies are not grown under perfusion. We choose here to validate the classical protocol of collagen coating.

Although the use of collagen allowed cell adhesion, we are aware that this protein could not be the most suitable for a final cryogel-integrated microchip. Indeed, collagen is a protein abundantly found, up to 50%, in the ECM of a fibrous liver [194]. A coating of fibronectin, the main ECM component of the liver, could therefore be preferable and should be investigated in further studies.

In this first part, we establish the proof of concept for the integration a porous 3D cryogel into a microchip. We hypothesize that such combination would be valuable for liver tissue engineering. This will be investigated in the next chapters. However, we can already here propose some additional studies that should be performed to improve this device.

The design of the microchip should allow a homogeneous distribution of the flow as previously shown by [159]. However, the integration of a porous structure may disturb this flow by creating preferential paths. Thus, some areas might be more irrigated than others, which leads to heterogeneity in cell culture. In order to go further in this study, the formation of preferential paths in the cryogel-integrated microchip should be evaluated. If the design of the microchip is no longer suitable in the presence of cryogel, a new design could be studied to limit any preferential paths.

We demonstrated that the cryogel-integrated microchip can be used to culture cells in two different ways: homogeneous and spheroid cell growth. In the same way, the Kumar's group developed a 3D porous cryogel, composed of alginate and gelatin, allowing

to perform these two culture cell types depending on the cross-linking agent [195]. The synthesis with glutaraldehyde leads to a homogeneous cell growth whereas the synthesis with EDC, without any grafted peptide, leads to a spheroid cell growth. Although we choose homogeneous cell growth by collagen coating in the following of the study, it could be interesting to investigate the spheroid cell growth, with or without RGD functionalization.

Chapter 5

Feasibility study : human liver cancer cell line HepG2/C3A culture in alginate cryogel integrated microchip

The second part of this work focuses on the culture of hepatic cells in the alginate cryogel-integrated microchip described in chapter 4. As seen previously, getting close to the *in vivo* conditions, that is to say creating a perfused 3D environment, should allow a more relevant cellular response. However, it is first necessary to ensure that cells can live and be functional within this device. Therefore, the well-known hepatic cell line, HepG2/C3A, is chosen for this feasibility study. Cell culture is performed in microchips containing the alginate 1% (w/v) (1:1) cryogel that has been previously selected and in cryogel-free microchips in order to compare the cellular response between these conditions.

First, the cell viability and organization within the microchip are studied up to 6 days in culture. The metabolic functions are then characterized by albumin and glucose quantifications. Moreover, the xenobiotic activity of the cells is assessed by APAP exposure. The synthesis of ECM and the possibility to remove the alginate cryogel are finally considered in the last part of the chapter.

5.1 Cell viability and structure

HepG2/C3A cells are seeded at 500 000 cells/microchip and cultured for 6 days with a 10 μL/min perfusion (see 3.5.2). Determining the cells viability and proliferation in the alginate cryogel-integrated microchip is the first step in this feasibility study.

The cell viability is assessed with a dead cell staining assay at day 2, 4 and 6. The samples are observed under confocal microscopy and stacks images are performed from the bottom to the top of the microchip for each condition: cryogel-free and cryogel-integrated microchip (Fig. 5.1). The images show a negligible amount of dead cells (red), meaning that most of them remain viable in both conditions. Cell proliferation is obvious from day 2 to 6 but a difference in the cell distribution between both conditions can be noticed. Indeed, in the cryogel-free microchips, cells are located in the lower part, between 0 and 100 μm from the bottom: they line the microstructures. In the microchip

with alginate cryogel, cells are found over the whole height of the microchip, from 0 to 200 μm as they occupy the 3D cryogel. Cells' density appears to be lower in the presence of alginate cryogel, but this is most likely due to a "volume effect" since they are not concentrated on a specific level.

Under optical microscope, it is difficult to distinguish the 3D cell structures (Fig. 5.2). In the cryogel-free microchips, HepG2/C3A cover the collagen-coated surfaces as seen during the viability assay and form a dense confluent layer comparable to that observed in classical 2D culture. Their distribution is less clear in cryogel-integrated microchip since we observe microstructures, alginate filaments and cells at the same time.

SEM observations of samples'cross-sections are also performed to better understand cell 3D organization (Fig. 5.3). The images confirm the previous results: without alginate cryogel, the cells cover the microstructures and proliferate "layer-by-layer" but are not able to colonize the whole thickness of the microchip, i.e. to reach the top surface. In the cryogel-integrated microchip, they are located from the bottom to the top of the microchip, forming a tissue-like structure. Moreover, we can observe spaces/holes corresponding to the cryogel's pores and by which the cell culture medium goes through.

5.2 Metabolic activities

The previous results are encouraging but cell functionality needs to be studied. Indeed, the high viability of the cells does not ensure that they are functional. Especially for hepatocytes, it is known that culture conditions influence functions. Here, we focus on glucose consumption and albumin production, , as first assays regarding the physiological functionality of HepG2/C3A. The cell culture medium is stored at each medium change, i.e. at day 2, 4 and 6, for quantifications. Before providing and analyzing the results, we would like to point out two specificities of such culture in microfluidic devices.

Since work volumes are very small, any changes have to be considered to ensure the results' accuracy. In order to take into account the phenomenon of medium evaporation and some occasional leaks, the total volume is measured at each sampling (Table 5.1). At the milliliter scale, the variations cannot be neglected. This volume is then used to calculate the different amounts released or consumed.

Microchip	**N**	**V_{Day2} (mL)**	**V_{Day4} (mL)**	**V_{Day6} (mL)**
Cryogel free	1	3.75	3.85	3.80
	2	3.70	3.90	3.80
	3	3.00	3.10	3.45
	4	3.10	3.55	3.50
1% (w/v) (1:1) alginate cryogel	1	3.65	3.80	3.82
	2	3.60	3.90	3.96
	3	3.40	3.60	3.75
	4	3.10	3.40	3.40

TABLE 5.1: Volume measured for each microchip at day 2, 4 and 6 (Initial volume: 4 mL).

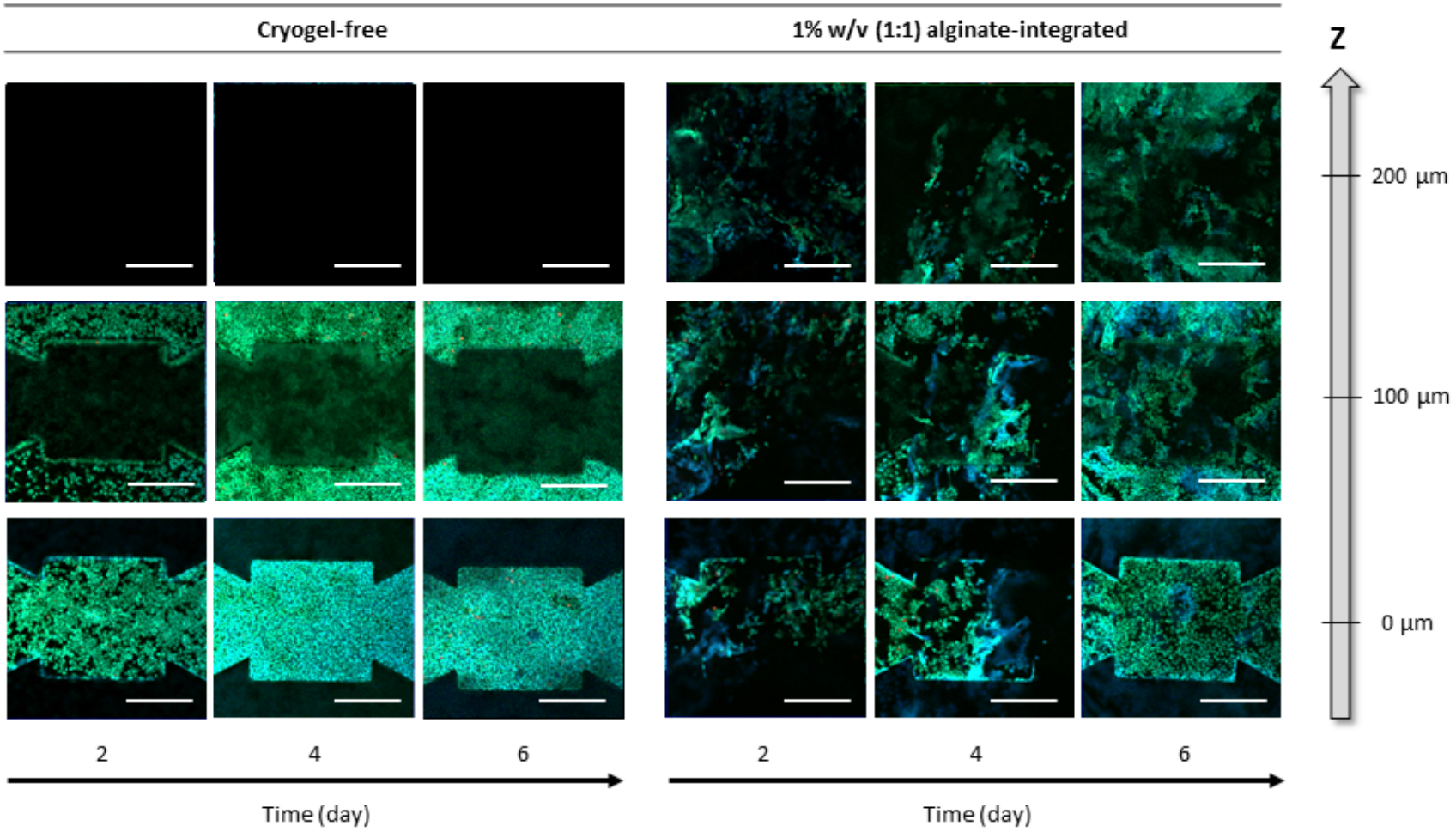

FIGURE 5.1: Cell viability of HepG2/C3A cells in cryogel-free and cryogel-integrated microchips. Confocal imaging at various time points and depths within the microchip with cell viability and mortality. (1:1) represents the (AAD:EDC) cross-linkers ratio. Cell staining: dead cell (red), cytoskeleton (green), and nucleus (blue). Scale bar = 150 μm.

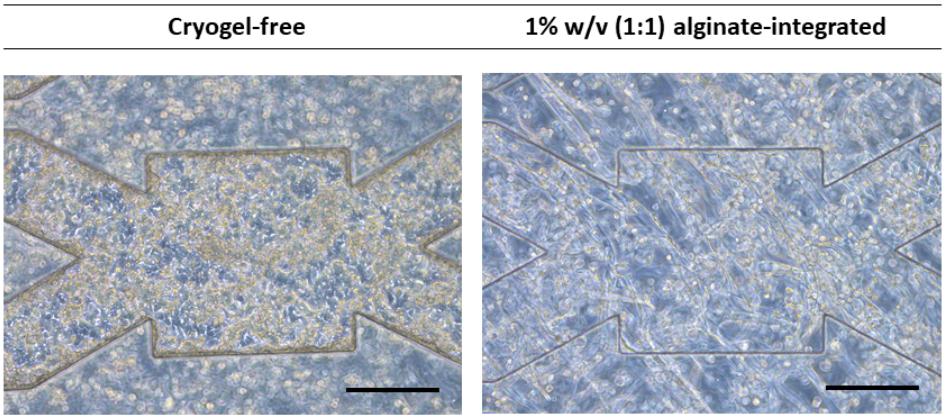

FIGURE 5.2: Microscopic observations of HepG2/C3A cultured in microchip at day 6. Scale bar = 200 μm.

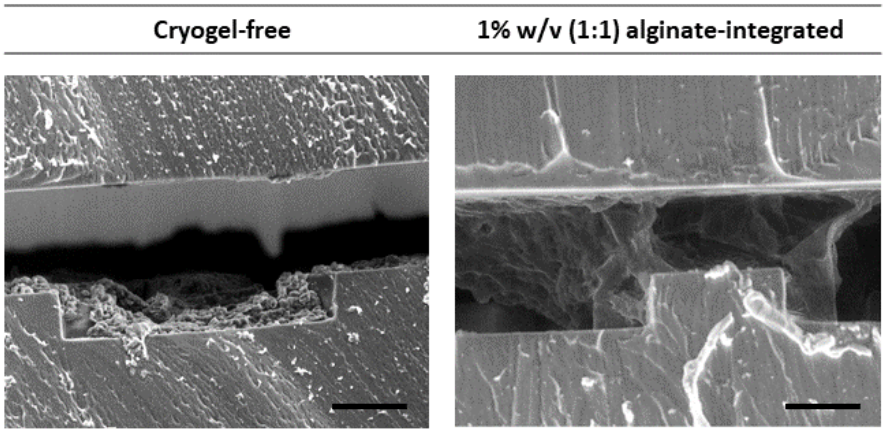

FIGURE 5.3: Cross-sectional SEM images of HepG2/C3A cultured at day 6. Scale bar = 100 μm.

Results are generally normalized by cell number in order to compare data. However, cell counting is difficult to perform in 3D culture, in the presence of a scaffold, and even more when it is within a microchip. We perform cell counting after alginate lyase and trypsin treatment (Table 5.2). Although the cell numbers obtained for the cryogel-free microchip show a cell proliferation, it is lower at day 2 and 4 than the initial number of cells seeded (0.5 million). Moreover, the results obtained for the alginate cryogel-integrated microchips are not consistent with the microscopic observations. Overall, the cell number seems to be much lower than reality. Since the number of cells is not known, the following quantifications cannot be normalized by cell number and are expressed in quantity per hour.

Microchip	N	Cell nbr_{Day2} (10^6)	Cell nbr_{Day4} (10^6)	Cell nbr_{Day6} (10^6)
Cryogel	1	0.172	0.102	1.396
free	2	0.1	0.308	1.62
1% (w/v) (1:1)	1	0.254	0.456	0.528
alginate cryogel	2	/	0.329	0.569

TABLE 5.2: Cell number counted with a Malassez's hemocytometer at day 2, 4 and 6 (Initial cell density: 0.5 million cells/microchip).

5.2.1 Glucose consumption

The consumption of glucose in the cell culture medium ensures that cells present a metabolic activity since the glycogenesis is negligeable for HepG2/C3A cell line. The results obtained are shown in figure 5.4.

The glucose consumption significantly increases in both conditions from day 2 to 6: 46 ng/h to 69 ng/h for cryogel-free microchip and 41 ng/h to 53 ng/h for alginate cryogel-integrated microchip. No significant difference is observed between both conditions. The increase of glucose consumption may be generally related to an increase of the cellular activity or of the cell number. However, since the HepG2/C3A cell line is stable regarding glucose consumption, the higher glucose consumption at day 6 than day 2 can be attributed to cell proliferation. These results confirm the previous observations showing this effect.

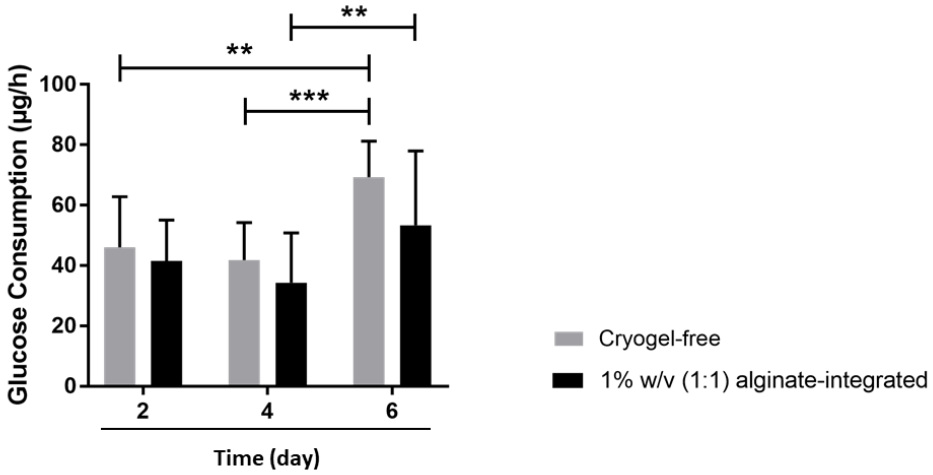

FIGURE 5.4: Glucose consumption of HepG2/C3A cells cultured in cryogel-free and 1% w/v (1:1) alginate cryogel-integrated microchips at various time points (2, 4 and 6 days). Values represent mean and SD (n=4). Data were analyzed using two-way ANOVA: * $p < 0.05$, ** $p < 0.01$, *** $p < 0.001$.

5.2.2 Albumin production

Albumin synthesis and release is one of the major hepatocytes' function. This function is also present in the HepG2/C3A cell line and can thus be used as a marker of metabolic activity. The albumin synthesis over the days is presented in figure 5.5.

In the same way as glucose consumption, the albumin production increases from day 2 to day 6. Although no significant difference is found between both conditions, the albumin production seems slightly lower when the cells are cultured in the alginate cryogel-integrated microchip. Indeed, at day 2, the albumin production is measured at 116 $\pm$ 30 ng/h and 84 $\pm$ 37 ng/h for cryogel-free and alginate cryogel-integrated microchips respectively. At day 6, the albumin production in the cryogel-free microchips is 463 $\pm$ 247 ng/h which is lower than the one in the cryogel-integrated microchips measured at 352 $\pm$ 232 ng/h. However, these results depend a lot on the number of cells in the microfluidic device which can vary from one microchip to another.

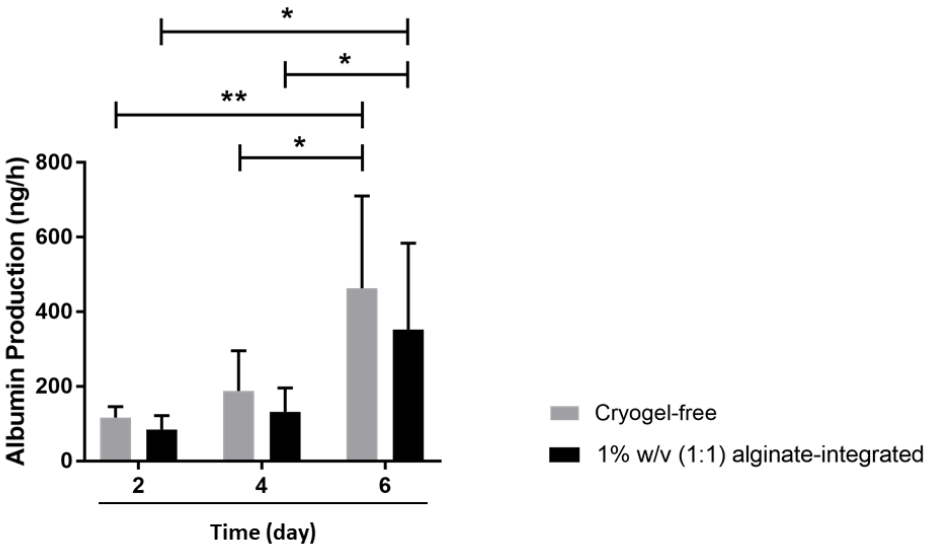

FIGURE 5.5: Albumin production of HepG2/C3A cells cultured in cryogel-free and 1% w/v (1:1) alginate cryogel-integrated microchips at various time points (2, 4 and 6 days). Values represent mean and SD (n=4). Data were analyzed using two-way ANOVA: * $p < 0.05$, ** $p < 0.01$, *** $p < 0.001$.

In order to normalize the albumin results, the albumin production is divided by the glucose consumption. Indeed, the latter represents an estimation of cell proliferation and is thus related to the cell number. The corresponding results are shown in figure 5.6.

The ratio between albumin production and glucose consumption increases over time. At day 2, it is estimated at 2.7 $\pm$ 0.9 and 1.9 $\pm$ 0.4 for the cryogel-free and cryogel-integrated microchips respectively. At day 6, both ratios are at 6.4. Although the results are not significant, it seems that the ratio is initially slightly lower in presence of alginate cryogel but then increases over time, up to reach the same level as the alginate-free condition.

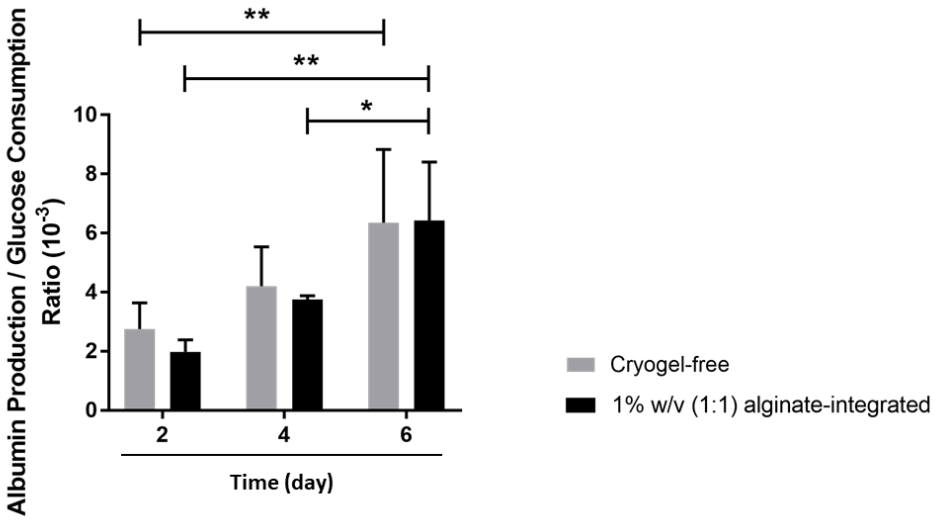

FIGURE 5.6: Albumin production over glucose consumption of HepG2/C3A cells cultured in cryogel-free and 1% w/v (1:1) alginate cryogel-integrated microchips at various time points (2, 4 and 6 days). Values represent mean and SD (n=4). Data were analyzed using two-way ANOVA: * $p < 0.05$, ** $p < 0.01$, *** $p < 0.001$.

5.3 Xenobiotic activity: APAP biotransformation

The biotransformation activity of liver cells is essential to follow since it is one of their main functions. Although HepG2/C3A cell line expresses lower phase I enzymes than human hepatocytes, its xenobiotic activity can be evaluated. It is assessed by exposing the cells to acetaminophen (APAP) (100 μM) during 24h every two days. The metabolites (see Fig. 1.8), APAP-SULF and APAP-GLU, are then measured in the cell culture medium to evaluate the biotransformation. APAP-GSH is not quantified since it is in minority, as seen in chapter 1. The results are presented in figure 5.7.

In both conditions, APAP biotransformation occurs, corresponding to about 50% of the initial exposure. Only APAP-sulfate, one of the metabolites, is significantly detected. No statistically significant differences are observed between both conditions. Only residues are detected for APAP-glucuronide.

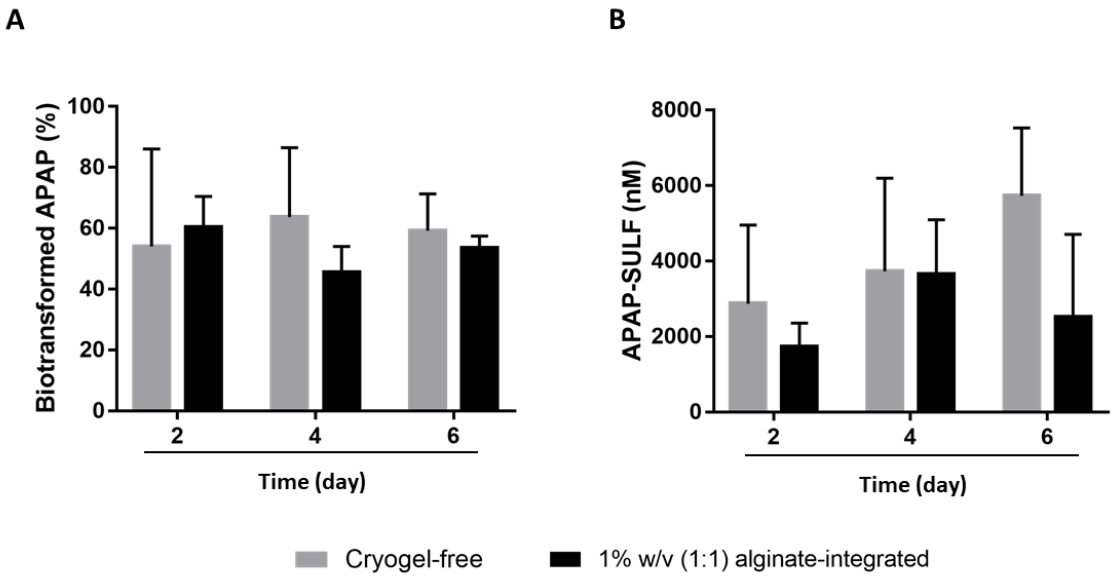

FIGURE 5.7: APAP and its metabolites quantification from HepG2/C3A cells cultured in cryogel-free and 1% (w/v) (1:1) alginate cryogel-integrated microchips at various time points (2, 4 and 6 days). (**A**) Biotransformed APAP. (**B**) APAP-sulfate.

5.4 Alginate cryogel removal

The alginate cryogel is used as a scaffold to perform 3D cell culture. The previous results have shown that this objective has been achieved, the cells being located over the entire height of the biochip. In order to let the cells completely free of their organization, it is necessary to remove the scaffold. Since this one is covalently cross-linked, we use alginate lyase, an enzyme that breaks down alginate, and which is not toxic to cells (Fig. 5.8).

After the removal of the alginate cryogel, the cells are observed under confocal microscope (Fig. 5.9). The images show that the HepG2/C3A are still in the microchip and that the 3D structure remains intact. Moreover, some pores can be distinguished.

In order to observe more precisely the 3D structures, SEM is performed on slices of microchip (Fig. 5.10). The previous observations are confirmed: 3D cell structures remain intact after alginate lyase treatment and the cells occupy the space from top to bottom of the microchip. Therefore, it seems that the cells neo-synthesized their own ECM allowing them to keep the 3D structure.

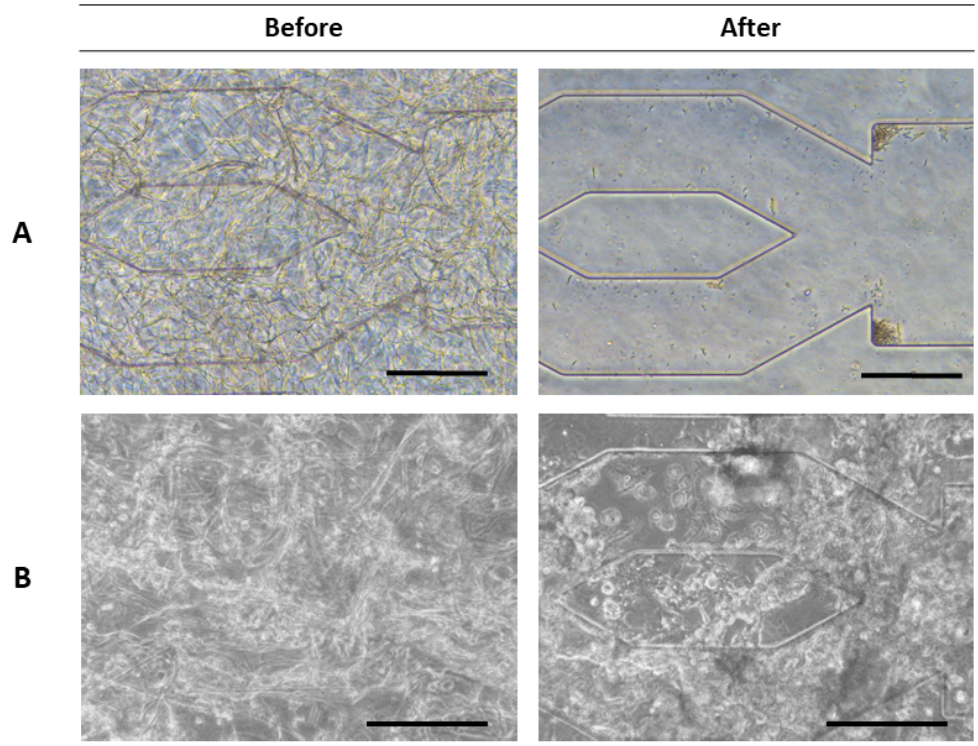

FIGURE 5.8: Microscopic observations of cryogel-integrated microchip before and after by alginate lyase treatment. (**A**) Without cells (**B**) With HepG2/C3A cells at day 6. Scale bar = 200 μm.

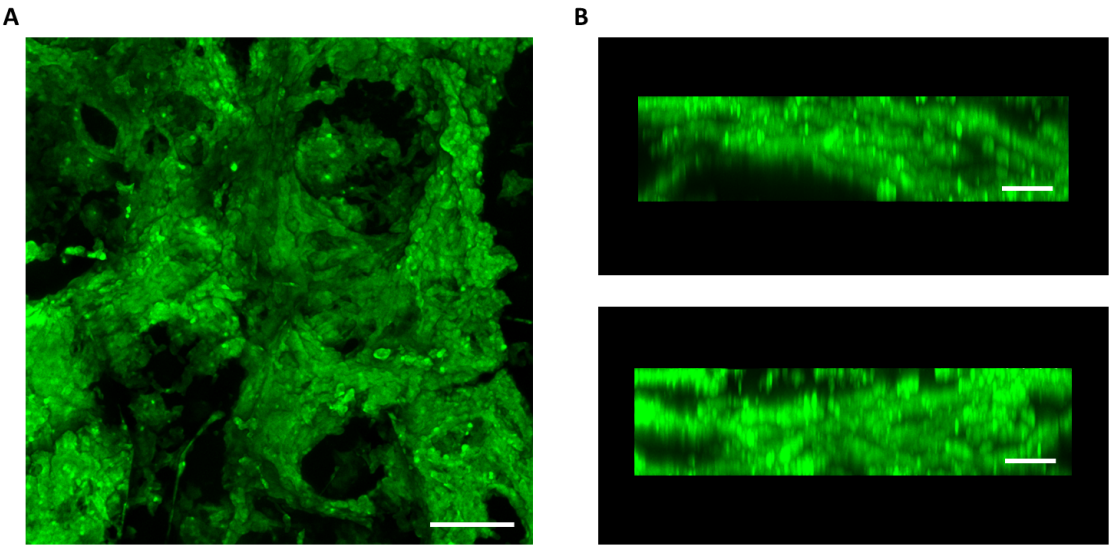

FIGURE 5.9: 3D reconstruction of HepG2/C3A cells inside mcirochip after alginate cryogel removal. Cytoskeleton (green). (**A**) Maximum intensity projection (**B**) Transverse view. Scale bar = 100 μm.

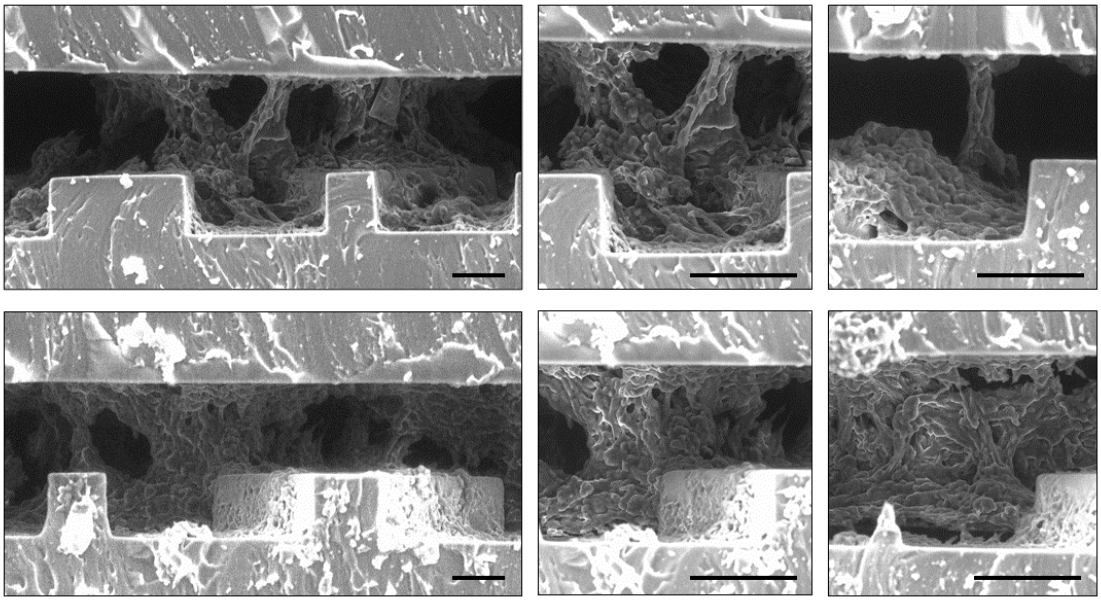

FIGURE 5.10: Cross-sectional SEM images of HepG2/C3A cell culture at day 6 after removal of alginate cryogel. Scale bar = 100 μm.

5.5 Discussion and conclusion

As already stated, we propose here a novel microfluidic device to culture hepatic cells organized as a 3D structure and even as a tissue under perfusion conditions. The objective is to bring together the potential of macroporous scaffold, to host the cells, and of microfluidic device to promote mass exchanges and induce mechanical (shear) stimuli on the cells.

First, we succeeded in maintaining HepG2/C3A viable, proliferative and functional during 6 days in perfusion in the cryogel-integrated microchips, the cryogel-free microchips being considered as controls. Cells are likely to adhere to any available surface. In the cryogel-free microchips, they grow mostly on the collagen-coated PDMS microscructures, leading to "semi-3D" organization. Very interestingly, in the cryogel-integrated microchips, they are able to spread all over the 3D alginate structure made available by the presence of very large pores achieved by the cryopolymerization process. After alginate lyase application to degrade the polymer, this 3D "tissue-like" organization remains stable, showing that the cells have produced their own ECM as support. One can thus consider that this environment will be much closer to *in vivo* situations. The cryogel could be used as a temporary scaffold to obtain 3D cell structures. To the best of our knowledge, no structures like this have been designed and evaluated before.

Using freeze-drying techniques, the Cohen's team demonstrated that alginate gels shaped as macroporous "sponge" helped hepatocytes to reorganize in spheroids [115]. More recently, Kumar's group synthesized cryogels of poly(AN-co-NVP) and poly(NiPAAm)-chitosan with pore size from 20 to 100 μm, that can be perfused in medium size bioreactors for bioartificial liver application [116]. HepG2 cells appear organized as small

clusters/aggregates in the structure. In our case, the spheroid organization could probably be achieved if the alginate cryogel is not coated with collagen. This could be further investigated with primary cells.

If we compare basic metabolic activities (glucose consumption, albumin synthesis, APAP biotransformation), we cannot demonstrate any improvement induced by this novel culture method compared to our standard microchips. This is not really surprising, considering the cells employed. HepG2/C3A are cells with limited metabolism compared to primary hepatocytes. We choose them as the classical first model widely described in the literature. Their behavior is very stable over the passages, which helps in a primary analysis and avoids huge variability always observed with primary cells (see next chapter for an example). Many authors, including our group, showed that glucose consumption is rather constant, while albumin synthesis reaches a peak after a few days. Our data completely fit with these observations. Our results are difficult to compare with literature since they are not normalized by the cell number. It should also be noted that the microsystems we use were designed to obtain optimized functions with these HepG2/C3A cells: our group demonstrated the benefit of the design compared to classical 2D culture, at the genomic, proteomic and metabolomic levels, probably due to the combined effect of structure and perfusion. It might thus be difficult to improve even more these features with such cells [159], [160].

The perfusion of the cryogel by the culture medium at a slow flow rate does not seem to affect cells' adherence and activities. The use of microfluidic chip allows the culture of a relevant number of cells under a continuous flow. This makes them interesting in predictive toxicology, for instance to mimic the admininistration phase of a drug, as for APAP that recirculate during 24 h in the circuit. The culture of liver cells in perfused microsystems has been reported in 2D [141], [196], as monolayers, semi 3D [159] or in 3D as spheroids [146]. In all cases, hepatocytes cultured under flow exhibit enhanced functional response. However, the cells' 3D organization or their functions might be hindered by limited diffusion and transport of nutrients towards cells far from the main flow. A recent study reported by Zhang et al. shows an organ on chip composed of an elastomer scaffold surrounding a microchannel [149]. Primary rat hepatocytes were seeded into the scaffold area and cultured for 7 days. Cells were present throughout the scaffold and secretion of urea was higher than that of collagen sandwich control. In our systems, the presence of large pores favored the perfusion, resulting in very low-pressure loss, ensuring a homogenous flow and thus convective mass transfer within the device.

However, the resistance of the microchips to flow, characterized in the previous chapter, might lead to unequal perfusion in the IDCCM device. We qualitatively observe differences in the hydraulic resistance during cell proliferation, highlighted by unequal volumes in the inlet and outlet chambers of the IDCCM. This suggests that the flow rates are not similar from one microchip to another. This observation is not so surprising since these variations among microchips exist due for example to handmade microchip fabrication or random alginate cryogel structure. It would thus be useful to design experimental set-ups able to achieve this follow-up, both qualitatively and quantitatively.

For further studies, some other improvements could be performed. A key point to overcome is the normalization of the biochemical results by cell number. Cell counting is known to be challenging in scaffold and even more when integrated in a microchip. However, this data is essential to compare results with literature. the relevance of DNA quantification should probably be analyzed, making sure that it does not interact with alginate.

Another difficulty, which could be rapidly be encountered, is imaging of cells. Indeed, 3D structures are not easy to observe *in situ*, unless confocal microscope is available. The thickness of the microchip is also a limitation to image the samples by limiting the focal length. Therefore, it would be useful to equip the microchip with on line sensors that could contribute to the daily follow-up of the culture.

Chapter 6

Towards a complex liver-on-chip: primary human hepatocytes and co-cultures

The third part of this work consists in exploring some potential applications of the microfluidic device, that we had in mind at the beginning of the PhD or that emerged from new collaborations. In the previous chapters, we have demonstrated that the alginate cryogel integrated microchip is suitable for HepG2/C3A culture under dynamic conditions. Although this first step is mandatory as proof of concept, we are aware that *in vitro* liver models and studies should be preferably performed with primary human hepatocytes (PHH). In parallel, it would be interesting to upgrade the model by performing co-cultures that mimic *in vivo* situations.

In the first part of this chapter, PHH seeding and culture in the device is evaluated by cell viability assay and metabolic functions measurements. This work is part of the WP6 "Liver in Chip" of the PIA Ilite program. Co-cultures are then investigated. The first type deals with the co-culture of HepG2/C3A with endothelial cells, so as to get closer to the liver sinusoidal structure. The second one is to follow up the behavior of circulating tumor cells in the microfluidic device, as model for metastasis mechanism in the liver. This latter part is motivated by the participation of BMBI lab in a project funded by Canderopole Nord-Ouest (P.I. A. Treizebré from IEMN).

6.1 Primary human hepatocytes culture

6.1.1 Context

PHH are still considered as the gold standard in the pharmaceutical industry as explained in chapter 2. They are preferred to study liver biology and function, DILI and liver diseases since they retain both phases I and II enzyme activities that are essential for the transformation of xenobiotics. However, maintaining viable and differentiated hepatocytes *in vitro* is still a major challenge *in vitro*. Cell-cell interactions, cell-matrix interactions, but also mechanical stimuli are key elements for the maintenance of hepatocytes' phenotype. The cryogel-integrated microchip has been initially designed to ensure such

environment, which needs to be evaluated with the dedicated cells. This work has been partially performed during the internship of Margaux Broussard, a BSc student at "École Supérieure de Biologie, Biochimie, Biotechnologies (ESTBB)" (Lyon).

6.1.2 Preliminary results

Non plateable cryopreserved PHH are used for the culture in cryogel-integrated microchip. They are seeded at 500 000 cells/cm^2 right after thawing and cultured for 15 days in the IDCCM device, as described in chapter 3. Half of them were exposed to APAP. After one day in static culture after cell injection, classical microscopy shows that the cells are quite homogeneously located in the microchips (Fig. 6.1).

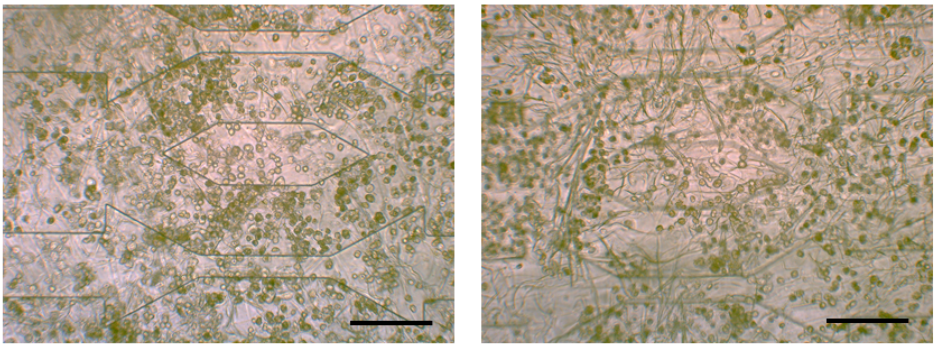

FIGURE 6.1: Microscope observations of PHH cultured in microchip at day 2. Scale bar = 200 μm.

Perfusion starts at day 2. Some microchips are unplugged from the perfusion device to perform a qualitative cell viability assay under confocal microscopy. The figure 6.2 shows that hepatocytes are present in the 3D structure. They present a cubic morphology and are plurinucleated, which corresponds to PHH's morphology within a tissue. However, a fraction of the cells is dead. At day 4, half of the microchips are exposed to APAP (15 M) following the protocol described in Figure 3.6. The cell viability is assessed later during this APAP exposure period (Fig. 6.2). At day 7 and 15, most of the cells seem to be dead, although some clusters remain stained in green corresponding to viable aggregates

To follow up cellular activity over time, the synthesized human albumin is measured in the supernatant for each perfused microchip (Fig. 6.3). The results differ from one microchip to another, so that no global can be identified. However, despite the probably high mortality, some albumin is produced and its amount even slightly increases from day 3 to 15, in a range from 20 ng/h to 40 ng/h, or remains stable around 30 ng/h. In some microchips, albumin production falls down to 0 ng/h at day 7, probably corresponding to cells' death (red curve). Only one microchip presents a significant increase in albumin synthesis over time (green curve). As many cells are probably dead, we cannot normalize the albumin production by the number of cells. Moreover, the exposure to APAP did not seem to affect PHH viability and activity since the albumin production

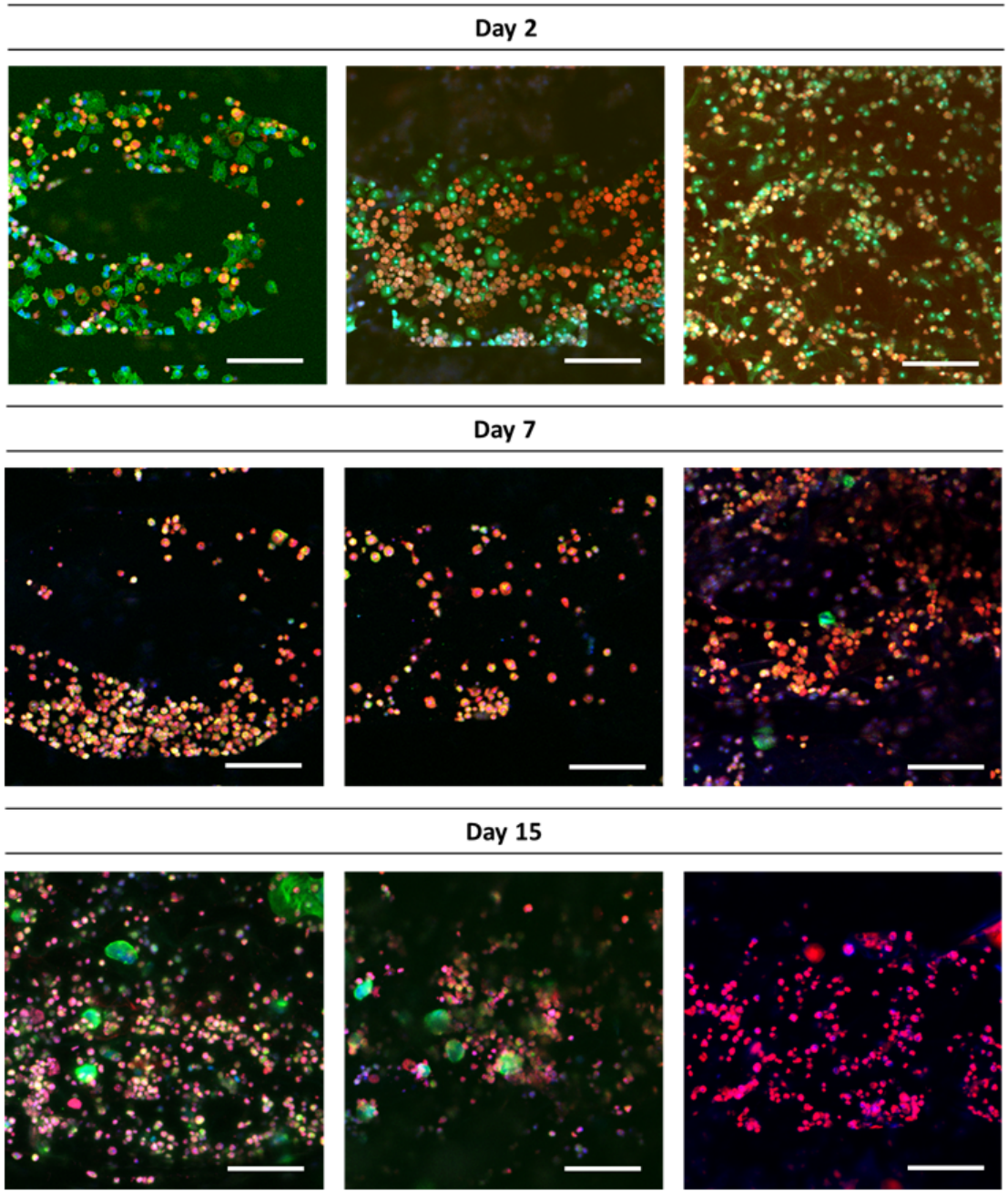

FIGURE 6.2: Confocal microscope observations of cell viability assay of PHH cultured in microchip at day 7 and 15, dead cell (red), cytoskeleton (green), nucleus (blue). Scale bar = 200 μm.

rates are in the same range. Based on these results, the analysis of APAP metabolites is thus not performed.

To study cell mortality in more details, lactate dehydrogenase (LDH) release is assessed. LDH concentration measured in the cell culture medium decreases over the days for each microchip: the cell damage mainly occurs at the beginning of the experiment (Fig. 6.4 **A**). The microchips in which albumin production falls down to zero (red), corresponding to cell death, do not release LDH on day 9: if all the cells were dead in the

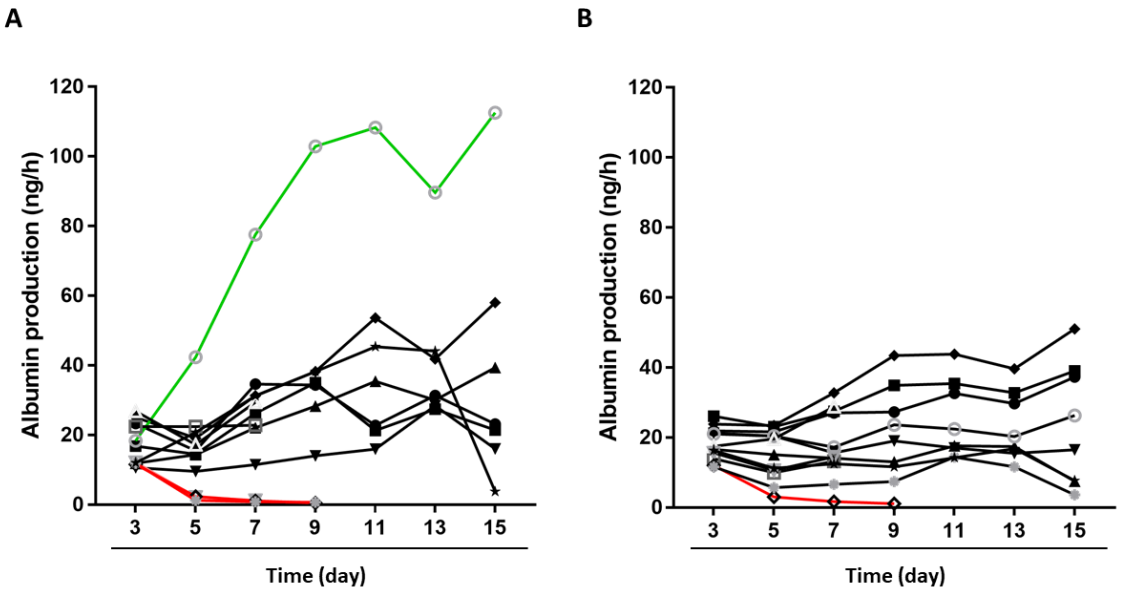

FIGURE 6.3: Albumin production of PHH cultured in cryogel-integrated microchips at various time points. (**A**) Cells not exposed to APAP (0 μM) (**B**) Cells exposed to APAP (15 μM).

previous days, LDH could not be released anymore. However, at day 3, these microchips contain a lower LDH quantity than the ones whose albumin production remains stable or even slightly increased (grey). To assess whether cell mortality occurs in the first 2 days, LDH is additionally quantified at day 2 (Fig. 6.4 **B**).

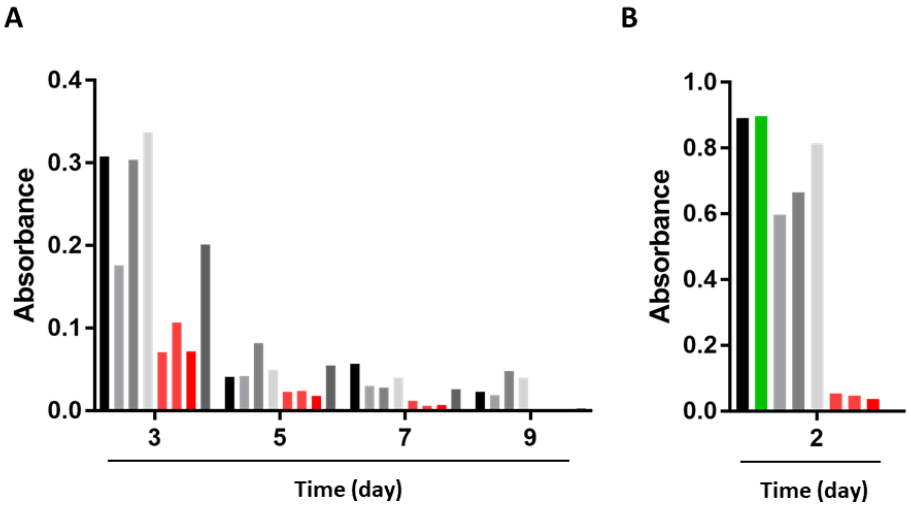

FIGURE 6.4: Absorbance of LDH assay of PHH cultured in cryogel-integrated microchips at various time points. (**A**) From day 3 to 9. (**B**) At day 2.

We observe that LDH related absorbance is much higher than in the next days, but are surprised about the low values exhibited in the "red" microchips, i.e. those where

cell death is very high. Therefore, we postulate that most of the cells probably die during the first day post seeding, and that the realeased LDH is already washed out at day 2, for these cultures. It is thus important in the future to closely monitor cell mortality in the post-seeding period.

6.1.3 Discussion and conclusion

Culturing PHH *in vitro* because of their high sensitivity to the environment and their rapid dedifferentiation if they lose their polarity. We also face this difficulty in this preliminary study. In addition, we choose to use non plateable PHH, to save costs but also to evaluate their capability to form aggregates or to rearrange themselves in the cryogels. It may be noted that these cells are usually discarded or used in suspension for a few hours, in toxicology studies, but are not recommended for long-term culture. It is thus difficult to compare our results with those in the literature.

PHH's viability is low from the beginning of culture in the cryogel-integrated microchip, as shown by dead cell assay and LDH release. We also observe a large variability in the albumin production in link with the status of the cells, with synthesized amounts much lower than others found in the literature [197]. In our group, Jellali et al. obtained an average albumin production rate of 1000 ng/h/106cells, with the original microchip geometry devoid of cryogel but also high quality PHH [164].

Nevertheless, some functions can be maintained in spite of a very low number of remaining cells. APAP exposure corresponds to rather low dose and not surprisingly does not shown specific additional toxicity. Due to the low number of cells, we decide not to perform the follow-up of its metabolites in the supernatant, which was an initial goal of the study.

Although disappointing, performing this preliminary work shows that such a culture is feasible, provided that the initial huge cell mortality can be prevented. We nevertheless manage to maintain some viable cells in the cryogel. For the next experiments, we propose to work on several axes: i) use high quality PHHs that are able to adhere on a culture support, or use fresh primary rat hepatocytes; ii) improve the thawing/seeding procedure: cells are cryopreserved in DMSO, which is toxic in classical cultures. Additional washing before cell inoculation in the microsystems, or preliminary short 2D culture could be of help to avoid the initial necrosis and withdraw the dead cells that can release *in situ* toxic factors; iii) let the cells reorganize before starting perfusion.

6.2 Co-culture of HepG2/C3A and HUVEC

6.2.1 Context

This part represents a first attempt to mimic a liver sinusoid (Fig. 1.6), based on the initial hepatocyte 3D structure reproduced in our cryogel-based microfluidic device. It has been shown in chapter 2 that hepatocytes co-cultured with endothelial cells improve their hepatic protein synthesis and detoxification activity [198]. Ideally, liver sinusoidal endothelial cells (LSEC), characterized by very specific fenestrations allowing mass transfer from the blood stream to the hepatocyte compartment, should be used. Unfortunately, they are not easily available, difficult to isolate and their phenotype is unstable *in vitro* [199], [200]. Therefore, several studies have used another endothelial cell type, i.e. human umbilical vein endothelial cells (HUVEC).

Not expensive and easy to isolate, they are widely used in *in vitro* studies. PHH or HepG2/C3A, co-cultured with HUVEC, exhibit higher albumin production, urea synthesis but also drug metabolism compared to monocultures [201], [202]. In addition to improve liver functions, co-cultures have an impact on the cellular organization. HUVEC and hepatocytes interact together, migrate and can create sinusoid-like structures [198], [203].

In order to improve the liver functions of our cryogel-integrated live-on-chip, co-culture of HepG2/C3A with HUVEC is performed. In this feasibility study, we will focus on the HUVEC interactions with the 3D cellular structure structure formed by the hepatic cells in the perfused cryogel.

6.2.2 Preliminary results

To perform the co-culture, two approaches are followed: seeding of both cell types could be either concomitant or sequential. Prior to the 3D conditions, the co-culture of HepG2/C3A with HUVEC is first evaluated in multi-well plates. To track them, both cell types are labelled with specific dyes: a red one for the HUVEC and a green one for the HepG2/C3A cells.

The first method consists in culturing the HepG2/C3A cells for several days and then seeding the HUVEC. Two situations were studied in multi-well plates: HUVEC seeding on confluent and non-confluent HepG2/C3A cell layers (Fig. 6.5). After 5 days of co-culture, HUVEC behaviour depends on the initial situation. If HepG2/C3A are not at confluence, HUVEC adhere on the free well surface and then, in contact with HepG2/C3A, form protrusions and sprout into them. On the contrary, if HUVEC are seeded on a confluent HepG2/C3A layer, they hardly adhere and proliferate on it. After these first investigations, the co-culture is then performed within the cryogel-integrated microchip. The HepG2/C3A are first seeded at 500 000 cells/microchip and cultured during several days in order to proliferate and produce their own ECM. The alginate cryogel is then removed with alginate lyase and finally 700 000 HUVEC are injected in

the microsystem. After 5 days of co-culture, some HUVEC are likely to adhere to the HepG2/C3A cells (Fig. 6.6).

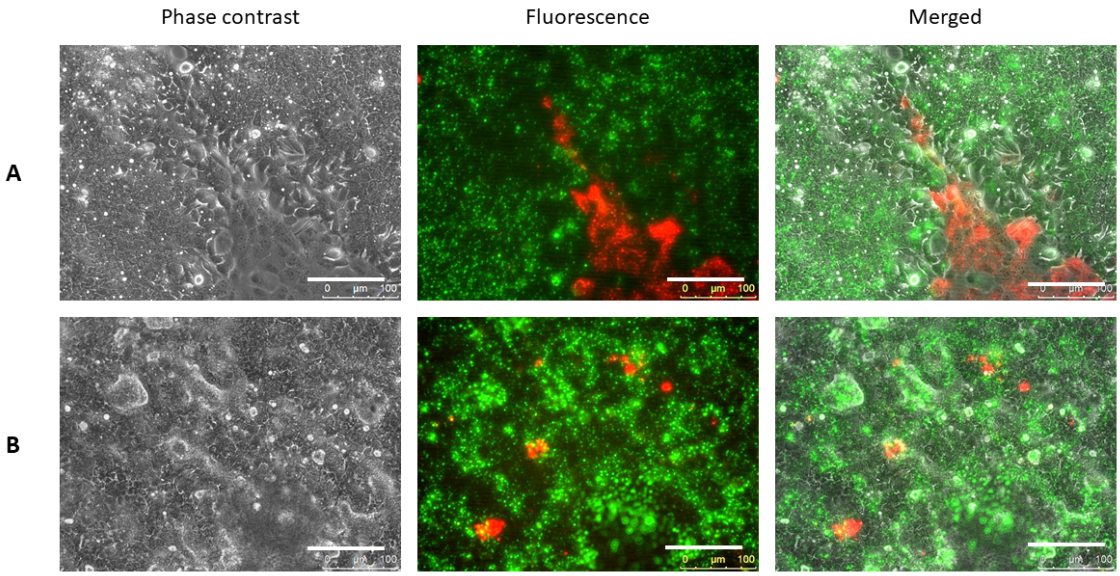

FIGURE 6.5: Co-culture of HepG2/C3A with HUVEC seeded at different time in multi-well plates, observations at day 5 using epifluorescence microscopy. (**A**) Low HepG2/C3A density and (**B**) High HepG2/C3A density. HepG2/C3A (green), HUVEC (red). Scale bar = 100 μm.

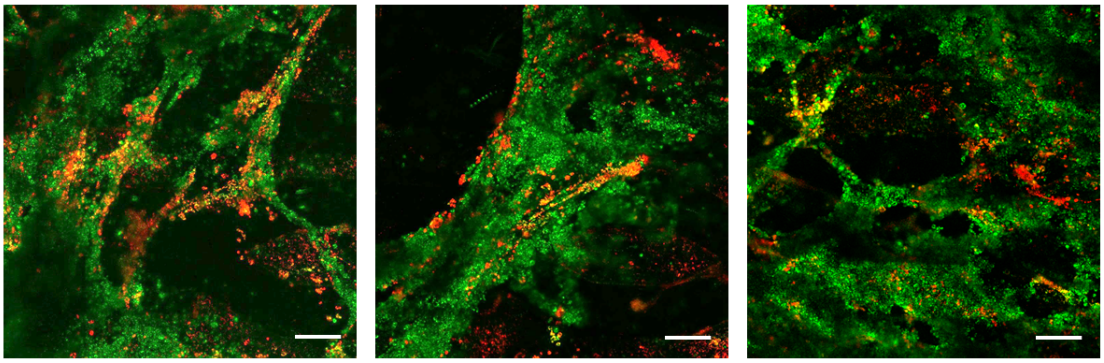

FIGURE 6.6: Co-culture of HepG2/C3A with HUVEC seeded at different time in the cryogel-integrated microchip, observations at day 5 using confocal microscopy. HepG2/C3A (green), HUVEC (red). Scale bar = 200 μm.

The second method consists in simultaneous seeding of HepG2/C3A and HUVEC. According to the literature, we apply the ratio of 2:1 HepG2/C3A:HUVEC [204]. After 5 days of co-culture in multi-well plates, cells are confluent and a well-defined structure can be observed: the HUVEC form tubular-like networks through the HepG2/C3A clusters (Fig. 6.7). However, when seeded both at the same time in the cryogel-integrated microchip, the structure appears to be lost: the previously observed organized network of HUVEC is not present (Fig. 6.8). Nevertheless, both cell types are randomly and homogeneously distributed on the alginate scaffold.

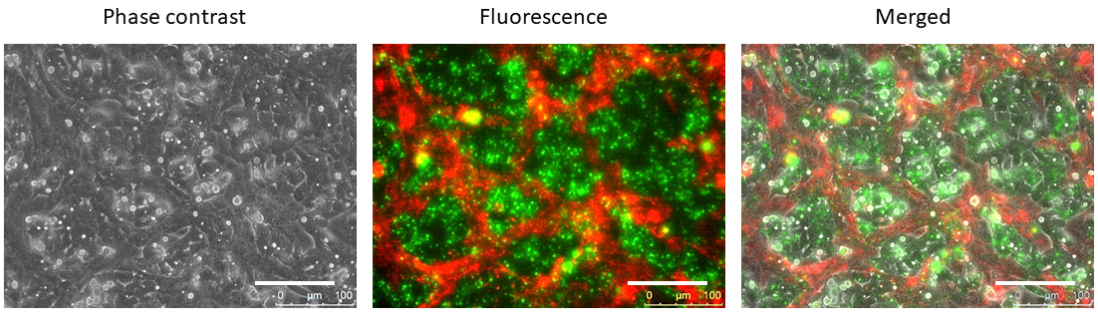

FIGURE 6.7: Co-culture of HepG2/C3A with HUVEC simultaneously seeded in multi-well plates, observations at day 5 using epifluorescence microscopy. HepG2/C3A (green), HUVEC (red). Scale bar = 100 μm.

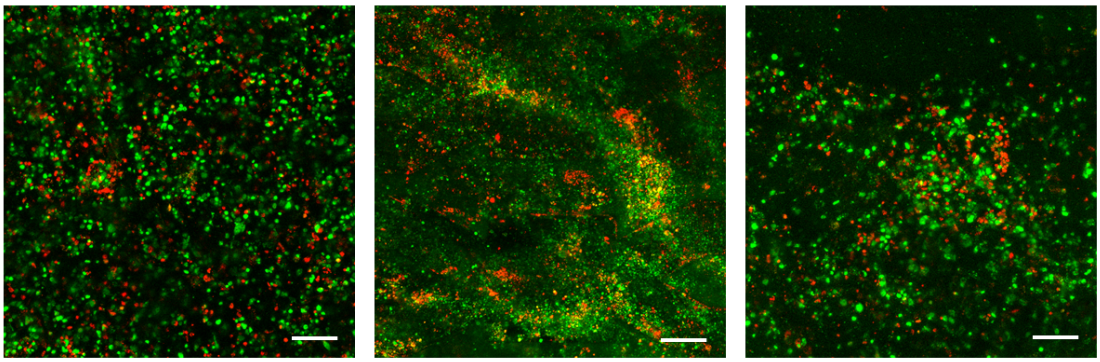

FIGURE 6.8: Co-culture of HepG2/C3A with HUVEC simultaneously seeded in the cryogel-integrated microchip, observations at day 5 using confocal microscopy. HepG2/C3A (green), HUVEC (red). Scale bar = 200 μm.

6.2.3 Discussion and conclusion

In order to design a complete liver-on-chip exhibiting all the functionalities of this organ, the culture of hepatocytes with NPC represents a significant step forward. As one of the major hurdles in bioengineering remains tissue's vascularization, the addition of endothelial cells is often foreseen to promote neovascularization. Moreover, this cell type plays an important role when culturing hepatocytes under dynamic condition by protecting them from the shear stress resulting from the flow. In this study, the improvement of our device is evaluated through the co-culture with HUVEC. Our objective is to form a 3D network of hepatocyte-like cells covered by endothelial cells, as a simplified sinusoid.

The question addressed here deals with the seeding protocol: concomitant and sequential seedings are studied to determine which one best promotes self-organization during the proliferation phase. In 2D culture, the simultaneous seeding appears promising since HUVEC are able to form a network that we do not observe following the sequential protocol. This network has also been described by Chiew et al. in multi-well plates [204]. However, we point out the relative difficulty of HUVEC to adhere and proliferate onto HepG2/C3A monolayer, a phenomenon that has not been reported in the

literature.

The application of the simultaneous seeding protocol in the cryogel-based microchip is rather disappointing: after 5 days of co-culture, we can not reproduce the results obtained in 2D: no specific structure could be observed. Both cell types are randomly distributed without many cell-cell interactions. In contrast with the 2D observations, the sequential co-culture in 3D appears more promising. Some HUVEC are likely to adhere on the pre-formed HepG2/C3A tissue. Nevertheless, it is difficult to say if they formed protrusions as observed in multi-well plates. In order to enhance the adhesion of HUVEC onto HepG2/C3A and mimic the space of Disse between the hepatocyte and the endothelial cells, a coating with proteins of this specific ECM could be performed on HepG2/C3A cells before HUVEC seeding. This method was carried out by Inamori et al. that coated hepatocyte spheroids with collagen I to obtain HUVEC-covered hepatocyte spheroids instead of HUVECs invaded hepatocyte spheroids [203].

The preliminary results generated during this co-culture between HepG2/C3A cells and HUVEC are promising and deserve further investigation. Although the sequential seeding has shown better cellular organization after 5 days, both co-culture methods should be performed on the long term to observe any specific structures formation. This model could be used to closely mimic the structure of the sinusoids. Moreover, it could become a study model of the hepatocellular carcinoma angiogenesis since this mechanism is crucial for tumor growth and is the target of some promising therapies against liver cancer [205], [206].

6.3 HepG2/C3A and MDA-MB-231: an example of study for circulating tumor cells

6.3.1 Context

The liver is the main organ in contact with xenobiotics but also with circulating tumor cells (CTCs). These cells come from a tumor in a specific organ from which they managed to reach the blood or lymphatic circulation. They can thus spread into the human body and generate new tumors, called metastases, distant from the primary one. The organ distribution is not random: depending on the primary tumor location, principal sites of metastasis have been identified [207]. Lungs, brain, bone and in particular liver are the main ones. This organ specific pattern is due to favorable interactions between the metastatic tumor cells and the organ microenvironment, known as "seed and soil" theory [208]. The mechanism for dissemination of CTCs is complex and diverse and its understanding is essential to find possible therapeutic interventions. Indeed, metastasis remains the cause of 90% of deaths from primary tumors [209].

The process of metastasis is composed of different steps [209], [210]. First, the primary tumor grows, cells invade the stromal tissue surrounding the tumor and activate the angiogenesis process in order to get blood supply that support their metabolic needs.

The resulting new blood vessels are closed to the cancer cells, and intravasation can occur: cancer cells cross the vessel wall and enter the circulation. Some of the CTCs survive into the body's circulatory system despite the immune system and shear stress, and circulate in the body until they are stopped. This usually happens in the capillaries which trap CTCs by size restriction and where they have been attracted by chemo-attractant molecules. They adhere to the vascular wall and can then begin extravasation: they leave the circulation by crossing the vessel wall. Cancer cells finally initiate their growth and colonize the new site thus developing metastasis.

The liver is one of the privileged sites for the development of metastasis due to its important vascularization and its numerous sinusoids but also due to its favorable microenvironment [211]. However, the metastasis process in this organ is not well understood yet. To this end, different research teams are working on one or more steps of this process including the team of Dr C. Lagadec (Inserm U908) at "Institut pour la Recherche contre le Cancer - Oscar Lambert" at Lille [212]. They study the extravasation step of breast CTCs in the liver, one of the specific organs along with lungs, brain and bones. Together with Dr A. Treizebré, from "Institut d'Electronique, de Microélectronique et de Nanotechnologie" (IEMN-UMR 8520), they developed a research program aiming at following the extravasation process in a microfluidic device that mimic the endothelial barrier [213], [214].

We decided thus to combine our efforts in the framework of a research project led by Dr Treizebré and funded by the "Cancéropole Nord Ouest (2019-2020)". One of the goals of the project, directly in link with my PhD thesis, is to evaluate the feasibility of following the behavior of CTCs in our biomimetic liver system. This study was partially performed during the internship of Solène Rousseau, a UTC student in bioengineering.

6.3.2 Preliminary results

When CTCs cross the liver endothelial wall, they reach the space of Disse where they can come into contact with hepatocytes and colonize the tissue. To recreate this process and study the interactions in our microsystems, we use a human breast cancer cell line, MDA-MB-231, that the team of Dr. Lagadec has transfected with GFP for imaging studies.

The parameters of the co-culture of HepG2/C3A and MDA-MB-231 are first evaluated in multi-well plates. The objectives are to fix the composition of the co-culture medium, the time course and respective concentrations for cell seeding. After analysis of both culture media employed by Dr Lagadec and our team, it appears that classical HepG2/C3A culture medium can be employed. The hepatic cells are first seeded at low and high density, 20 000 cells/cm^2 and 200 000 cells/cm^2 respectively. After adhesion, breast CTCs are inoculated at a density of 1 000 cells/cm^2 and the evolution of the co-culture is monitored under epifluorescent microscope after a cell viability assay (Fig. 6.9). HepG2/C3A cells adhere, proliferate and become confluent in both conditions, although mortality seems slightly higher for the high density condition. The MDA-MB-231 cells, in green, exhibit different behaviours depending on the HepG2/C3A cell density: at low

density (Fig. 6.9 **A**) they succeed to adhere and seem to proliferate contrary to high density (Fig. 6.9 **B**) where they do not adhere and die. However, their morphology is not the one usually observed, they are spherical instead of being elongated with pseudopods.

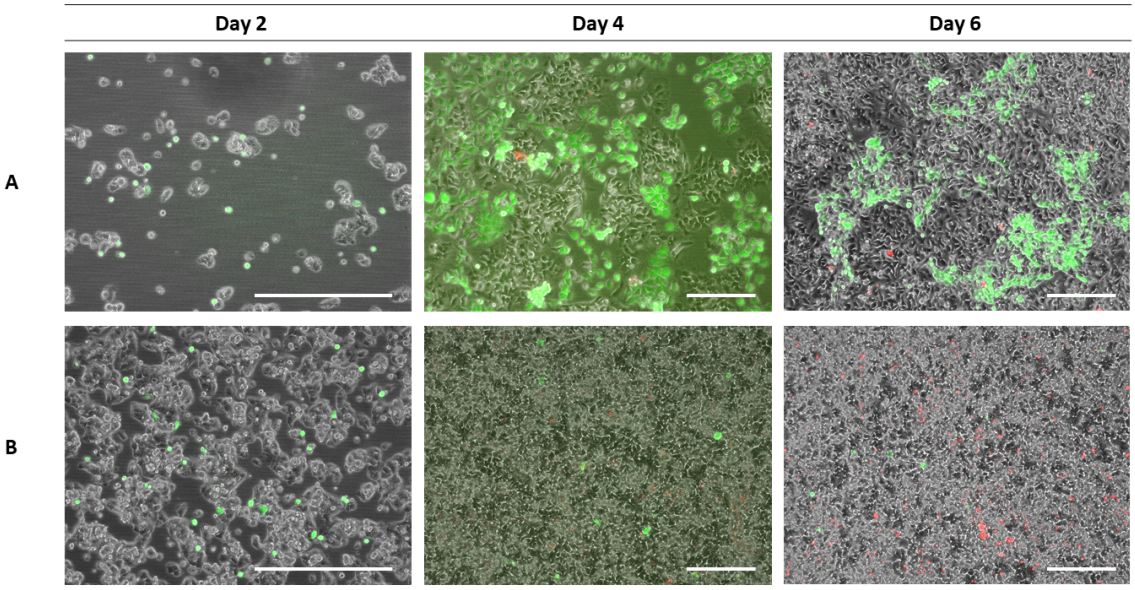

FIGURE 6.9: Epifluorescent microscope observations of HepG2/C3A cells seeded at different densities in well plates co-cultured with MDA-MB-231 cells seeded at 1 000 cells/cm^2 at day 2, 4 and 6. (**A**) HepG2/C3A seeded at 20 000 cells/cm^2 (**B**) HepG2/C3A seeded at 200 000 cells/cm^2. Far-Red Fixable Dead Cell (red), GFP (green). Scale bar = 200 μm.

In order to confirm the microscopic observations, cell counts are performed for each cell type in co-culture and alone as a control 6.10. On the one hand, the HepG2/C3A proliferation in co-culture is similar to that of the control (without CTCs) for both densities. On the other hand, the number of MDA-MB-231 cells in co-culture is much lower than that of the control: at day 6, it is 3 times lower in the low HepG2/C3A cells density condition and almost equal to zero in the high HepG2/C3A cells density condition. Therefore, these results confirm the previous microscopic observations: the HepG2/C3A cells density seems to influence MDA-MB-231 cells adhesion and further proliferation. At low HepG2/C3A cells density, the breast cancer cells proliferate but at HepG2/C3A cells high density they do not succeed to adhere and die.

A preliminary study is consequently performed in the alginate cryogel-integrated microchip in order to evaluate the suitability of this device to study the metastasis mechanism. HepG2/C3A cells are first seeded at 1 million/microchip and then MDA-MB-231 cells at 1 000 cells/microchip following the protocol established in chapter 3. The co-culture is maintained for 4 days and observed under epifluorescent microscope after a cell viability assay (Fig. 6.11).

At day 1, HepG2/C3A cells are located all over the microchip. The MDA-MB-231 cells can be observed inside the microchip and appear spherical, just after their seeding. One day after, the presence of green areas suggests that some MDA-MB-231 cells

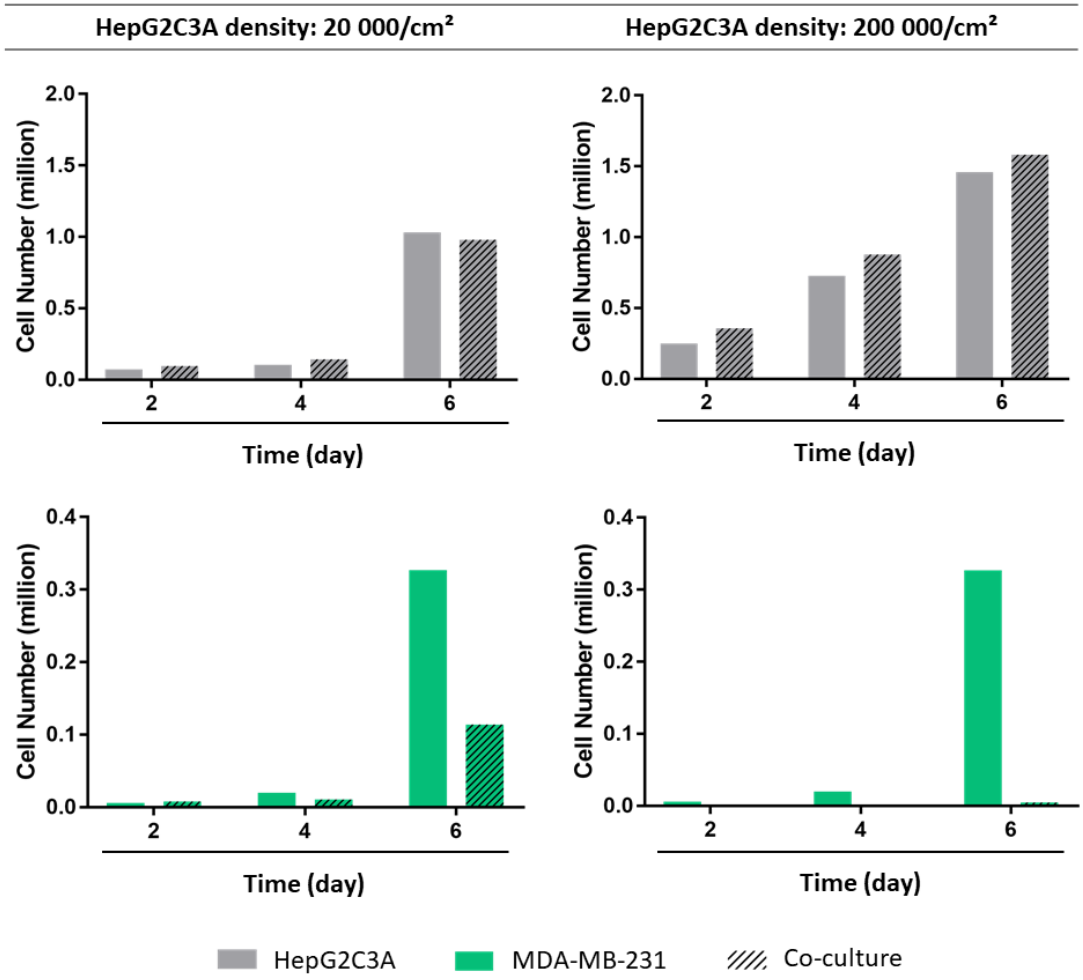

FIGURE 6.10: Cell counting of HepG2/C3A cells at 20 000 cells/cm^2 and 200 000 cells/cm^2 and MDA-MB-231 cells at 1 000 cells/cm^2 in co-culture and their respective control.

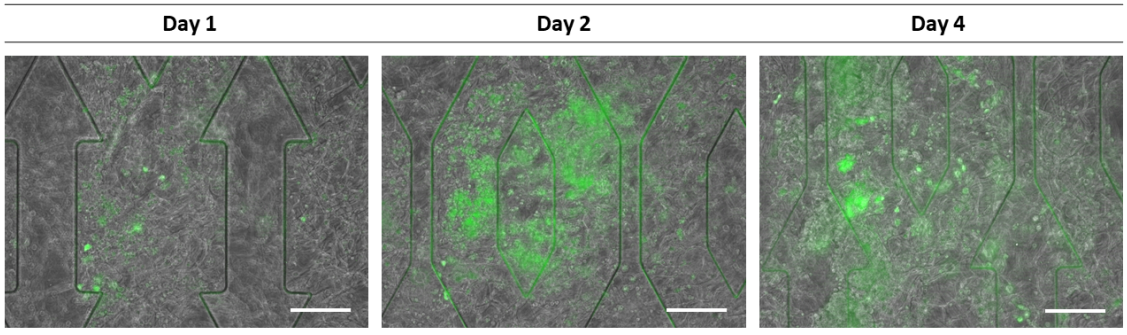

FIGURE 6.11: Epifluorescent microscope observations of HepG2/C3A cells seeded at 1 million in microchip alginate 1% (1:1) co-cultured with MDA-MB-231 cells seeded at 1 000 cells/microchip at day 1, 2 and 4. Far-Red Fixable Dead Cell (red), GFP (green). Scale bar = 200 μm.

have proliferated. However, at day 4, we distinguish different intensities of green areas. The most intense are probably MDA-MB-231 cell clusters. The other spots can be

attributed either to MDA-MB-231 cells located at another level in the microchip or to auto-fluorescence from PDMS.

6.3.3 Discussion and conclusion

Although the formation of metastasis in specific organs have been recognized for many years, this phenomenon is still not well understood. Metastasis formation is a highly complex mechanism that involves a wide variety of mediators, including growth factors, cytokines and adhesion molecules. For example, some interactions between breast CTCs and their target organs have been discovered: lungs, brain, bones and liver secrete chemokines whose receptors are highly expressed in cancer cells leading to their migration to these sites [215]. Microcirculation and resulting shear conditions play probably an important role too. New tools mimicking the full microenvironment are needed to study these interactions in detail and further develop host-directed anticancer therapies. They are currently only few studies dealing with this type of approach. We can only cite the group of Wells and Griffith in Pittsburgh, using hygrogels to co-culture an hepatic tissue with CTCs in view of understanding dormancy [216]

Before studying the possibility to use the cryogel-integrated microchip, the two cell types used, HepG2/C3A and MDA-MB-231 cells, are first co-cultured in multi-well plates. The microscopic observations show that the breast CTCs do not seem to be able to adhere on HepG2/C3A cells, but only to the plastic support. These observations are confirmed by cell counting: the number of MDA-MB-231 cells decreases over the days probably due to cell culture change. They are thus washed out of the wells. We did not find in the literature any report regarding such a co-culture. Receptors responsible for MDA-MB-231 adhesion might not be present on the membrane of HepG2/C3A. In addition, it has been shown that during the process of extravasation, a release of chemokines by different cellular actors leads to the development of an inflammatory microenvironment. This induces the upregulation of some receptors present on the LSEC. For example, the intercellular adhesion molecule 1 (ICAM-1) receptor is activated by the tumor necrosis factor alpha (TNF-α), thus allowing the fixation of circulating cancer cells bearing the ligand of this receptor. Since this receptor is also present on hepatocytes, an activation with TNF-α might be necessary [217]. However, we are also aware that chemokines are only one part of the complex metastasis mechanism and that other factors are involved.

The introduction of MDA-MB-231 cells in the cryogel-integrated microchip containing HepG2/C3A cells is then performed. Very interestingly, and in contrast with 2D culture, breast CTCs remain in the microchip despite the perfusion. They probably adhere to PDMS or alginate coated with collagen, i.e. the biomimetic extracellular matrix, or remain trapped in the pores of the cryogel. In the same way as before, this experiment should be probably performed in an inflammatory environment and all the necessary factors to induce metastasis cascade. However, this preliminary experiment shows that MDA-MB-231 cells can be successfully injected in the cryogel-integrated microchip already occupied by the hepatic cells.

To conclude, the cryogel-integrated microchip could be an interesting tool to study breast CTCs mechanisms, as well as potential therapies. Indeed, under appropriate conditions that induce the metastasis cascade, cell behaviour could be studied in 3D. Moreover, in case of a co-culture between hepatocytes and LSEC, the complete mechanism of extravasation could be reproduced with breast CTCs circulating in the microfluidic system. In such perfused systems, the effect of cytotoxics on the tumor, but also in the surrounding healthy tissues could be analyzed. These first promising results regarding the proof of concept deserve thus to be persued in more ambitious projects.

Conclusion and perspectives

Obtaining liver's *in vitro* relevant model remains a key challenge today. Despite the abundant literature in the field, rapidly growing in the last years, none of the proposed advanced techniques has been successfully translated to routine tests in the pharmaceutical companies yet, and animal experiments are still considered as the gold standard. Indeed, the current *in vitro* liver models do not reproduce the complete set of features necessary to maintain a functional tissue. This results in poor reliability and accuracy, especially for predictive toxicology or drug metabolism studies. The development of a liver model that mimics in vivo conditions as closely as possible is therefore crucial. In this thesis project, we developed a cryogel-integrated microchip, gathering therefore the cell culture in 3D and in perfusion in a bioinspired approach.

First, we designed and characterized the 3D scaffold, i.e. alginate cryogel, at the microscopic and macroscopic levels. By varying the alginate concentration and the AAD:EDC ratio, we were able to obtain cryogels with tunable mechanical properties, ranging from those of a healthy to a pathological liver. The study of the porosity, the degree of pore connectivity, the swelling ratio but also the flow resistance in the microchip showed that the cryogel properties change with the alginate concentration and the AAD:EDC ratio. These results led us to choose only one condition for the cryogel-integrated microchip.

Then, the proof of concept of this new microchip was performed with the human hepatocyte cell line HepG2/C3A. We demonstrated the viability and proliferation of cells in the cryogel-integrated microchip and their 3D distribution in the device. Basic hepatic functions, albumin synthesis and APAP biotransformation, were found to be close to the standard cryogel-free microchip. This similarity was expected since HepG2/C3A behavior is rather independent from 3D culture conditions. Very interestingly, applying alginate lyase to remove alginate cryogel did not alter the 3D cell structures, leading to a highly porous 3D liver tissue.

Finally, during this PhD framework, we had the opportunity to explore several ways to upgrade this new device for its further use to understand physiological and pathological processes occurring in the liver. The culture of the gold standard cells, i.e. PHH, is not straightforward and will need improvement to propose a model for hepatotoxicity or drug metabolism studies. The complexification of the HepG2/C3A model with HUVEC, as an example of non parenchymal cells, showed promising results, especially on the sequences of co-culture to be performed. This is a first step towards a biomimetic liver sinusoid, in which endothelial cells will be in direct contact with the

flow, while hepatocytes are entrapped into an extracellular matrix. A preliminary study of the interaction between liver cells with breast tumor cells highlighted the potential of the device for such investigations involving circulating cells.

This thesis project has thus led to the development of an innovative model of perfused liver, with a functional 3D structure that can be used for the pharmaceutical industry as a healthy and pathological model. The results shown here only correspond to the first characterizations of the device and many improvements can be proposed for the next stages.

Concerning the healthy liver model, the next step is to successfully grow PHH. The proof of concept has been done here with a cell line, but the first attempts to culture PHH were not successful. The protocol should be improved to culture such sensitive cells. Moreover, in order to be used as a new *in vitro* liver model, a reliable method to count cells in the device should be found. DNA quantification should be tested, ensuring that the alginate does not adsorb DNA. The biological studies need to be further investigated. Cell polarity could be observed by immunostaining of transporters (MRP2, OATP) for example. Proteomic and genomic analysis could also be performed to study in more details the cell activity in this new device.

Concerning, the pathological models, in particular the cirrhotic liver, new conditions varying alginate concentration and AAD:EDC ratio should be tested. Indeed, we succeeded in this work to develop a cryogel with tunable mechanical properties but the one close to pathological liver rigidity did not exhibit a porous structure. Therefore, a balance between alginate concentration and AAD:EDC ratio should probably be found. Another possibility could be to use alginate with another polymer such as agarose which allow to create rigid structures. Concerning the metastatic model, the next step is to inject the CTC in the circulating cell culture medium to mimic the process of extravasation. Moreover, to faithfully reproduce this process, the sinusoidal model must be improved. The adhesion of endothelial cells should thus be enhanced. A coating with molecules of the ECM could be performed on the 3D structure formed by the hepatic cells. This sinusoidal model is essential to have a metastatic model but it could also be used in the healthy and cirrhotic liver models.

Concerning the device itself, a study of fluid mechanics inside the cryogel-integrated microchip should be performed to understand the perfusion in details and identify its main parameters. This would enable a better characterization of local velocities, pressures, shear stresses, preferential paths, and dead zones. Some parameters such as the pore size and the stiffness of the alginate cryogel should probably be adapted once more to optimize the perfusion. In the same way, the design of the microchip plays a role on the flow distribution and could be adapted accordingly.

Another improvement deals with the perfusion platform, the IDCCM. It was originally designed for "empty" microchips. The addition of the cryogel inside of these microfludic devices and the resulting resistance to flow do not allow an optimal use anymore. Actually, it could be interesting to develop a new perfusion system gathering the

advantages of both devices we used here, i.e. IDCCM and bubble traps. It should meet several criteria: observable under microscope during the experiment and directly perfused like the bubble traps system but also easy to handle with a microchip support and an easily measurable circuit volume like the IDCCM device. In addition, the integration of a pressure controller would be a great improvement to control the flow rate through the cryogel-integrated microchips. In the same ways, oxygen, glucose or lactate sensors could be integrated to improve the culture follow-up.

The work presented here has enabled to take a new step towards the realization of a liver-on-chip. In the future, it could represent a reliable *in vitro* model for predictive toxicology and therefore improve the drug development process. Moreover, it could be used as a physiological and pathological liver model. In the development of personalized medicine, it could also be an interesting tool against liver cancers.

Beyond the liver, this cryogel integrated microchip represents a new cell culture system, in a 3D and dynamic environment, and could be adapted to other cell types and therefore other organs.

Communications

Congress

L. Boulais, M. Beldjilali-Labro, U. Pereira, R. Jellali, P. Paullier, C. Legallais, S. Bencherif, "Cryogel-based hepatic cell culture devices for liver tissue engineering" - Presentation
2nd BIOMAT Congress, June 2017, Ambleteuse, France

L. Boulais, U. Pereira, R. Jellali, P. Paullier, E. Leclerc, S. Bencherif, C. Legallais, "Cryogel-integrated cell culture microchips for liver tissue engineering" - Poster
5th TERMIS World Congress, September 2018, Kyoto, Japan

L. Boulais, R. Jellali, U. Pereira, P. Paullier, E. Leclerc, S. Bencherif, C. Legallais, "Cryogel integrated microchip : towards a human 3D model of liver cancer" - Presentation
Cancer Cells-on-Chip Workshop, March 2019, Lyon, France

L. Boulais, R. Jellali, U. Pereira, P. Paullier, E. Leclerc, S. Bencherif, C. Legallais, "Cryogel integrated microchip : towards a human 3D model of liver cancer" - Poster
STCM Congress, June 2019, Paris, France

Publications

Published :
L. Boulais, M. Pasqua, C. D. Lartigue, R. Jellali, U. Pereira, and C. Legallais, "Bioartificial liver: Biomechanical considerations", *Computer Methods in Biomechanics and Biomedical Engineering*, vol. 22, no. sup1, S370–S372, 2019. DOI:10.1080/10255842.2020.1714948.143

In preparation:
L. Boulais, R. Jellali, U. Pereira, P. Paullier, E. Leclerc, S. Bencherif, C. Legallais, "Cryogel-integrated biochip for liver tissue engineering"

Bibliography

[1] G. A. V. Norman, "Drugs and Devices Comparison of European and U.S. Approval Processes", *JACC: Basic to Translational Science*, vol. 1, no. 5, pp. 399–412, 2016. DOI: 10.1016/j.jacbts.2016.06.003.

[2] European Medicines Agency, "User guide for micro , small and medium-sized enterprises", 2016.

[3] G. A. V. Norman, "Drugs, Devices, and the FDA: Part 1: An Overview of Approval Processes for Drugs", *JACC: Basic to Translational Science*, vol. 1, no. 3, pp. 170–179, 2016. DOI: 10.1016/j.jacbts.2016.03.002.

[4] D. Cook, D. Brown, R. Alexander, R. March, P. Morgan, G. Satterthwaite, and M. N. Pangalos, "Lessons learned from the fate of AstraZeneca's drug pipeline: A five-dimensional framework", *Nature Reviews Drug Discovery*, vol. 13, no. 6, pp. 419–431, 2014. DOI: 10.1038/nrd4309.

[5] I. Kola and J. Landis, "Can the pharmaceutical industry reduce attrition rates?", *Nature Reviews Drug Discovery*, vol. 3, no. August, pp. 1–5, 2004. DOI: 10.1038/nrd1470.

[6] C. L. D. Schuster and T. Langer, "Why drugs fail - a study on side effects in new chemical entities", *Current Pharmaceutical Design*, vol. 11, no. 27, pp. 3545–3559, 2005. DOI: 10.2174/138161205774414510.

[7] J. A. DiMasi, R. W. Hansen, and H. G. Grabowski, "The price of innovation: New estimates of drug development costs", *Journal of Health Economics*, vol. 22, no. 2, pp. 151–185, 2003. DOI: 10.1016/S0167-6296(02)00126-1.

[8] J. A. DiMasi, H. G. Grabowski, and R. W. Hansen, "Innovation in the pharmaceutical industry: New estimates of R&D costs", *Journal of Health Economics*, vol. 47, pp. 20–33, 2016. DOI: 10.1016/j.jhealeco.2016.01.012.

[9] S. Morgan, P. Grootendorst, J. Lexchin, C. Cunningham, and D. Greyson, "The cost of drug development: A systematic review", *Health Policy*, vol. 100, no. 1, pp. 4–17, 2011. DOI: 10.1016/j.healthpol.2010.12.002.

[10] M. D. Rawlins, "Cutting the cost of drug development?", *Nature Reviews Drug Discovery*, vol. 3, no. 4, pp. 360–364, 2004. DOI: 10.1038/nrd1347.

[11] E. P. A. on Therapeutic Innovation. (). The key principles of pharmacokinetics – the study of the effect the body has on a medicine – are represented in the acronym adme., [Online]. Available: https://www.eupati.eu/fr/glossary/pharmacocinetique/. (accessed: 02.2020).

[12] V. J. Navarro and J. R. Senior, "Drug-related hepatotoxicity", *New England Journal of Medicine*, vol. 354, no. 7, pp. 731–739, 2006. DOI: 10.1056/NEJMra052270.

[13] D. Larrey, "Epidemiology and individual susceptibility to adverse drug reactions affecting the liver", *Seminars in liver disease*, vol. 22, pp. 145–55, Feb. 2002. DOI: 10.1055/s-2002-30105.

[14] W. Bernal and J. Wendon, "Acute liver failure", *New England Journal of Medicine*, vol. 369, no. 26, pp. 2525–2534, 2013. DOI: 10.1056/NEJMra1208937.

[15] M. Krishna, "Microscopic anatomy of the liver", *Clinical Liver Disease*, vol. 2, no. SUPPL. 1, pp. 4–7, 2013. DOI: 10.1002/cld.147.

[16] R. Saxena, N. D. Theise, and J. M. Crawford, "Microanatomy of the human liver - Exploring the hidden interfaces", *Hepatology*, vol. 30, no. 6, pp. 1339–1346, 1999. DOI: 10.1002/hep.510300607.

[17] A. M. Rappaport, Z. J. Borowy, W. M. Lougheed, and N. Lotto, "Subdivisions of Hexagonal Liver Lobules into a Structural and Functional Unit", *Role in hepatic physiology and pathology*, pp. 11–33, 1952. DOI: 10.1002/ar.1091190103.

[18] T. H.-Y. Medicine. (). Liver acinus, [Online]. Available: https://www.thehymedicine.com/gi. (accessed: 02.2020).

[19] M. N. H. System. (), [Online]. Available: https://www.mountnittany.org/articles/healthsheets/35761. (accessed: 02.2020).

[20] D. E. Malarkey, K. Johnson, L. Ryan, G. Boorman, and R. R. Maronpot, "New Insights into Functional Aspects of Liver Morphology", *Toxicologic Pathology*, vol. 33, no. 1, pp. 27–34, 2005. DOI: 10.1080/01926230590881826.

[21] E. Wisse, F. Braet, D. Luo, R. De Zanger, D. Jans, E. Crabbé, and A. Vermoesen, "Structure and function of sinusoidal lining cells in the liver", *Toxicologic Pathology*, vol. 24, no. 1, pp. 100–111, 1996. DOI: 10.1177/019262339602400114.

[22] A. Treyer and A. Müsch, "Hepatocyte Polarity", *Comprehensive Physiology*, pp. 243–287, 2013. DOI: 10.1002/cphy.c120009.Hepatocyte.

[23] A. Mescher, *Junqueira's Basic Histology: Text Atlas*. 2010.

[24] U. Frevert, S. Engelmann, S. Zougbédé, J. Stange, B. Ng, K. Matuschewski, L. Liebes, and H. Yee, "Intravital observation of plasmodium berghei sporozoite infection of the liver", *PLoS Biology*, vol. 3, no. 6, pp. 1034–1046, 2005. DOI: 10.1371/journal.pbio.0030192.

[25] I. Arias, H. Alter, J. Boyer, D. Cohen, N. Fausto, D. Shafritz, and A. Wolkoff, *The Liver: Biology and Pathobiology: Fifth Edition*, English (US). John Wiley and Sons, Oct. 2009, ISBN: 9780470723135. DOI: 10.1002/9780470747919.

[26] R. Gebhardt, "Metabolic zonation of the liver: Regulation and implications for liver function", *Pharmacology Therapeutics*, vol. 53, no. 3, pp. 275–354, 1992. DOI: 10.1016/0163-7258(92)90055-5.

[27] P. Godoy, N. J. Hewitt, U. Albrecht, M. E. Andersen, N. Ansari, S. Bhattacharya, J. Georg, B. Jennifer, B. Christoph, B. Jan, R. A. Budinsky, B. Burkhardt, N. R. Cameron, G. Camussi, T. Vanhaecke, M. Vinken, T. S. Weiss, A. Widera, C. G. Woods, J. James, X. Kathy, M. Y. Jan, P. Godoy, N. J. Hewitt, and J. G. Hengstler, *Recent advances in 2D and 3D in vitro systems using primary hepatocytes , alternative hepatocyte sources and non-parenchymal liver cells and their use in investigating mechanisms of hepatotoxicity , cell signaling and ADME*. 2013, pp. 1315–1530, ISBN: 0020401310. DOI: 10.1007/s00204-013-1078-5.

[28] L. L. Mazaleuskaya, K. Sangkuhl, C. F. Thorn, G. A. Fitzgerald, R. B. Altman, T. E. Klein, T. Therapeutics, and T. Medicine, "PharmGKB summary: Pathways of acetaminophen metabolism at the therapeutic versus toxic doses", *Pharmacogenetics Genomics*, vol. 25, no. 8, pp. 416–426, 2016. DOI: 10.1097/FPC.0000000000000150.PharmGKB.

[29] J. R. Mitchell, D. J. Jollow, W. Z. Potter, J. R. Gillette, and B. B. Brodie, "Acetaminophen-induced hepatic necrosis", *Journal of Pharmacology and Experimental Therapeutics*, vol. 187, no. 1, pp. 211–217, 1973.

[30] W. Russell and R. Burch, *The Principles of Humane Experimental Technique*, 1959.

[31] J. Tannenbaum and B. T. Bennett, "Russell and Burch's 3Rs then and now: The need for clarity in definition and purpose", *Journal of the American Association for Laboratory Animal Science*, vol. 54, no. 2, pp. 120–132, 2015.

[32] N. Burden, K. Chapman, F. Sewell, and V. Robinson, "Pioneering better science through the 3Rs: An introduction to the National Centre for the Replacement, Refinement, and Reduction of Animals in Research (NC3Rs)", *Journal of the American Association for Laboratory Animal Science*, vol. 54, no. 2, pp. 198–208, 2015.

[33] I. A. S. Olsson, S. P. d. Silva, D. Townend, and P. Sandøe, "Protecting Animals and Enabling Research in the European Union: An Overview of Development and Implementation of Directive 2010/63/EU", *ILAR Journal*, vol. 57, no. 3, pp. 347–357, May 2017. DOI: 10.1093/ilar/ilw029.

[34] H. Olson, G. Betton, D. Robinson, K. Thomas, A. Monro, G. Kolaja, P. Lilly, J. Sanders, G. Sipes, W. Bracken, M. Dorato, and K. V. Deun, "Concordance of the Toxicity of Pharmaceuticals in Humans and in Animals", *Regulatory Toxicology and Pharmacology*, vol. 67, pp. 56–67, 2000. DOI: 10.1006/rtph.2000.1399.

[35] K. Bayne and H. Würbel, "The impact of environmental enrichment on the outcome variability and scientific validity of laboratory animal studies", *OIE Revue Scientifique et Technique*, vol. 33, no. 1, pp. 273–280, 2014. DOI: 10.20506/rst.33.1.2282.

[36] G. C. Terstappen and A. Reggiani, "In silico research in drug discovery", *Trends in Pharmacological Sciences*, vol. 22, no. 1, pp. 23–26, 2001. DOI: 10.1016/S0165-6147(00)01584-4.

[37] H. Yu and A. Adedoyin, "Adme–tox in drug discovery: Integration of experimental and computational technologies", *Drug Discovery Today*, vol. 8, no. 18, pp. 852–861, 2003. DOI: 10.1016/S1359-6446(03)02828-9.

[38] Y. Low, T. Uehara, Y. Minowa, H. Yamada, Y. Ohno, T. Urushidani, A. Sedykh, E. Muratov, V. Kuz'min, D. Fourches, H. Zhu, I. Rusyn, and A. Tropsha, "Predicting drug-induced hepatotoxicity using qsar and toxicogenomics approaches", *Chemical Research in Toxicology*, vol. 24, no. 8, pp. 1251–1262, 2011. DOI: 10.1021/tx200148a.

[39] T. Hou and J. Wang, "Structure – adme relationship: Still a long way to go?", *Expert Opinion on Drug Metabolism & Toxicology*, vol. 4, no. 6, pp. 759–770, 2008. DOI: 10.1517/17425255.4.6.759.

[40] P. Zhao, L. Zhang, J. Grillo, Q. Liu, J. Bullock, Y. Moon, P. Song, S. Brar, R. Madabushi, T. Wu, B. Booth, N. Rahman, K. Reynolds, E. Gil Berglund, L. Lesko, and S.-M. Huang, "Applications of physiologically based pharmacokinetic (pbpk) modeling and simulation during regulatory review", *Clinical Pharmacology & Therapeutics*, vol. 89, no. 2, pp. 259–267, 2011. DOI: 10.1038/clpt.2010.298.

[41] V. Y. Soldatow, E. L. Lecluyse, L. G. Griffith, and I. Rusyn, "In vitro models for liver toxicity testing", *Toxicology Research*, vol. 2, no. 1, pp. 23–39, 2013. DOI: 10.1039/c2tx20051a.

[42] E. F. Brandon, C. D. Raap, I. Meijerman, J. H. Beijnen, and J. H. Schellens, "An update on in vitro test methods in human hepatic drug biotransformation research: Pros and cons", *Toxicology and Applied Pharmacology*, vol. 189, no. 3, pp. 233–246, 2003. DOI: 10.1016/S0041-008X(03)00128-5.

[43] P. Fasinu, P. J. Bouic, and B. Rosenkranz, "Liver-Based In Vitro Technologies for Drug Biotransformation Studies - A Review", *Current Drug Metabolism*, vol. 13, no. 2, pp. 215–224, 2012. DOI: 10.2174/138920012798918426.

[44] J. R. C. European Commission. (). Eurl ecvam dataset on alternative methods to animal experimentation (db-alm), [Online]. Available: http://data.europa.eu/89h/b7597ada-148d-4560-9079-ab0a5539cad3. (accessed: 01.2020).

[45] N. J. Hewitt, M. J. G. Lechón, J. B. Houston, D. Hallifax, H. S. Brown, P. Maurel, J. G. Kenna, L. Gustavsson, C. Lohmann, C. Skonberg, A. Guillouzo, G. Tuschl, A. P. Li, E. LeCluyse, G. M. M. Groothuis, and J. G. Hengstler, "Primary hepatocytes: Current understanding of the regulation of metabolic enzymes and transporter proteins, and pharmaceutical practice for the use of hepatocytes in metabolism, enzyme induction, transporter, clearance, and hepatotoxicity studies", *Drug Metabolism Reviews*, vol. 39, no. 1, pp. 159–234, 2007. DOI: 10.1080/03602530601093489.

[46] E. L. LeCluyse, E. Alexandre, G. A. Hamilton, C. Viollon-Abadie, D. J. Coon, S. Jolley, and L. Richert, "Isolation and culture of primary human hepatocytes", in

Basic Cell Culture Protocols, C. D. Helgason and C. L. Miller, Eds. Totowa, NJ: Humana Press, 2005, pp. 207–229, ISBN: 978-1-59259-838-0. DOI: 10.1385/1-59259-838-2:207.

[47] M. J. Gómez-Lechón, L. Tolosa, I. Conde, and M. T. Donato, "Competency of different cell models to predict human hepatotoxic drugs", *Expert Opinion on Drug Metabolism & Toxicology*, vol. 10, no. 11, pp. 1553–1568, 2014. DOI: 10.1517/17425255.2014.967680.

[48] M. J. Gomez-Lechon, M. T. Donato, A. Lahoz, and J. V. Castell, "Cell lines: A tool for in vitro drug metabolism studies", *Current Drug Metabolism*, vol. 9, no. 1, pp. 1–11, 2008. DOI: doi:10.2174/138920008783331086.

[49] C. Hilgendorf, G. Ahlin, A. Seithel, P. Artursson, A.-L. Ungell, and J. Karlsson, "Expression of thirty-six drug transporter genes in human intestine, liver, kidney, and organotypic cell lines", *Drug Metabolism and Disposition*, vol. 35, no. 8, pp. 1333–1340, 2007. DOI: 10.1124/dmd.107.014902.

[50] L. Guo, S. Dial, L. Shi, W. Branham, J. Liu, J.-L. Fang, B. Green, H. Deng, J. Kaput, and B. Ning, "Similarities and differences in the expression of drug-metabolizing enzymes between human hepatic cell lines and primary human hepatocytes", *Drug Metabolism and Disposition*, vol. 39, no. 3, pp. 528–538, 2011. DOI: 10.1124/dmd.110.035873.

[51] H. H. J. Gerets, K. Tilmant, B. Gerin, H. Chanteux, B. O. Depelchin, S. Dhalluin, and F. A. Atienzar, "Characterization of primary human hepatocytes, hepg2 cells, and heparg cells at the mrna level and cyp activity in response to inducers and their predictivity for the detection of human hepatotoxins", *Cell Biology and Toxicology*, vol. 28, pp. 69–87, 2012. DOI: 10.1007/s10565-011-9208-4.

[52] E. L. LeCluyse, R. P. Witek, M. E. Andersen, and M. J. Powers, "Organotypic liver culture models: Meeting current challenges in toxicity testing", *Critical Reviews in Toxicology*, vol. 42, no. 6, pp. 501–548, 2012. DOI: 10.3109/10408444.2012.682115.

[53] S. Wilkening, F. Stahl, and A. Bader, "Comparison of primary human hepatocytes and hepatoma cell line hepg2 with regard to their biotransformation properties", *Drug Metabolism and Disposition*, vol. 31, no. 8, pp. 1035–1042, 2003. DOI: 10.1124/dmd.31.8.1035.

[54] W. M. Westerink and W. G. Schoonen, "Cytochrome p450 enzyme levels in hepg2 cells and cryopreserved primary human hepatocytes and their induction in hepg2 cells", *Toxicology in Vitro*, vol. 21, no. 8, pp. 1581–1591, 2007. DOI: 10.1016/j.tiv.2007.05.014.

[55] S. Anthérieu, C. Chesné, R. Li, C. Guguen-Guillouzo, and A. Guillouzo, "Optimization of the heparg cell model for drug metabolism and toxicity studies", *Toxicology in Vitro*, vol. 26, no. 8, pp. 1278–1285, 2012. DOI: 10.1016/j.tiv.2012.05.008.

[56] A. Guillouzo, A. Corlu, C. Aninat, D. Glaise, F. Morel, and C. Guguen-Guillouzo, "The human hepatoma heparg cells: A highly differentiated model for studies of liver metabolism and toxicity of xenobiotics", *Chemico-Biological Interactions*, vol. 168, no. 1, pp. 66–73, 2007. DOI: 10.1016/j.cbi.2006.12.003.

[57] T. B. Andersson, K. P. Kanebratt, and J. G. Kenna, "The heparg cell line: A unique in vitro tool for understanding drug metabolism and toxicology in human", *Expert Opinion on Drug Metabolism & Toxicology*, vol. 8, no. 7, pp. 909–920, 2012. DOI: 10.1517/17425255.2012.685159.

[58] K. Takahashi and S. Yamanaka, "Induction of pluripotent stem cells from mouse embryonic and adult fibroblast cultures by defined factors", *Cell*, vol. 126, no. 4, pp. 663–676, 2006. DOI: 10.1016/j.cell.2006.07.024.

[59] J. C. Davila, G. G. Cezar, M. Thiede, S. Strom, T. Miki, and J. Trosko, "Use and Application of Stem Cells in Toxicology This article summarizes in part the Stem Cell Symposium presented at the 42nd Annual Meeting of the Society of Toxicology, Salt Lake City, Utah, March 2003.", *Toxicological Sciences*, vol. 79, no. 2, pp. 214–223, Jun. 2004. DOI: 10.1093/toxsci/kfh100.

[60] C. Guguen-Guillouzo, A. Corlu, and A. Guillouzo, "Stem cell-derived hepatocytes and their use in toxicology", *Toxicology*, vol. 270, no. 1, pp. 3–9, 2010. DOI: 10.1016/j.tox.2009.09.019.

[61] C. N. Medine, B. Lucendo-Villarin, C. Storck, F. Wang, D. Szkolnicka, F. Khan, S. Pernagallo, J. R. Black, H. M. Marriage, J. A. Ross, M. Bradley, J. P. Iredale, O. Flint, and D. C. Hay, "Developing high-fidelity hepatotoxicity models from pluripotent stem cells", *STEM CELLS Translational Medicine*, vol. 2, no. 7, pp. 505–509, 2013. DOI: 10.5966/sctm.2012-0138.

[62] K. Si-Tayeb, F. K. Noto, M. Nagaoka, J. Li, M. A. Battle, C. Duris, P. E. North, S. Dalton, and S. A. Duncan, "Highly efficient generation of human hepatocyte–like cells from induced pluripotent stem cells", *Hepatology*, vol. 51, no. 1, pp. 297–305, 2010. DOI: 10.1002/hep.23354.

[63] B. Anson, K. Kolaja, and T. Kamp, "Opportunities for use of human ips cells in predictive toxicology", *Clinical Pharmacology & Therapeutics*, vol. 89, no. 5, pp. 754–758, 2011. DOI: 10.1038/clpt.2011.9.

[64] J. Deng, W. Wei, Z. Chen, B. Lin, W. Zhao, Y. Luo, and X. Zhang, "Engineered liver-on-a-chip platform to mimic liver functions and its biomedical applications: A review", *Micromachines*, vol. 10, no. 10, 2019. DOI: 10.3390/mi10100676.

[65] S. Hasmall, N. James, K. Hedley, K. Olsen, and R. Roberts, "Mouse hepatocyte response to peroxisome proliferators: Dependency on hepatic nonparenchymal cells and peroxisome proliferator activated receptor (ppar)", *Archives of Toxicology*, vol. 75, no. 6, pp. 357–361, 2001. DOI: 10.1007/s002040100246.

[66] R. A. Roberts, P. E. Ganey, C. Ju, L. M. Kamendulis, I. Rusyn, and J. E. Klaunig, "Role of the Kupffer Cell in Mediating Hepatic Toxicity and Carcinogenesis", *Toxicological Sciences*, vol. 96, no. 1, pp. 2–15, Nov. 2006. DOI: 10.1093/toxsci/kfl173.

[67] R. Kostadinova, F. Boess, D. Applegate, L. Suter, T. Weiser, T. Singer, B. Naughton, and A. Roth, "A long-term three dimensional liver co-culture system for improved prediction of clinically relevant drug-induced hepatotoxicity", *Toxicology and Applied Pharmacology*, vol. 268, no. 1, pp. 1–16, 2013. DOI: 10.1016/j.taap.2013.01.012.

[68] Y. B. (Kang, S. Rawat, J. Cirillo, M. Bouchard, and H. (Noh, "Layered long-term co-culture of hepatocytes and endothelial cells on a transwell membrane: Toward engineering the liver sinusoid", *Biofabrication*, vol. 5, no. 4, p. 045 008, 2013. DOI: 10.1088/1758-5082/5/4/045008.

[69] M. Ohno, K. Motojima, T. Okano, and A. Taniguchi, "Induction of drug-metabolizing enzymes by phenobarbital in layered co-culture of a human liver cell line and endothelial cells", *Biological and Pharmaceutical Bulletin*, vol. 32, no. 5, pp. 813–817, 2009. DOI: 10.1248/bpb.32.813.

[70] M. West, G. Keller, B. Hyland, F. Cerra, and R. Simmons, "Further characterization of kupffer cell/macrophage-mediated alterations in hepatocyte protein synthesis", *Surgery*, vol. 100, no. 2, pp. 416–423, Aug. 1986.

[71] V. Kegel, E. Pfeiffer, B. Burkhardt, J. L. Liu, K. Zeilinger, A. K. Nüssler, D. Seehofer, and G. Damm, "Subtoxic concentrations of hepatotoxic drugs lead to kupffer cell activation in a human in vitro liver model: An approach to study dili", *Mediators of Inflammation*, 2015. DOI: 10.1155/2015/640631.

[72] J. Kasuya, R. Sudo, T. Mitaka, M. Ikeda, and K. Tanishita, "Hepatic stellate cell-mediated three-dimensional hepatocyte and endothelial cell triculture model", *Tissue Engineering Part A*, vol. 17, no. 3-4, pp. 361–370, 2011. DOI: 10.1089/ten.tea.2010.0033.

[73] C. A. Goubko and X. Cao, "Patterning multiple cell types in co-cultures: A review", *Materials Science and Engineering: C*, vol. 29, no. 6, pp. 1855–1868, 2009. DOI: 10.1016/j.msec.2009.02.016.

[74] W. F. Liu and C. S. Chen, "Engineering biomaterials to control cell function", *Materials Today*, vol. 8, no. 12, pp. 28–35, 2005. DOI: 10.1016/S1369-7021(05)71222-0.

[75] H.-W. Chien and W.-B. Tsai, "Fabrication of tunable micropatterned substrates for cell patterning via microcontact printing of polydopamine with poly(ethylene imine)-grafted copolymers", *Acta Biomaterialia*, vol. 8, no. 10, pp. 3678–3686, 2012. DOI: 10.1016/j.actbio.2012.06.033.

[76] S. N. Bhatia, M. L. Yarmush, and M. Toner, "Controlling cell interactions by micropatterning in co-cultures: Hepatocytes and 3T3 fibroblasts", *Journal of Biomedical Materials Research*, vol. 34, no. 2, pp. 189–199, 1997. DOI: 10.1002/(SICI)1097-4636(199702)34:2<189::AID-JBM8>3.0.CO;2-M.

[77] S. N. Bhatia, U. J. Balis, M. L. Yarmush, and M. Toner, "Microfabrication of hepatocyte/fibroblast co-cultures: Role of homotypic cell interactions", *Biotechnology Progress*, vol. 14, no. 3, pp. 378–387, 1998. DOI: 10.1021/bp980036j.

[78] C. H. Cho, J. Park, A. W. Tilles, F. Berthiaume, M. Toner, and M. L. Yarmush, "Layered patterning of hepatocytes in co-culture systems using microfabricated stencils", *BioTechniques*, vol. 48, no. 1, pp. 47–52, 2010. DOI: 10.2144/000113317.

[79] S. R. Khetani and S. N. Bhatia, "Microscale culture of human liver cells for drug development", *Nature Biotechnology*, vol. 26, no. 1, pp. 120–126, 2008. DOI: 10.1038/nbt1361.

[80] Y. S. Zinchenko and R. N. Coger, "Engineering micropatterned surfaces for the coculture of hepatocytes and Kupffer cells", *Journal of Biomedical Materials Research - Part A*, vol. 75, no. 1, pp. 242–248, 2005. DOI: 10.1002/jbm.a.30399.

[81] B. R. Ware, D. R. Berger, and S. R. Khetani, "Prediction of Drug-Induced Liver Injury in Micropatterned Co-cultures Containing iPSC-Derived Human Hepatocytes", *Toxicological Sciences*, vol. 145, no. 2, pp. 252–262, Feb. 2015. DOI: 10.1093/toxsci/kfv048.

[82] W. W. Wang, S. R. Khetani, S. Krzyzewski, D. B. Duignan, and R. S. Obach, "Assessment of a micropatterned hepatocyte coculture system to generate major human excretory and circulating drug metabolites", *Drug Metabolism and Disposition*, vol. 38, no. 10, pp. 1900–1905, 2010. DOI: 10.1124/dmd.110.034876.

[83] E. L. LeCluyse, K. L. Audus, and J. H. Hochman, "Formation of extensive canalicular networks by rat hepatocytes cultured in collagen-sandwich configuration", *American Journal of Physiology-Cell Physiology*, vol. 266, no. 6, pp. C1764–C1774, 1994. DOI: 10.1152/ajpcell.1994.266.6.C1764.

[84] G. Tuschl and S. O. Mueller, "Effects of cell culture conditions on primary rat hepatocytes—cell morphology and differential gene expression", *Toxicology*, vol. 218, no. 2, pp. 205–215, 2006. DOI: 10.1016/j.tox.2005.10.017.

[85] A. Kern, A. Bader, R. Pichlmayr, and K.-F. Sewing, "Drug metabolism in hepatocyte sandwich cultures of rats and humans", *Biochemical Pharmacology*, vol. 54, no. 7, pp. 761–772, 1997. DOI: 10.1016/S0006-2952(97)00204-9.

[86] K. Mathijs, A. S. Kienhuis, K. J. J. Brauers, D. G. J. Jennen, A. Lahoz, J. C. S. Kleinjans, and J. H. M. van Delft, "Assessing the metabolic competence of sandwich-cultured mouse primary hepatocytes", *Drug Metabolism and Disposition*, vol. 37, no. 6, pp. 1305–1311, 2009. DOI: 10.1124/dmd.108.025775.

[87] Y.-a. Bi, D. Kazolias, and D. B. Duignan, "Use of cryopreserved human hepatocytes in sandwich culture to measure hepatobiliary transport", *Drug Metabolism and Disposition*, vol. 34, no. 9, pp. 1658–1665, 2006. DOI: 10.1124/dmd.105.009118.

[88] S. S. Bale, I. Golberg, R. Jindal, W. J. McCarty, M. Luitje, M. Hegde, A. Bhushan, O. B. Usta, and M. L. Yarmush, "Long-term coculture strategies for primary hepatocytes and liver sinusoidal endothelial cells", *Tissue Engineering Part C: Methods*, vol. 21, no. 4, pp. 413–422, 2015. DOI: 10.1089/ten.tec.2014.0152.

[89] N. Yamada, T. Okano, H. Sakai, F. Karikusa, Y. Sawasaki, and Y. Sakurai, "Thermo-responsive polymeric surfaces; control of attachment and detachment of cultured cells", *Die Makromolekulare Chemie, Rapid Communications*, vol. 11, no. 11, pp. 571–576, 1990. DOI: 10.1002/marc.1990.030111109.

[90] M. Yamato, C. Konno, M. Utsumi, A. Kikuchi, and T. Okano, "Thermally responsive polymer-grafted surfaces facilitate patterned cell seeding and co-culture", *Biomaterials*, vol. 23, no. 2, pp. 561–567, 2002. DOI: 10.1016/S0142-9612(01)00138-7.

[91] K. Kim, K. Ohashi, R. Utoh, K. Kano, and T. Okano, "Preserved liver-specific functions of hepatocytes in 3d co-culture with endothelial cell sheets", *Biomaterials*, vol. 33, no. 5, pp. 1406–1413, 2012. DOI: 10.1016/j.biomaterials.2011.10.084.

[92] B. Swift, N. D. Pfeifer, and K. L. Brouwer, "Sandwich-cultured hepatocytes: An in vitro model to evaluate hepatobiliary transporter-based drug interactions and hepatotoxicity", *Drug Metabolism Reviews*, vol. 42, no. 3, pp. 446–471, 2010. DOI: 10.3109/03602530903491881.

[93] C. Rowe, C. E. P. Goldring, N. R. Kitteringham, R. E. Jenkins, B. S. Lane, C. Sanderson, V. Elliott, V. Platt, P. Metcalfe, and B. K. Park, "Network analysis of primary hepatocyte dedifferentiation using a shotgun proteomics approach", *Journal of Proteome Research*, vol. 9, no. 5, pp. 2658–2668, 2010. DOI: 10.1021/pr1001687.

[94] R. Z. Lin and H. Y. Chang, "Recent advances in three-dimensional multicellular spheroid culture for biomedical research", *Biotechnology Journal*, vol. 3, no. 9-10, pp. 1172–1184, 2008. DOI: 10.1002/biot.200700228.

[95] E. Fennema, N. Rivron, J. Rouwkema, C. van Blitterswijk, and J. de Boer, "Spheroid culture as a tool for creating 3d complex tissues", *Trends in Biotechnology*, vol. 31, no. 2, pp. 108–115, 2013. DOI: 10.1016/j.tibtech.2012.12.003.

[96] S. F. Abu-Absi, J. R. Friend, L. K. Hansen, and W. S. Hu, "Structural polarity and functional bile canaliculi in rat hepatocyte spheroids", *Experimental Cell Research*, vol. 274, no. 1, pp. 56–67, 2002. DOI: 10.1006/excr.2001.5467.

[97] S. C. Ramaiahgari, M. W. den Braver, B. Herpers, V. Terpstra, J. N. M. Commandeur, B. van de Water, and L. S. Price, "A 3D in vitro model of differentiated HepG2 cell spheroids with improved liver-like properties for repeated dose high-throughput toxicity studie", *Archives of Toxicology*, vol. 88, no. 1, pp. 1083–1095, 2014. DOI: 10.1007/s00204-014-1215-9.

[98] C. C. Bell, D. F. G. Hendriks, S. M. L. Moro, E. Ellis, J. Walsh, A. Renblom, L. F. Puigvert, A. C. A. Dankers, F. Jacobs, J. Snoeys, R. L. Sison-young, R. E. Jenkins, Å. Nordling, S. Mkrtchian, B. K. Park, N. R. Kitteringham, C. E. P. Goldring, and V. M. Lauschke, "Characterization of primary human hepatocyte spheroids as a model system for drug-induced liver injury , liver function and disease", *Nature Publishing Group*, vol. 6, no. April, 2016. DOI: 10.1038/srep25187.

[99] R. M. Tostões, S. B. Leite, M. Serra, J. Jensen, P. Björquist, M. J. T. Carrondo, C. Brito, and P. M. Alves, "Human liver cell spheroids in extended perfusion bioreactor culture for repeated-dose drug testing", *Hepatology*, vol. 55, no. 4, pp. 1227–1236, 2012. DOI: 10.1002/hep.24760.

[100] S. Nayak, S. Dey, and S. C. Kundu, "Silk sericin–alginate–chitosan microcapsules: Hepatocytes encapsulation for enhanced cellular functions", *International Journal of Biological Macromolecules*, vol. 65, pp. 258–266, 2014. DOI: 10.1016/j.ijbiomac.2014.01.042.

[101] M. B. Phillips, P. Balbuena-Venancio, J. R. Enders, R. L. Norini, Y.-S. Shim, E. Burgunder, L. Rao, D. Billings, J. Pedersen, J. M. Macdonald, M. Andersen, H. J. Clewell, and M. Yoon, "Xenobiotic metabolism in alginate-encapsulated primary human hepatocytes over long timeframes", *Applied In Vitro Toxicology*, vol. 4, no. 3, pp. 238–247, 2018. DOI: 10.1089/aivt.2017.0029.

[102] C. Guyomard, L. Rialland, B. Fremond, C. Chesne, and A. Guillouzo, "Influence of alginate gel entrapment and cryopreservation on survival and xenobiotic metabolism capacity of rat hepatocytes", *Toxicology and Applied Pharmacology*, vol. 141, no. 2, pp. 349–356, 1996. DOI: 10.1006/taap.1996.0299.

[103] L. Canaple, N. Nurdin, N. Angelova, D. Saugy, D. Hunkeler, and B. Desvergne, "Maintenance of primary murine hepatocyte functions in multicomponent polymer capsules – in vitro cryopreservation studies", *Journal of Hepatology*, vol. 34, no. 1, pp. 11–18, 2001. DOI: 10.1016/S0168-8278(00)00086-6.

[104] T. Aoki, T. Koizumi, Y. Kobayashi, D. Yasuda, Y. Izumida, Z. Jin, N. Nishino, Y. Shimizu, H. Kato, N. Murai, T. Niiya, Y. Enami, K. Mitamura, T. Yamamoto, and M. Kusano, "A novel method of cryopreservation of rat and human hepatocytes by using encapsulation technique and possible use for cell transplantation", *Cell Transplantation*, vol. 14, no. 9, pp. 609–620, 2005. DOI: 10.3727/000000005783982710.

[105] M. J. Bissell, H. Hall, and G. Parry, "How does the extracellular matrix direct gene expression?", *Journal of Theoretical Biology*, vol. 99, no. 1, pp. 31–68, 1982. DOI: 10.1016/0022-5193(82)90388-5.

[106] J. L. Drury and D. J. Mooney, "Hydrogels for tissue engineering: Scaffold design variables and applications", *Biomaterials*, vol. 24, no. 24, pp. 4337–4351, 2003. DOI: 10.1016/S0142-9612(03)00340-5.

[107] A. S. Hoffman, "Hydrogels for biomedical applications", *Advanced Drug Delivery Reviews*, vol. 64, pp. 18–23, 2012. DOI: 10.1016/j.addr.2012.09.010.

[108] M. W. Tibbitt and K. S. Anseth, "Hydrogels as extracellular matrix mimics for 3d cell culture", *Biotechnology and Bioengineering*, vol. 103, no. 4, pp. 655–663, 2009. DOI: 10.1002/bit.22361.

[109] A. Skardal, L. Smith, S. Bharadwaj, A. Atala, S. Soker, and Y. Zhang, "Tissue specific synthetic ecm hydrogels for 3-d in vitro maintenance of hepatocyte function", *Biomaterials*, vol. 33, no. 18, pp. 4565–4575, 2012. DOI: 10.1016/j.biomaterials.2012.03.034.

[110] M. Bhattacharya, M. M. Malinen, P. Lauren, Y.-R. Lou, S. W. Kuisma, L. Kanninen, M. Lille, A. Corlu, C. GuGuen-Guillouzo, O. Ikkala, A. Laukkanen, A. Urtti, and M. Yliperttula, "Nanofibrillar cellulose hydrogel promotes three-dimensional liver cell culture", *Journal of Controlled Release*, vol. 164, no. 3, pp. 291–298, 2012. DOI: 10.1016/j.jconrel.2012.06.039.

[111] A. Memic, T. Colombani, L. J. Eggermont, M. Rezaeeyazdi, J. Steingold, Z. J. Rogers, K. J. Navare, and H. S. Mohammed, "Latest Advances in Cryogel Technology for Biomedical Applications", vol. 1800114, pp. 1–45, 2019. DOI: 10.1002/adtp.201800114.

[112] S. Zmora, R. Glicklis, and S. Cohen, "Tailoring the pore architecture in 3-d alginate scaffolds by controlling the freezing regime during fabrication", *Biomaterials*, vol. 23, no. 20, pp. 4087–4094, 2002. DOI: 10.1016/S0142-9612(02)00146-1.

[113] M. Rezaeeyazdi, T. Colombani, A. Memic, and S. Bencherif, "Injectable hyaluronic acid-co-gelatin cryogels for tissue-engineering applications", *Materials*, vol. 11, no. 8, p. 1374, Aug. 2018. DOI: 10.3390/ma11081374.

[114] J. Yang, T. Woong Chung, M. Nagaoka, M. Goto, C. S. Cho, and T. Akaike, "Hepatocyte-specific porous polymer-scaffolds of alginate/galactosylated chitosan sponge for liver-tissue engineering", *Biotechnology Letters*, vol. 23, no. 17, pp. 1385–1389, 2001. DOI: 10.1023/A:1011600414225.

[115] R. Glicklis, L. Shapiro, R. Agbaria, J. C. Merchuk, and S. Cohen, "Hepatocyte behavior within three-dimensional porous alginate scaffolds", *Biotechnology and Bioengineering*, vol. 67, no. 3, pp. 344–353, 2000. DOI: 10.1002/(SICI)1097-0290(20000205)67:3<344::AID-BIT11>3.0.CO;2-2.

[116] E. Jain, A. Damania, A. K. Shakya, A. Kumar, S. K. Sarin, and A. Kumar, "Fabrication of macroporous cryogels as potential hepatocyte carriers for bioartificial liver support", *Colloids and Surfaces B: Biointerfaces*, vol. 136, pp. 761–771, 2015. DOI: 10.1016/j.colsurfb.2015.10.012.

[117] P. L. Lewis and R. N. Shah, "3D Printing for Liver Tissue Engineering: Current Approaches and Future Challenges", *Current Transplantation Reports*, vol. 3, no. 1, pp. 100–108, 2016. DOI: 10.1007/s40472-016-0084-y.

[118] Y. S. Zhang, K. Yue, J. Aleman, K. Mollazadeh-Moghaddam, S. M. Bakht, J. Yang, W. Jia, V. Dell'Erba, P. Assawes, S. R. Shin, M. R. Dokmeci, R. Oklu, and A. Khademhosseini, "3D Bioprinting for Tissue and Organ Fabrication", *Annals of Biomedical Engineering*, vol. 45, no. 1, pp. 148–163, 2017. DOI: 10.1007/s10439-016-1612-8.

[119] S. Ji and M. Guvendiren, "Recent Advances in Bioink Design for 3D Bioprinting of Tissues and Organs", *Frontiers in Bioengineering and Biotechnology*, vol. 5, no. APR, pp. 1–8, 2017. DOI: 10.3389/fbioe.2017.00023.

[120] S. V. Murphy and A. Atala, "3D bioprinting of tissues and organs", *Nature Biotechnology*, vol. 32, no. 8, pp. 773–785, 2014. DOI: 10.1038/nbt.2958.

[121] W. Zhu, X. Ma, M. Gou, D. Mei, K. Zhang, and S. Chen, "3d printing of functional biomaterials for tissue engineering", *Current Opinion in Biotechnology*, vol. 40, pp. 103–112, 2016. DOI: 10.1016/j.copbio.2016.03.014.

[122] J. Li, M. Chen, X. Fan, and H. Zhou, "Recent advances in bioprinting techniques: Approaches, applications and future prospects", *Journal of Translational Medicine*, vol. 14, no. 1, pp. 1–15, 2016. DOI: 10.1186/s12967-016-1028-0.

[123] Y. Kim, K. Kang, J. Jeong, S. S. Paik, J. S. Kim, S. A. Park, W. D. Kim, J. Park, and D. Choi, "Three-dimensional (3D) printing of mouse primary hepatocytes to generate 3D hepatic structure", *Annals of Surgical Treatment and Research*, vol. 92, no. 2, pp. 67–72, 2017. DOI: 10.4174/astr.2017.92.2.67.

[124] D. G. Nguyen, J. Funk, J. B. Robbins, C. Crogan-Grundy, S. C. Presnell, T. Singer, and A. B. Roth, "Bioprinted 3D primary liver tissues allow assessment of organ-level response to clinical drug induced toxicity in vitro", *PLoS ONE*, vol. 11, no. 7, pp. 1–17, 2016. DOI: 10.1371/journal.pone.0158674.

[125] A. Faulkner-Jones, C. Fyfe, D. J. Cornelissen, J. Gardner, J. King, A. Courtney, and W. Shu, "Bioprinting of human pluripotent stem cells and their directed differentiation into hepatocyte-like cells for the generation of mini-livers in 3D", *Biofabrication*, vol. 7, no. 4, 2015. DOI: 10.1088/1758-5090/7/4/044102.

[126] X. Ma, X. Qu, W. Zhu, Y. S. Li, S. Yuan, H. Zhang, J. Liu, P. Wang, C. S. E. Lai, F. Zanella, G. S. Feng, F. Sheikh, S. Chien, and S. Chen, "Deterministically patterned biomimetic human iPSC-derived hepatic model via rapid 3D bioprinting", *Proceedings of the National Academy of Sciences of the United States of America*, vol. 113, no. 8, pp. 2206–2211, 2016. DOI: 10.1073/pnas.1524510113.

[127] A. Dash, M. B. Simmers, T. G. Deering, D. J. Berry, R. E. Feaver, N. E. Hastings, T. L. Pruett, E. L. LeCluyse, B. R. Blackman, and B. R. Wamhoff, "Hemodynamic flow improves rat hepatocyte morphology, function, and metabolic activity in vitro", *American Journal of Physiology-Cell Physiology*, vol. 304, no. 11, pp. C1053–C1063, 2013. DOI: 10.1152/ajpcell.00331.2012.

[128] H. Rashidi, S. Alhaque, D. Szkolnicka, O. Flint, and D. C. Hay, "Fluid shear stress modulation of hepatocyte-like cell function", *Archives of Toxicology*, vol. 90, no. 7, pp. 1757–1761, 2016. DOI: 10.1007/s00204-016-1689-8.

[129] M. R. Ebrahimkhani, J. A. S. Neiman, M. S. B. Raredon, D. J. Hughes, and L. G. Griffith, "Bioreactor technologies to support liver function in vitro", *Advanced Drug Delivery Reviews*, vol. 69-70, pp. 132–157, 2014. DOI: 10.1016/j.addr.2014.02.011.

[130] J. W. Allen, T. Hassanein, and S. N. Bhatia, "Advances in bioartificial liver devices", *Hepatology*, vol. 34, no. 3, pp. 447–455, 2001. DOI: 10.1053/jhep.2001.26753.

[131] C. Legallais, B. David, and E. Doré, "Bioartificial livers (bal): Current technological aspects and future developments", *Journal of Membrane Science*, vol. 181, no. 1, pp. 81–95, 2001. DOI: 10.1016/S0376-7388(00)00539-1.

[132] S. Chen, J. Wang, H. Ren, Y. Liu, C. Xiang, C. Li, S. Lu, Y. Shi, H. Deng, and X. Shi, "Hepatic spheroids derived from human induced pluripotent stem cells in bio-artificial liver rescue porcine acute liver failure", *Cell Research*, vol. 30, no. 1, pp. 95–97, 2020. DOI: 10.1038/s41422-019-0261-5.

[133] V. Arumugaswami and Clive Svendsen, *Induced pluripotent stem cell-derived hepatocyte based bioartificial liver device*, 2016.

[134] K. Zeilinger, T. Schreiter, M. Darnell, T. Söderdahl, M. Lübberstedt, B. Dillner, D. Knobeloch, A. K. Nüssler, J. C. Gerlach, and T. B. Andersson, "Scaling down of a clinical three-dimensional perfusion multicompartment hollow fiber liver bioreactor developed for extracorporeal liver support to an analytical scale device useful for hepatic pharmacological in vitro studies", *Tissue Engineering Part C: Methods*, vol. 17, no. 5, pp. 549–556, 2011. DOI: 10.1089/ten.tec.2010.0580.

[135] V. N. Goral, Y.-C. Hsieh, O. N. Petzold, J. S. Clark, P. K. Yuen, and R. A. Faris, "Perfusion-based microfluidic device for three-dimensional dynamic primary human hepatocyte cell culture in the absence of biological or synthetic matrices or coagulants", *Lab Chip*, vol. 10, pp. 3380–3386, 24 2010. DOI: 10.1039/C0LC00135J.

[136] J. Park, F. Berthiaume, M. Toner, M. L. Yarmush, and A. W. Tilles, "Microfabricated grooved substrates as platforms for bioartificial liver reactors", *Biotechnology and Bioengineering*, vol. 90, no. 5, pp. 632–644, 2005. DOI: 10.1002/bit.20463.

[137] E. Leclerc, Y. Sakai, and T. Fujii, "Perfusion culture of fetal human hepatocytes in microfluidic environments", vol. 20, pp. 143–148, 2004. DOI: 10.1016/j.bej.2003.09.010.

[138] Y.-C. Toh, T. C. Lim, D. Tai, G. Xiao, D. van Noort, and H. Yu, "A microfluidic 3d hepatocyte chip for drug toxicity testing", *Lab Chip*, vol. 9, pp. 2026–2035, 14 2009. DOI: 10.1039/B900912D.

[139] P. Chao, T. Maguire, E. Novik, K.-C. Cheng, and M. Yarmush, "Evaluation of a microfluidic based cell culture platform with primary human hepatocytes for the prediction of hepatic clearance in human", *Biochemical Pharmacology*, vol. 78, no. 6, pp. 625–632, 2009. DOI: 10.1016/j.bcp.2009.05.013.

[140] L. Xia, S. Ng, R. Han, X. Tuo, G. Xiao, H. L. Leo, T. Cheng, and H. Yu, "Laminar-flow immediate-overlay hepatocyte sandwich perfusion system for drug hepatotoxicity testing", *Biomaterials*, vol. 30, no. 30, pp. 5927–5936, 2009. DOI: 10.1016/j.biomaterials.2009.07.022.

[141] M. Hegde, R. Jindal, A. Bhushan, S. S. Bale, W. J. McCarty, I. Golberg, O. B. Usta, and M. L. Yarmush, "Dynamic interplay of flow and collagen stabilizes primary hepatocytes culture in a microfluidic platform", *Lab Chip*, vol. 14, pp. 2033–2039, 12 2014. DOI: 10.1039/C4LC00071D.

[142] L. Prodanov, R. Jindal, S. S. Bale, M. Hegde, W. J. McCarty, I. Golberg, A. Bhushan, M. L. Yarmush, and O. B. Usta, "Long-term maintenance of a microfluidic 3d human liver sinusoid", *Biotechnology and Bioengineering*, vol. 113, no. 1, pp. 241–246, 2016. DOI: 10.1002/bit.25700.

[143] J. Deng, X. Zhang, Z. Chen, Y. Luo, Y. Lu, T. Liu, Z. Wu, Y. Jin, W. Zhao, and B. Lin, "A cell lines derived microfluidic liver model for investigation of hepatotoxicity induced by drug-drug interaction", *Biomicrofluidics*, vol. 13, no. 2, 2019. DOI: 10.1063/1.5070088.

[144] S. Bauer, C. Wennberg Huldt, K. P. Kanebratt, I. Durieux, D. Gunne, S. Andersson, L. Ewart, W. G. Haynes, I. Maschmeyer, A. Winter, C. Ämmälä, U. Marx, and T. B. Andersson, "Functional coupling of human pancreatic islets and liver spheroids on-a-chip: Towards a novel human ex vivo type 2 diabetes model", *Scientific Reports*, vol. 7, no. 1, pp. 1–11, 2017. DOI: 10.1038/s41598-017-14815-w.

[145] K. Moshksayan, N. Kashaninejad, M. E. Warkiani, J. G. Lock, H. Moghadas, B. Firoozabadi, M. S. Saidi, and N.-T. Nguyen, "Spheroids-on-a-chip: Recent advances and design considerations in microfluidic platforms for spheroid formation and culture", *Sensors and Actuators B: Chemical*, vol. 263, pp. 151–176, 2018. DOI: 10.1016/j.snb.2018.01.223.

[146] S.-A. Lee, D. Y. No, E. Kang, J. Ju, D.-S. Kim, and S.-H. Lee, "Spheroid-based three-dimensional liver-on-a-chip to investigate hepatocyte–hepatic stellate cell interactions and flow effects", *Lab Chip*, vol. 13, pp. 3529–3537, 18 2013. DOI: 10.1039/C3LC50197C.

[147] Y. Y. Choi, J. Kim, S. H. Lee, and D. S. Kim, "Lab on a chip-based hepatic sinusoidal system simulator for optimal primary hepatocyte culture", *Biomedical Microdevices*, vol. 18, no. 4, pp. 1–9, 2016. DOI: 10.1007/s10544-016-0079-6.

[148] F. Yu and D. Choudhury, "Microfluidic bioprinting for organ-on-a-chip models", *Drug Discovery Today*, vol. 24, no. 6, pp. 1248–1257, 2019. DOI: 10.1016/j.drudis.2019.03.025.

[149] J. Zhang, F. Chen, Z. He, Y. Ma, K. Uchiyama, and J.-M. Lin, "A novel approach for precisely controlled multiple cell patterning in microfluidic chips by inkjet printing and the detection of drug metabolism and diffusion", *Analyst*, vol. 141, pp. 2940–2947, 10 2016. DOI: 10.1039/C6AN00395H.

[150] N. S. Bhise, V. Manoharan, S. Massa, A. Tamayol, M. Ghaderi, M. Miscuglio, Q. Lang, Y. S. Zhang, S. R. Shin, G. Calzone, N. Annabi, T. D. Shupe, C. E. Bishop, A. Atala, M. R. Dokmeci, and A. Khademhosseini, "A liver-on-a-chip platform with bioprinted hepatic spheroids", *Biofabrication*, vol. 8, no. 1, p. 014 101, Jan. 2016. DOI: 10.1088/1758-5090/8/1/014101.

[151] H. Lee and D. W. Cho, "One-step fabrication of an organ-on-a-chip with spatial heterogeneity using a 3D bioprinting technology", *Lab on a Chip*, vol. 16, no. 14, pp. 2618–2625, 2016. DOI: 10.1039/c6lc00450d.

[152] J. M. Prot, A. S. Briffaut, F. Letourneur, P. Chafey, F. Merlier, Y. Grandvalet, C. Legallais, and E. Leclerc, "Integrated proteomic and transcriptomic investigation of the acetaminophen toxicity in liver microfluidic biochip", *PLoS ONE*, vol. 6, no. 8, 2011. DOI: 10.1371/journal.pone.0021268.

[153] J. M. Prot, A. Bunescu, B. Elena-Herrmann, C. Aninat, L. C. Snouber, L. Griscom, F. Razan, F. Y. Bois, C. Legallais, C. Brochot, A. Corlu, M. E. Dumas, and E. Leclerc, "Predictive toxicology using systemic biology and liver microfluidic "on chip" approaches: Application to acetaminophen injury", *Toxicology and Applied Pharmacology*, vol. 259, no. 3, pp. 270–280, 2012. DOI: 10.1016/j.taap.2011.12.017.

[154] A. Gautier, B. Carpentier, M. Dufresne, Q. V. Dinh, P. Paullier, and C. Legallais, "Impact of alginate type and bead diameter on mass transfers and the metabolic activities of encapsulated C3A cells in bioartificial liver applications", *European Cells and Materials*, vol. 21, no. 0, pp. 94–106, 2011.

[155] S. Figaro, U. Pereira, H. Rada, N. Semenzato, D. Pouchoulin, and C. Legallais, "Development and validation of a bioartificial liver device with fluidized bed bioreactors hosting alginate-encapsulated hepatocyte spheroids *", *2015 37th Annual International Conference of the IEEE Engineering in Medicine and Biology Society (EMBC)*, pp. 1335–1338, 2015. DOI: 10.1109/EMBC.2015.7318615.

[156] S. M. Coward, C. Legallais, B. David, M. Thomas, Y. Foo, D. Mavri-damelin, H. J. Hodgson, and C. Selden, "Alginate-encapsulated HepG2 Cells in a Fluidized Bed Bioreactor Maintain Function in Human Liver Failure Plasma", *Artificial Orgnas*, vol. 33, no. 12, pp. 1117–1126, 2009. DOI: 10.1111/j.1525-1594.2009.00821.x.

[157] T. Fujii, "Pdms-based microfluidic devices for biomedical applications", *Microelectronic Engineering*, vol. 61-62, pp. 907–914, 2002. DOI: 10.1016/S0167-9317(02)00494-X.

[158] C. Legallais, R. Baudoin, and E. Leclerc, *Bioreactor for culturing cells, wo 2010/149567 a2*, 2010.

[159] R. Baudoin, L. Griscom, J. M. Prot, C. Legallais, and E. Leclerc, "Behavior of HepG2/C3A cell cultures in a microfluidic bioreactor", *Biochemical Engineering Journal*, vol. 53, no. 2, pp. 172–181, 2011. DOI: 10.1016/j.bej.2010.10.007.

[160] J. M. Prot, C. Aninat, L. Griscom, F. Razan, C. Brochot, C. G. Guillouzo, C. Legallais, A. Corlu, and E. Leclerc, "Improvement of HepG2/C3a cell functions in a microfluidic biochip", *Biotechnology and Bioengineering*, vol. 108, no. 7, pp. 1704–1715, 2011. DOI: 10.1002/bit.23104.

[161] L. C. Snouber, A. Bunescu, M. Naudot, C. Legallais, C. Brochot, M. E. Dumas, B. Elena-Herrmann, and E. Leclerc, "Metabolomics-on-a-chip of hepatotoxicity induced by anticancer drug flutamide and its active metabolite hydroxyflutamide using hepg2/c3a microfluidic biochips", *Toxicological Sciences*, vol. 132, no. 1, pp. 8–20, 2013. DOI: 10.1093/toxsci/kfs230.

[162] R. Baudoin, G. Alberto, A. Legendre, P. Paullier, M. Naudot, M. J. Fleury, S. Jacques, L. Griscom, and E. Leclerc, "Investigation of expression and activity levels of primary rat hepatocyte detoxication genes under various flow rates and cell densities in microfluidic biochips", *Biotechnology Progress*, vol. 30, no. 2, pp. 401–410, 2014. DOI: 10.1002/btpr.1857.

[163] R. Jellali, P. Zeller, F. Gilard, A. Legendre, M. J. Fleury, S. Jacques, G. Tcherkez, and E. Leclerc, "Effects of DDT and permethrin on rat hepatocytes cultivated in microfluidic biochips: metabolomics and gene expression study", *Environmental Toxicology and Pharmacology*, no. 2010, 2018. DOI: 10.1016/j.etap.2018.02.004.

[164] R. Jellali, T. Bricks, S. Jacques, M.-j. Fleury, P. Paullier, F. Merlier, and E. Leclerc, "Long-term human primary hepatocyte cultures in a micro fluidic liver biochip show maintenance of mRNA levels and higher drug metabolism compared with Petri cultures", *Biopharmaceutics & Drug Disposition*, vol. 275, no. March, pp. 264–275, 2016. DOI: 10.1002/bdd.

[165] J. M. Prot, O. Videau, C. Brochot, C. Legallais, H. Bénech, and E. Leclerc, "A cocktail of metabolic probes demonstrates the relevance of primary human hepatocyte cultures in a microfluidic biochip for pharmaceutical drug screening", *International Journal of Pharmaceutics*, vol. 408, no. 1-2, pp. 67–75, 2011. DOI: 10.1016/j.ijpharm.2011.01.054.

[166] G. Orive, A. M. Carcaboso, R. M. Hernández, A. R. Gascón, and J. L. Pedraz, "Biocompatibility evaluation of different alginates and alginate-based microcapsules", *Biomacromolecules*, vol. 6, no. 2, pp. 927–931, 2005. DOI: 10.1021/bm049380x.

[167] K. Y. Lee and D. J. Mooney, "Alginate: Properties and biomedical applications", *Progress in Polymer Science (Oxford)*, vol. 37, no. 1, pp. 106–126, 2012. DOI: 10.1016/j.progpolymsci.2011.06.003.

[168] M. Szekalska, A. Puciłowska, E. Szymańska, P. Ciosek, and K. Winnicka, "Alginate: Current Use and Future Perspectives in Pharmaceutical and Biomedical Applications", *International Journal of Polymer Science*, vol. 2016, 2016. DOI: 10.1155/2016/7697031.

[169] T. Henderson, K. Ladewig, D. Haylock, K. McLean, and A. J. O. Connor, "Cryogels for Biomedical Applications", *Journal of Materials Chemistry*, vol. 1, no. May, pp. 2682–2695, 2013. DOI: 10.1039/C3TB20280A.

[170] F. M. Plieva, I. Y. Galaev, W. Noppe, and B. Mattiasson, "Cryogel applications in microbiology", *Trends in Microbiology*, no. October, pp. 543–551, 2008. DOI: 10.1016/j.tim.2008.08.005.

[171] V. Lozinsky, "Polymeric cryogels as a new family of macroporous and supermacroporous materials for biotechnological purposes", *Russ Chem Bull*, vol. 57, no. 5, pp. 1015–1032, 2008. DOI: 10.1007/s11172-008-0131-7.

[172] K. R. Hixon, T. Lu, and S. A. Sell, "A comprehensive review of cryogels and their roles in tissue engineering applications", *Acta Biomaterialia*, vol. 62, pp. 29–41, 2017. DOI: 10.1016/j.actbio.2017.08.033.

[173] G. Ingavle, L. Baillie, Y. Zheng, E. Lis, I. Savina, C. Howell, S. Mikhalovsky, and S. Sandeman, "Affinity binding of antibodies to supermacroporous cryogel adsorbents with immobilized protein a for removal of anthrax toxin protective antigen", *Biomaterials*, vol. 50, May 2015. DOI: 10.1016/j.biomaterials.2015.01.039.

[174] C. Legallais, R. Baudoin, E. Leclerc, J. M. Prot, and P. Paullier, *Multi-reactor unit for dynamic cell culture, wo 201 1/107519 a2*, 2011.

[175] C. Legallais, R. Baudoin, E. Leclerc, J.-M. Prot, and P. Paullier, *Multi-reactor unit for dynamic cell culture, us 2013/0084632 a1*, 2013.

[176] Y. S. Heo, L. M. Cabrera, J. W. Song, N. Futai, Y.-C. Tung, G. D. Smith, and S. Takayama, "Characterization and resolution of evaporation-mediated osmolality shifts that constrain microfluidic cell culture in poly(dimethylsiloxane) devices", *Analytical Chemistry*, vol. 79, no. 3, pp. 1126–1134, 2007. DOI: 10.1021/ac061990v.

[177] R. Baudoin, "Développement et caractérisation d'une puce à cellules pour le criblage d'agents toxiques", PhD thesis, Université de Technologie de Compiègne, 2008.

[178] G. Ferraioli, P. Parekh, A. B. Levitov, and C. Filice, "Shear wave elastography for evaluation of liver fibrosis", *Journal of Ultrasound in Medicine*, vol. 33, no. 2, pp. 197–203, 2014. DOI: 10.7863/ultra.33.2.197.

[179] C. H. Suh, S. Y. Kim, K. W. Kim, Y.-S. Lim, S. J. Lee, M.-G. Lee, J. Lee, S.-G. Lee, and E. Yu, "Determination of normal hepatic elasticity by using real-time shear-wave elastography", *Radiology*, vol. 271, no. 3, pp. 895–900, 2014. DOI: 10.1148/radiol.14131251.

[180] M. E. Hoque, W. Y. San, F. Wei, S. Li, M.-H. Huang, M. Vert, and D. W. Hutmacher, "Processing of polycaprolactone and polycaprolactone-based copolymers into 3d scaffolds, and their cellular responses", *Tissue Engineering Part A*, vol. 15, no. 10, pp. 3013–3024, 2009. DOI: 10.1089/ten.tea.2008.0355.

[181] N. Sultana and M. Wang, "PHBV/PLLA-based composite scaffolds fabricated using an emulsion freezing/freeze-drying technique for bone tissue engineering: Surface modification and in vitro biological evaluation", *Biofabrication*, vol. 4, no. 1, 2012. DOI: 10.1088/1758-5082/4/1/015003.

[182] C. Bossard, H. Granel, Y. Wittrant, É. Jallot, J. Lao, C. Vial, and H. Tiainen, "Polycaprolactone / bioactive glass hybrid scaffolds for bone regeneration", *Biomedical Glasses*, vol. 4, no. 1, pp. 108–122, 2018. DOI: 10.1515/bglass-2018-0010.

[183] R. Baudoin, G. Alberto, P. Paullier, C. Legallais, and E. Leclerc, "Parallelized microfluidic biochips in multi well plate applied to liver tissue engineering", *Sensors and Actuators B: Chemical*, vol. 173, pp. 919–926, 2012. DOI: 10.1016/j.snb.2012.06.050.

[184] E. Ruoslahti, "Rgd and other recognition sequences for integrins", *Annual Review of Cell and Developmental Biology*, vol. 12, no. 1, pp. 697–715, 1996. DOI: 10.1146/annurev.cellbio.12.1.697.

[185] U. Hersel, C. Dahmen, and H. Kessler, "Rgd modified polymers: Biomaterials for stimulated cell adhesion and beyond", *Biomaterials*, vol. 24, no. 24, pp. 4385–4415, 2003. DOI: 10.1016/S0142-9612(03)00343-0.

[186] C. K. Kuo and P. X. Ma, "Maintaining dimensions and mechanical properties of ionically crosslinked alginate hydrogel scaffolds in vitro", *Journal of Biomedical Materials Research Part A*, vol. 84A, no. 4, pp. 899–907, 2008. DOI: 10.1002/jbm.a.31375.

[187] J. You, S.-A. Park, D.-S. Shin, D. Patel, V. K. Raghunathan, M. Kim, C. J. Murphy, G. Tae, and A. Revzin, "Characterizing the effects of heparin gel stiffness on function of primary hepatocytes", *Tissue Engineering Part A*, vol. 19, no. 23-24, pp. 2655–2663, 2013. DOI: 10.1089/ten.tea.2012.0681.

[188] V. Natarajan, E. J. Berglund, D. X. Chen, and S. Kidambi, "Substrate elasticity regulates primary hepatocyte functions", *RSC Advances*, 2016. DOI: 10.17303/jber.2016.101.

[189] B. David, L. Barbe, D. BarthèS-Biesel, and C. Legallais, "Mechanical properties of alginate beads hosting hepatocytes in a fluidized bed bioreactor", *The International Journal of Artificial Organs*, vol. 29, no. 8, pp. 756–763, 2006. DOI: 10.1177/039139880602900805.

[190] T. M. Henderson, K. Ladewig, D. N. Haylock, K. M. McLean, and A. J. OConnor, "Formation and characterisation of a modifiable soft macro-porous hyaluronic acid cryogel platform", *Journal of Biomaterials Science, Polymer Edition*, vol. 26, no. 13, pp. 881–897, 2015. DOI: 10.1080/09205063.2015.1065597.

[191] A. Tripathi and J. S. Melo, "Preparation of a sponge-like biocomposite agarose–chitosan scaffold with primary hepatocytes for establishing an in vitro 3d liver tissue model", *RSC Adv.*, vol. 5, pp. 30 701–30 710, 39 2015. DOI: 10.1039/C5RA04153H.

[192] A. Tripathi and A. Kumar, "Multi-featured macroporous agarose–alginate cryogel: Synthesis and characterization for bioengineering applications", *Macromolecular Bioscience*, vol. 11, no. 1, pp. 22–35, 2011. DOI: 10.1002/mabi.201000286.

[193] S. Yan, J. Wei, Y. Liu, H. Zhang, J. Chen, and X. Li, "Hepatocyte spheroid culture on fibrous scaffolds with grafted functional ligands as an in vitro model for predicting drug metabolism and hepatotoxicity", *Acta Biomaterialia*, vol. 28, pp. 138–148, 2015. DOI: 10.1016/j.actbio.2015.09.027.

[194] D. Schuppan, "Structure of the extracellular matrix in normal and fibrotic liver: Collagens and glycoproteins", *Seminars in Liver Disease*, vol. 10, no. 1, pp. 1–10, 1990. DOI: 10.1055/s-2008-1040452.

[195] A. Tripathi, T. Vishnoi, D. Singh, and A. Kumar, "Modulated crosslinking of macroporous polymeric cryogel affects in vitro cell adhesion and growth", *Macromolecular Bioscience*, vol. 13, no. 7, pp. 838–850, 2013. DOI: 10.1002/mabi.201200398.

[196] B. J. Kane, M. J. Zinner, M. L. Yarmush, and M. Toner, "Liver-specific functional studies in a microfluidic array of primary mammalian hepatocytes", *Analytical Chemistry*, vol. 78, no. 13, pp. 4291–4298, 2006. DOI: 10.1021/ac051856v.

[197] H. Ijima, S. Nakamura, R. P. Bual, and K. Yoshida, "Liver-specific extracellular matrix hydrogel promotes liver-specific functions of hepatocytes in vitro and survival of transplanted hepatocytes in vivo", *Journal of Bioscience and Bioengineering*, vol. 128, no. 3, pp. 365–372, 2019. DOI: 10.1016/j.jbiosc.2019.02.014.

[198] Y. Nahmias, R. E. Schwartz, W.-S. Hu, C. M. Verfaillie, and D. J. Odde, "Endothelium-mediated hepatocyte recruitment in the establishment of liver-like tissue in vitro", *Tissue Engineering*, vol. 12, no. 6, pp. 1627–1638, 2006. DOI: 10.1089/ten.2006.12.1627.

[199] L. D. DeLeve, X. Wang, L. Hu, M. K. McCuskey, and R. S. McCuskey, "Rat liver sinusoidal endothelial cell phenotype is maintained by paracrine and autocrine regulation", *American Journal of Physiology-Gastrointestinal and Liver Physiology*, vol. 287, no. 4, G757–G763, 2004. DOI: 10.1152/ajpgi.00017.2004.

[200] K. Elvevold, B. Smedsrød, and I. Martinez, "The liver sinusoidal endothelial cell: A cell type of controversial and confusing identity", *American Journal of Physiology-Gastrointestinal and Liver Physiology*, vol. 294, no. 2, G391–G400, 2008. DOI: 10.1152/ajpgi.00167.2007.

[201] Y. Toyoda, M. Tamai, K. Kashikura, S. Kobayashi, Y. Fujiyama, T. Soga, and Y.-i. Tagawa, "Acetaminophen-induced hepatotoxicity in a liver tissue model consisting of primary hepatocytes assembling around an endothelial cell network", *Drug Metabolism and Disposition*, vol. 40, no. 1, pp. 169–177, 2012. DOI: 10.1124/dmd.111.041137.

[202] L. J. Nelson, M. Navarro, P. Treskes, K. Samuel, O. Tura-Ceide, S. D. Morley, P. C. Hayes, and J. N. Plevris, "Acetaminophen cytotoxicity is ameliorated in a human liver organotypic co-culture model", *Scientific Reports*, vol. 5, 2015. DOI: 10.1038/srep17455.

[203] M. Inamori, H. Mizumoto, and T. Kajiwara, "An approach for formation of vascularized liver tissue by endothelial cell–covered hepatocyte spheroid integration", *Tissue Engineering Part A*, vol. 15, no. 8, pp. 2029–2037, 2009. DOI: 10.1089/ten.tea.2008.0403.

[204] G. G. Y. Chiew, A. Fu, K. Perng Low, and K. Q. Luo, "Physical supports from liver cancer cells are essential for differentiation and remodeling of endothelial cells in a HepG2-HUVEC co-culture model", *Scientific Reports*, vol. 5, no. April, pp. 1–16, 2015. DOI: 10.1038/srep10801.

[205] J. M. Llovet and J. Bruix, "Molecular targeted therapies in hepatocellular carcinoma", *Hepatology*, vol. 48, no. 4, pp. 1312–1327, 2008. DOI: 10.1002/hep.22506.

[206] L. Liu, Y. Cao, C. Chen, X. Zhang, A. McNabola, D. Wilkie, S. Wilhelm, M. Lynch, and C. Carter, "Sorafenib blocks the RAF/MEK/ERK pathway, inhibits tumor angiogenesis, and induces tumor cell apoptosis in hepatocellular carcinoma model PLC/PRF/5", *Cancer Research*, vol. 66, no. 24, pp. 11 851–11 858, 2006. DOI: 10.1158/0008-5472.CAN-06-1377.

[207] D. X. Nguyen, P. D. Bos, and J. Massagué, "Metastasis: From dissemination to organ-specific colonization", *Nature Reviews Cancer*, vol. 9, no. 4, pp. 274–284, 2009. DOI: 10.1038/nrc2622.

[208] R. R. Langley and I. J. Fidler, "The seed and soil hypothesis revisited—the role of tumor-stroma interactions in metastasis to different organs", *International Journal of Cancer*, vol. 128, no. 11, pp. 2527–2535, 2011. DOI: 10.1002/ijc.26031.

[209] G. P. Gupta and J. Massagué, "Cancer metastasis: Building a framework", *Cell*, vol. 127, no. 4, pp. 679–695, 2006. DOI: 10.1016/j.cell.2006.11.001.

[210] A. F. Chambers, A. C. Groom, and I. C. MacDonald, "Dissemination and growth of cancer cells in metastatic sites", *Nature Reviews Cancer*, vol. 2, no. 8, pp. 563–572, 2002. DOI: 10.1038/nrc865.

[211] P. Brodt, "Role of the microenvironment in liver metastasis: From pre- to prometastatic niches", *Clinical Cancer Research*, vol. 22, no. 24, pp. 5971–5982, 2016. DOI: 10.1158/1078-0432.CCR-16-0460.

[212] N. Bidan, J. Bailleul-Dubois, J. Duval, M. Winter, M. Denoulet, K. Hannebicque, I. Y. El-Sayed, C. Ginestier, V. Forissier, E. Charafe-Jauffret, M. Macario, Y. T. Matsunaga, S. Meignan, F. Anquez, S. Julien, A. Bonnefond, M. Derhourhi, X. Le Bourhis, and C. Lagadec, "Transcriptomic analysis of breast cancer stem cells and development of a paldh1a1:mneptune reporter system for live tracking", *Proteomics*, vol. 19, no. 21-22, p. 1 800 454, 2019. DOI: 10.1002/pmic.201800454.

[213] A. Treizebre, A. Sivery, J. Duval, V. Senez, X. Lebourhis, and C. Lagadec, "Microfluidic metastasis-on-a-chip models for investigation of breast cancer stem cells (bcscs)", *22nd International Conference on Miniaturized Systems for Chemistry and Life Sciences, MicroTAS*, 2018.

[214] A. Sivery, J. Duval, V. Senez, X. Lebourhis, C. Lagadec, and A. Treizebre, "Development of a microlfuidic biomimetic device for triple negative breast cancer stem cells extravasation studies", *MicroNanofluidics Conference*, 2018.

[215] S. Ali and G. Lazennec, "Chemokines: Novel targets for breast cancer metastasis", *Cancer and Metastasis Reviews*, vol. 26, no. 3, pp. 401–420, 2007. DOI: 10.1007/s10555-007-9073-z.

[216] A. M. Clark, S. E. Wheeler, C. L. Young, L. Stockdale, J. Shepard Neiman, W. Zhao, D. B. Stolz, R. Venkataramanan, D. Lauffenburger, L. Griffith, and A. Wells, "A liver microphysiological system of tumor cell dormancy and inflammatory responsiveness is affected by scaffold properties", *Lab Chip*, vol. 17, pp. 156–168, 1 2017. DOI: 10.1039/C6LC01171C.

[217] A. Benedicto, I. Romayor, and B. Arteta, "Role of liver ICAM-1 in metastasis", *Oncology Letters*, vol. 14, no. 4, pp. 3883–3892, 2017. DOI: 10.3892/ol.2017.6700.